Tom Brenner

Aggregation behaviour of cod muscle proteins

Department of Chemistry, Faculty of Physical Sciences,
University of Iceland, Reykjavík, 2009

Matís ohf.

Aggregation behaviour of cod muscle proteins

PhD thesis

Tom Brenner

Department of Chemistry
Faculty of Physical Sciences
University of Iceland
Reykjavík 2009

Academic dissertation,
submitted to the Department of Chemistry, Faculty of Physical Sciences,
University of Iceland, for the degree of PhD in Physical Chemistry

PhD committee

Dr. Ragnar Jóhannsson, Matís ohf.
Dr. Taco Nicolai, Université Du Maine, France
Dr. Ágúst Kvaran, University of Iceland

Opponents

Dr. E. Allen Foegeding, North Carolina State University, US
Dr. Erik van der Linden, Wageningen University, The Netherlands

PhD thesis
Printed by Háskólaprent in Iceland, Reykjavík 2009,
ISBN 978-9979-9633-9-4

Abstract

Aggregation of cod muscle proteins was studied, mainly using light scattering and rheology. The main muscle protein, myosin, was studied in purified form at pH close to neutral (6-8) and high salt concentration (0.5M KCl). It was found that limited aggregation took place upon heating to 30-70°C at pH ≥ 6.5, while the aggregation was very extensive at pH 6.0. Cooling of solution at pH ≥ 6.5 led to a stronger, thermo-reversible aggregation step. The aggregates formed were characterized in terms of a single fractal dimension. Similar aggregates had been observed earlier for other types of proteins, but never for myosin or muscle proteins in general, from fish or otherwise.

The second part of the research dealt with isolates of cod muscle proteins obtained using homogenization at pH ~11. This isolation mimics the large-scale protein solubilisation used in 2 Icelandic processing plants aimed at recovering muscle proteins of cod (and other fish) from cut-offs and frames. Proteins thus solubilised yielded a gel if the protein concentration C was 6g/L or higher when the pH was lowered below pH 9.5, but these gels melted above about 25°C. Gels could also be produced at higher pH, up to 11, when solutions (C≥15g/L) were first heated for several minutes to 30°C or higher and then cooled below 25°C. Gels deformed under application of constant stresses, but did not break and flow below certain stresses that may be referred to as proper yield stresses. Broken gels reformed under application of stresses below this proper yield stress, making their use

in food processing easier, since gelation is spontaneously retained for fractured gels at low temperatures and at rest.

Finally, it was observed that gels at all pH undergo a slow phase separation and exude water. Visualization using confocal scanning light microscopy showed formation of protein poor regions believed to be the first step in the macroscopic phase separation.

Ágrip

Klösun vöðvapróteina úr þorski var rannsökuð. Stuðst var aðallega við ljósdreifingu og viskoelastískar mælingar í þessum rannsóknum. Í fyrstu var aðalvöðvapróteinið, mýosin, einangrað og rannsakað við pH 6-8 og 0.5M KCl. Ljósdreifimælingar vörpuðu ljósi á takmarkaða klösun við 30-70°C og pH≥6.5, en klösunin var mun sterkari við pH 6.0. Kæling upphitaðra lausna við pH≥6.5 leiddi til frekari klösunar, sem var afturkræf að því leyti að upphitun rauf þau tengi sem mynduð voru við kælingu. Próteinklasarnir sýndu brotvíddarbyggingu á þeim skala sem ljósdreifitækni mælir. Slík bygging er þekkt fyrir mörg önnur protein, en þetta er í fyrsta skipti sem sýnt er fram á þessa byggingu fyrir vöðvaprótein.

Seinni hluti rannsóknarinnar fjallar um hegðun vöðvapróteinlausna sem fást við uppleysingu við pH ~11. Slíkri uppleysingu er beitt á iðnaðarskala hér á landi til að ná vöðvapróteinum úr þorskafskurði sem og öðrum fiskafskurði. Próteinlausnir fengnar með þessum ferli sýndu gelmyndun þegar próteinstyrkur er hærri en 6g/L á sýrustigsbilinu 8.5-9.5, en þessi gel voru einungis stöðug undir 25°C. Gel voru einnig útbúin við hærra pH (upp í 11) með því að lausnir við þetta háa pH og með próteinstyrk hærri en 15g/L voru hitaðar upp í 30°C og síðan kældar aftur niður fyrir 25°C.

Öll þau gel sem fengin voru fram, skriðu undir fastri skerspennu (e. shear stress), en brotnuðu ekki og sýndu þau ekki flæði ef skerspennan var lægri en sú spenna sem skilgreina má sem eiginlega brotspennu.

Brotin gel endurmynduðust undir skerspennu sem var lægri en þessi brotspenna, en það mun hafa þýðingu í matvælaiðnaði fyrst vinnsluferlar mega gera ráð fyrir broti gelja svo fremi sem þau eru látin endurmyndast við lágt hitastig og kyrrstöðu.

Almennt sýndu öll kerfin hæga skiljun í tvo fasa, þar sem vatn skildist út úr próteingeljunum. Notkun “confocal scanning light microscopy” varpaði ljósi á myndun próteinsnauðra svæða í gelinu.

List of publications

This thesis is based on the following publications:

1. Brenner Tom, Johannsson Ragnar and Nicolai Taco. *Characterization of fish myosin aggregates using static and dynamic light scattering.* Food Hydrocolloids, 2009. **23**(2): p. 296-305.

2. Brenner Tom, Johannsson Ragnar and Nicolai Taco. *Characterisation and thermo-reversible gelation of cod muscle protein isolates.* Food Chemistry, 2009. **115**(1): p. 26-31.

3. Brenner Tom, Nicolai Taco and Johannsson Ragnar. *Rheology of thermo-reversible fish protein isolate gels.* Food Research International, doi:10.1016/j.foodres.2009.04.020.

Table of contents

Introduction

Of the ~10^8 tonnes of fish and marine catch caught annually world-wide, only 50-60% are used for human consumption [1]. The efforts to utilize better the remaining parts of the catch have significance both in terms of profitability and of minimizing waste. Underutilized fish species are usually small, dark-meat fish with a high lipid content, and are in general less-acceptable to consumers [2]. Fish cut-offs and by-products, on the other hand, are those parts of any fish which are removed from the main product (usually the fish fillet) during its processing. Various efforts have been put into processing both underutilized fish and fish cut-offs into more lucrative products, preferably for human consumption.

The fishing industry is traditionally an important aspect of Icelandic economy, and accounted for 6% of the gross domestic production in 2007 [3]. The Atlantic Cod (Gadhus Morhua), henceforth referred to as cod, accounted for 40% of revenue generated by the Icelandic fishing industry the same year [3]. Since 2007, the Icelandic food research company Matís has been operating a processing plant aiming to isolate muscle proteins from cod cut-offs and frames, while a second processing plant was opened in Iceland in 2008. The total amount of cut-offs processed in the former plant is about 50 tonnes per year. Interest in the behaviour of protein isolates obtained in a similar

manner to that employed in the processing plants was the main impetus for the research reported herein.

Elucidating aggregation mechanism of proteins has been the focus of extensive research, spanning nearly a century. The research reported herein capitalized on an opportunity to compare aggregation and structure of aggregates and gels from fish muscle proteins to the universal behaviour exhibited by globular proteins [4, 5].

The research reported herein concentrated at first on the aggregation of purified cod myosin, the main results of which were reported in Ref. [6]. The main technique used for this investigation was light scattering. It was found that large self similar aggregates were formed during heating that could be characterized in terms of a so-called fractal dimension. Such aggregates had been observed earlier for other types of proteins [5], but never for myosin or muscle proteins in general, from fish or otherwise. The other important finding for purified myosin was that for pH≥6.5, cooling of solution heated to 30°C or higher leads to a thermo-reversible step of aggregation. This finding agreed with an aggregation mechanism previously suggested for myosin [7]. The results allowed an understanding of the mechanism in play for purified myosin.

After elucidating the behaviour of myosin, attention was turned to the protein isolates prepared from cod muscle at a high pH. This part of the research is more applied, since these solutions resemble those prepared at the processing plants, and are of a higher total protein

concentration, which we found to suffice for production of gels. It was found that protein solubilisation of cod muscle proteins is about 60% if homogenization at pH 11 is employed [8]. An extensive study was then made of the rheological properties of these protein solutions and their ability to yield gels, which is perhaps the most important prerequisite to use of the solution in food products [8, 9]. The novelty in this part of the research is the observation of solution behaviour directly post solubilisation, without precipitation of the proteins at their iso-electric point. Other reports on gelation of protein solutions obtained from fish using extreme pH without their precipitation at the iso-electric point have not been given in the literature, to the author's knowledge.

Background

Underutilized fish and fish cut-offs

As noted in the introduction, waste from fish and marine catch process is an economical and environmental issue, with about 50-60% of total catch currently either discarded or underutilized. The most important fish by-products are the head, skin, viscera, direct cut-offs and the frame [1]. The component to have enjoyed the greatest attention in terms of isolation from the above by-products are the edible muscle proteins which are abundant in the cut-offs and in meat left on frames and heads. There are 2 main approaches to isolation of the muscle proteins. The first involves removal of undesirable substances from the muscle by extensive washing and refining, yielding a recovered heterogeneous suspension of the muscle proteins. The second approach involves solubilising the muscle proteins to obtain a protein solution.

Perhaps the best known example of muscle protein recovery is the preparation of surimi. Surimi is prepared from recovered muscle which is washed extensively in water at neutral or slightly alkaline pH. Further refinement of the resulting suspension from bones and skin yields the cured surimi paste, to which salt is added as well. While surimi processing is an often cited example of an effort towards improved fish utilization, industry scale production is still nearly exclusive to surimi from lean, white fish (such as the Alaska pollock, the over-supply of which is often quoted as the main reason of surimi

processing having developed to its current scale), from which nearly fully separated muscle mince is used [2]. Current efforts are made to extend surimi processing to smaller and dark-meat fish, such as menhaden and red pike [2]. A better example of "proper" curing of muscle protein from underutilized portions of the catch is the production of fish protein concentrate (FPC), which follows in principle the same steps as surimi processing, except that organic solvents (such as ethanol or iso-propanol) are used in the washing instead of water. The processing of FPC allows for a more complete use of different fish by-products as a starting material, especially the inclusion of the fish head in the processing. The resulting protein suspension lacks proper gelling properties [2, 10] and as such is usually either processed into a powder or used for preparation of hydrolysates. FPC has not found wide spread use in food products for human consumption, except as an additive to such products as pasta and bread [2, 10, 11]. Its main uses are still either in animal-feed or in silage [2].

Hydrolysis of muscle proteins enhances their solubility and can be used to prepare a solution of muscle proteins. The hydrolysis can be accomplished either chemically or enzymatically, and the starting material may be either unprocessed fish muscle (and cut-offs) or pre-processed concentrates, such as FPC. Fish protein hydrolysates have traditionally found uses in such products as fish soup flavourings, and outside the food industry in fertilizers and silage [2]. Growing

attention is currently being paid to possible bioactivity and positive health effects of hydrolyzed fish muscle proteins [12].

Solubilisation of muscle proteins at extreme pH (without added salt) has been noted widely [13-16]. Solutions of proteins obtained through extreme pH solubilisation are referred to in the current work as fish protein isolates, or FPI. Most attention has been paid to the gelling properties and possible use of FPI after concentration at the iso-electric point (pH ~5.5), which yields a heterogeneous precipitate with protein concentration 150-200 g/L. Such concentrated FPI have been shown to gel after addition of salt and heating [17-23].

Muscle structure and muscle proteins

Muscle cells and muscle fibres are highly organized entities, a fact which has allowed them to be investigated using x-ray and electron microscopy [24]. Striated muscle is composed of many long fibres. The fibre is divided into many smaller myofibrils - While the diameter of a muscle fibre might be of the order of 0.05-0.1 mm, the myofibril has a diameter of about 1 μm. Each myofibril is divided longitudinally into a repeating unit referred to sarcomeres.

The total protein content in muscle is about 20%, and the dominant part of the rest is water. The fat content in muscle is quite variable between different animals, and is ~0.3% for cod [25]. It is customary to classify the protein content of muscles into 3 classes of proteins, according to their solubility at neutral pH- stromal proteins (non-water soluble), sarcoplasmic proteins (soluble in water at neutral pH) and

myofibrillar proteins (soluble in water at neutral pH and high salt concentrations). The myofibrillar protein comprise at least 70% of the muscle protein content in general, and usually over 80% in fish muscle [25]. It should be noted that despite the conventional classification of myofibrillar proteins as soluble in water at high salt concentrations, enhanced solubility has also been reported for myofibrillar proteins at neutral pH under extremely low ionic strength conditions, the attaining of which requires several dilutions in deionised water [26].

The main stromal protein is the main component of the lamina, the membrane encapsulating the muscle fibre, that is, collagen 4. Other stromal proteins are reticulin and elastin. Sarcoplasmic proteins are mainly enzymes- haemoglobin, myoglobin and other membrane associated proteins.

The main proteins composing the myofibril are myosin and actin, which are arranged into the so called thick filaments and thin filaments, respectively. Each thick filament contains between 200 and 400 myosin molecules, while the thin filament is a double helix of strands of actin molecules.

The repeating sarcomere unit can be seen in figure 1. The sarcomere is demarcated by 2 Z discs, one on each side.

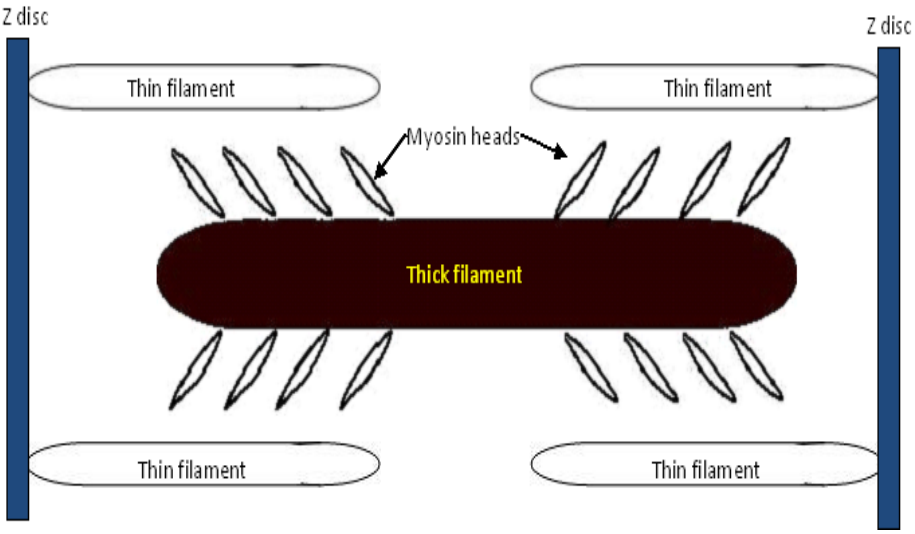

Figure 1. The sarcomere (not drawn to scale).

Two myofibrillar proteins that should be mentioned here are tropomyosin and troponin. Tropomyosin is a fibrous protein, woven along the thin actin filaments. Each tropomyosin molecule in bound to a troponin complex which has 3 subunits called troponin-I, C and T. During rest this tropomyosin-troponin complex blocks myosin from interacting with actin. When a nerve signal leads to a Ca^{2+} concentration increase in the cytoplasm, one Ca^{2+} ion binds to troponin-C which is ensued by a shift in the troponin complex. This exposes the myosin binding sites on actin, with which myosin can then interact. One actin-binding site is found on each head of the myosin molecule.

Table 1 lists the main myofibrillar proteins and their mass percentage in the myofibril, adapted in part from Ref. [26].

Table 1. The different myofibrillar proteins and their relative weight fraction in the muscle.

Protein	Wt% of total myofibrillar content	(No. of sub-units)	MW (kD)
Myosin	45-55	2	210-220
		1 (LC1 or A1)	23-25
		2 (LC2 or RLC)	18-19
		1 (LC3 or A2)	17-18
Actin	20-25	1	42
Tropomyosin	5-7	2	35
Troponin	4-6	1 (TnT)	37
		1 (TnI)	22
		1 (TnC)	18
Titin	7-10	1	2800
Nebulin	3-5	1	600
M protein	1-2	1	165
C protein	1-2	1	140
F Protein	<1	1	110
α actinin	1-2	2	100
Desmin	1-5	1	55

Myosin

The myosin molecule is composed of 2 heavy chains of molecular weight 210-220 kD plus 4 light chains (LC), designated LC1, LC2 and LC3 in order of decreasing molecular weight. There are 2 identical LC2 light chains, which are also called the regulatory light chains (RLC), with a molecular weight 18-19kD. LC1 and LC3 are referred to as the essential light chains (ELC), and have a M_w of about 23-25kD and 17-18kD, respectively. Since they can be released by alkaline treatment, they're also referred to as A1 and A2 light chains.

The heavy chain of myosin folds into 2 distinct regions, the globular head and the tail. The myosin molecule is formed by two heavy chains, with the 2 tails forming a super-helix while the 2 heads are distinct as 2 lobes on the same end of the super-helix, often also referred to as myosin tail or rod. The light chains are woven around the heads, with the regulatory chains (LC2) close to the joint-region (between the heads and the tail), while the essential chains seem to span the entire length of the head [24, 27]. Enzymatic digestion of myosin heavy chain with trypsin cleaves it to the so-called heavy meromyosin (HMM) and light meromyosin (LMM), while cleavage using papain yields the myosin head and the tail (rod) [27]. Cleaving using chemotrypsin with or without divalent cations yields the former or latter segments, respectively. Figure 2 illustrates the myosin molecule and its proteolytic fragments. The head is referred to as S-1, while the tail portion of HMM is referred to as S-2.

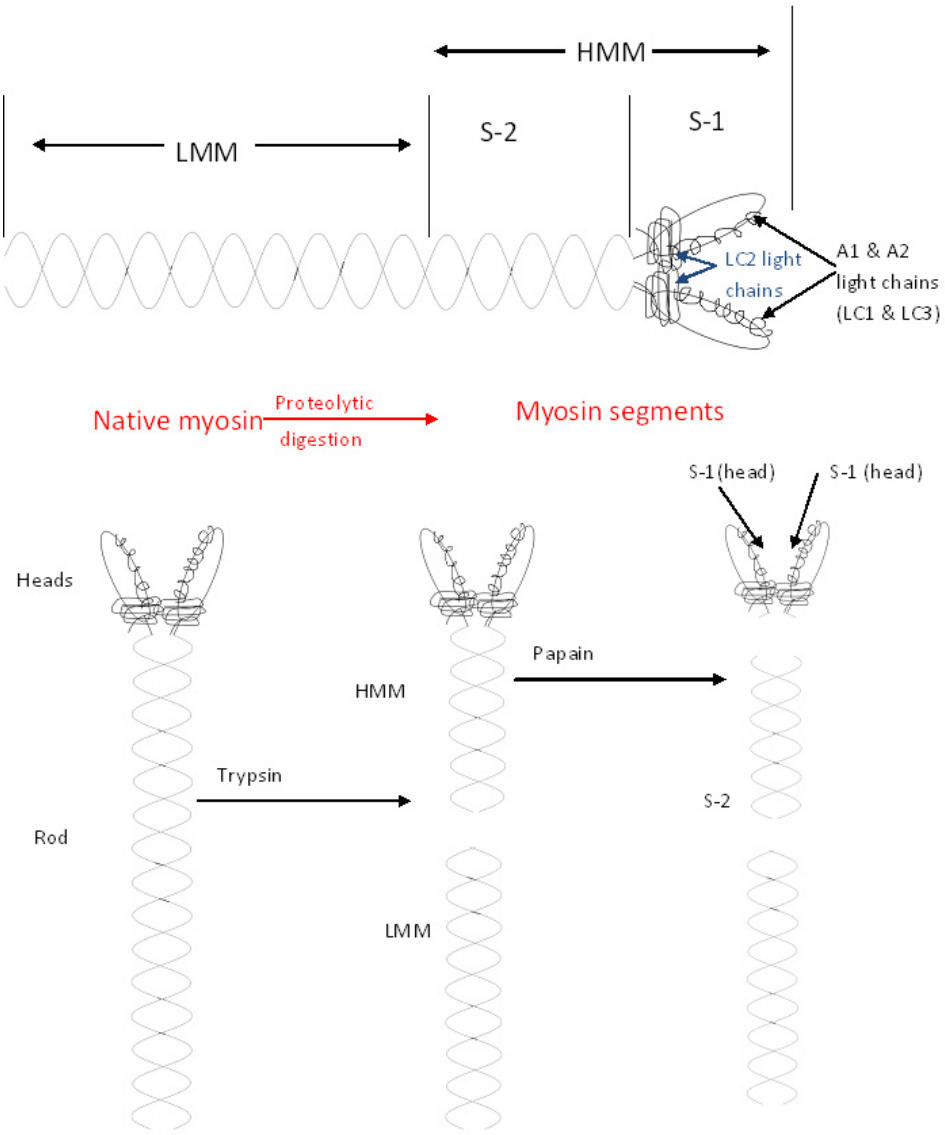

Figure 2. Native myosin and the fragments of myosin obtained after different enzymatic treatments.

The dimensions of the myosin molecule have been estimated from electron microscopy images. The tail has a contour length of about 155nm, and a diameter of 2nm [28, 29]. It is far from being rigid, and possesses at least 2 bending regions, about 43nm and 70nm from the head-tail joint [28-30]. The region between the 2 bending "points" is susceptible to enzymes producing LMM and HMM, and both bending regions are assumed to be thermally unstable and to facilitate myosin movement in the myofibril [27]. The myosin heads seem closer to an ellipsoid than a sphere, 19nm long and 6.5nm at its widest in the plane of the myosin moiety, and 3nm perpendicular to it [28]. The myosin heads also assume a wide range of angles compared to the tail, as if on a swivel joint [28, 31].

The amino-acid sequence of the myosin tail can be described as a heptad-repeat (a,b,c,d,e,f,g) where positions a and d are frequently occupied by hydrophobic residues [27, 32]. This arrangement is considered to be the main driving force for the coiled-coil formation. Positions b, c and f are often occupied by polar amino-acids, the presence of which not only stabilizes the coiled-coil, but also drives the thick filament formation in muscle. This serves to explain why thick filaments are dissociated at high salt concentrations [27].

Aggregation processes

Predicting structures formed by random aggregation is probably only possible using computer simulations. Computer simulations of randomly aggregating particles have shown two distinct regimes:

flocculation, the initial aggregation when aggregates are still on average far apart, and percolation, the nearly static formation of a network from the aggregates formed in the first step, taking place once their volume fraction is approximately unity (i.e., when the aggregates overlap) [33].

One fundamental property of aggregates formed by random aggregation is that they have a self-similar structure characterized by a fractal dimension. Until the advance of the fractal concept, most physicists would define a dimension by the number of coordinates needed to specify a point in a curve or a body; a fractal resists such specification [34]. A definition of the dimension applicable to fractals is the scaling exponent of the number of units of the fractal (and, in physical terms, its mass) with its characteristic size:

$$N \propto r^{df} \quad (1)$$

with N the number of units, d_f the fractal dimension, and r a characteristic size of the body. The fractal dimensions characterizing aggregates formed by diffusion limited aggregation processes (where every collision of particles leads to binding) and reaction limited aggregation processes (where only a very small fraction of the collisions with a sufficient energy to overcome the energy barrier leads to binding) have been determined using computer simulations as 1.8 and 2.1, respectively. The aggregates formed in the percolation process follow universal scaling laws and are characterized by a fractal dimension 2.5 [35]. Aggregates are thus more properly referred

to as multi-fractals, but this is very difficult to appreciate experimentally using light scattering measurements [33].

Aggregation processes may lead to stable finite aggregates, (thermodynamically) stable gels (where a single aggregate spans the entire volume), or meta-stable gels which keep developing until the aggregating particles phase-separate from the solvent [36]. The lifetime of meta-stable gels depends strongly on the volume fraction of the aggregating particles and the inter-particle interaction [36]; it is common in the food industry, for instance, that an effort is made to produce gels which are stable on time-scales larger than the desired shelf-life of the product. Such products include, for instance, yoghurts, surimi and various meat sausages.

Aggregation and gelation of muscle proteins

Compared to the extent of research of aggregation exhibited by denatured (heat, pressure, additives) globular proteins, the understanding of muscle protein aggregation is rather limited. For globular proteins, a universal feature is that exposure of hydrophobic patches after denaturation is the first step leading to aggregation and gelation at sufficiently high concentrations [4]. Denatured globular protein assembly is furthermore most often irreversible. It is more difficult to find conclusive results on the mechanism behind muscle protein aggregation, since often, as in the case of surimi, they are precipitated before gelation is induced through heating. This precludes

a complete study from a homogenous solution to a gel and observation of proper sol-to-gel transitions.

For surimi pastes, it was found that deactivating endogenous trans-glutaminase (TGase) led to weaker gels, while addition of exogenous TGase led to an increase in gel strength [37]. This seems to suggest involvement of enzymatically-mediated covalent bonds in gel formation. On the other hand, increase of surface hydrophobicity in surimi pastes was observed during holding at low temperatures (5-30°C), leading a stronger final gel (after subsequent heating). This phenomenon is referred to as setting and is considered to involve both enhanced TGase activity and increase in hydrophobic interactions (35).

Heat induced gels of muscle protein mixture, such as surimi, are invariably white. This means that they are heterogeneous in structure (sometimes referred to as phase-separated gels [4]).It is well established that such gels are obtained at conditions where electro-static repulsions between proteins are either lacking (at pH near pI) or are effectively screened by addition of salt [4, 5]. This suggests that for muscle protein mixtures, electro-static repulsion needs to be completely eliminated (or nearly so) to allow gel formation.

Most research on aggregation of individual muscle proteins has been done on myosin, though fundamental research is occasionally reported (e.g. Ref. [38]) on actin since it serves as a model system for formation of long linear aggregates. The heat-induced aggregation of myosin from rabbit was understood in terms of a 2-step process,

involving oligomerization of myosin through their heads into star-like aggregates [29, 39-42], followed by formation of larger aggregates by association of the tails [7, 43-45]. While a weak decrease in surface thiol groups on myosin, S-1and HMM segments during heating led to speculation that disulphide bridges were stabilizing the star-like aggregates, studies of the changes in hydrophobicity of the same segments seem like a more conclusive indication as to mechanism of the initial aggregation step [44, 45]. Further assembly of the star-like aggregates has been attributed to tail interaction [29, 44, 45]. Such interaction between tails has been speculated to account for the cooling-induced aggregation of preheated rod fragments of myosin from carp, with the interesting modification that reformation of coiled-coil structure from tails on different rods could facilitate such aggregation only after cooling. Observations of the heat-induced melting of the tail fragment of myosin and the coiled-coil to random coil have been widely given in the literature [7, 29, 41-43, 45-49], and often to be nearly completely reversible [7, 44, 45, 48], in agreement with the tail aggregation mechanism proposed in Ref. [7].

Myosin gels

Production of myosin gels has shown that there some similarities between myosin from different sources, but also important differences. Gelation induced by heating has been reported for myosin from different sources [38, 43, 47, 50-53]. Rheological studies have demonstrated that cooling of gels produced at elevated temperatures led to an increase in gel strength of myosin from white croaker [52] as

well as from catfish [54]. On the other hand, no effect was of cooling was observed for red muscle chicken myosin and the gel strength of white muscle chicken myosin slightly decreased after cooling [53]. This could suggest a greater importance of hydrogen bonds in the stabilizing of myosin gels from fish sources.

Microscopy of myosin gels has shown that very different structures are obtained at high or low salt concentrations and pH close to neutral or slightly acidic. So-called particulate structure, where coarse aggregates are visible in the gel structure, has been observed for myosin gels at pH 6.0 and salt concentration 0.2-0.25M for rabbit [47] and cattle myosin [50], while at the same pH and salt concentration 0.6M fine-stranded gels were obtained. The latter structure was observed even at 0.6M salt if the pH was lowered to 4.0, where gel was observed without heating. However, further studies reported differences in the thickness of the strands of when gels were obtained at pH 6.0 and 0.25M NaCl or pH 4.0 and 0.6M NaCl have been reported [51].

While the structure of globular protein aggregates formed at different conditions of pH and salt is similar, the structure of gels is not. It is well established that globular proteins form transparent gels, where the local structure consists of well-defined strands of aggregates, under conditions where long-range repulsion is present, i.e. at pH far from the pI at low ionic strength [5]. When the charge density on the proteins is decreased by setting the pH closer to pI or when salt is

added to screen the electric charges, the strand-structure transforms into more coarse grains of aggregates, which results in so-called particulate gels. These gels have larger correlation lengths and are more opaque [5]. Thus, the production of fine-stranded gels from myosin at the lower ionic strength (and at a pH not far from the pI) and of particulate gels at the higher ionic strength fits nicely with the known behaviour of globular proteins. Myosin does have specific characteristics as well, such as the ability to form at low ionic strength (without heating) filaments which resemble thick muscle filaments [27]. However, it should be stresses again that heating myosin solutions at a low ionic strength where such filaments are present before heating, as reported in Refs. [50, 51], results in gels very similar to those obtained at similar conditions with globular proteins.

Techniques used in this study

Light scattering

To realize the strength of light scattering (LS) as a spectroscopy technique, it is important to realize how the main relations used in LS are derived and what approximations are made in the generally cited analyses. The following follows derivations in Refs [55-57]. Starting with the imposed electric field E, and the scattered field E_s:

$$\vec{E}(\vec{r},t) = \vec{n}E_0 \exp(i\vec{k}\cdot\vec{r} - i\omega t + i\delta) \quad (2)$$

$$\vec{E_s}(\vec{r'},t') = \frac{b}{|\vec{r'}-\vec{r}|}E_0 \exp(i((\vec{k}-\vec{k_s})\cdot\vec{r} - \omega t' + \vec{k_s}\cdot\vec{r'} + \delta)) \quad (3)$$

The arrows designate vector notation. The wave vector is designated with k, and is equal to $2\pi/\lambda$ (λ being the wavelength), δ is the phase angle and ω is the wave's frequency. The scattered field is measured at position r' and time t', and $\vec{n}$ designates the polarization vector. A measure of the scattering 'power' of the scatterer is given by the parameter b, sometimes referred to as the scattering length. The scattering vector $\vec{k} - \vec{k}_s$ is usually designated $\vec{q}$, and using geometry it can be shown that (as long as the wavelength of the scattered light is the same as that of the incident light, i.e. the scattering is elastic):

$$|q| = \frac{4\pi n}{\lambda}\sin(\theta/2) \tag{4}$$

with λ the light's wave-length in vacuum, n the refractive index of the sample, and θ the scattering angle.

In practice the measurement corresponds to the sum of scattering from all point scatterers in the scattering volume, V_s:

$$\vec{E}_s(\vec{r}',t') = E_0 \exp(i(-\omega_j t' + \vec{k}_s \cdot \vec{r}' + \delta)) \sum_{j=1}^{N} \frac{b_j \exp(i\vec{q} \cdot \vec{r}_j)}{\left|\vec{r}' - \vec{r}_j\right|} \tag{5}$$

where N point scatterers are assumed to be in V_s. The size of V_s is typically negligible compared to the distance to the detector, so that $\left|\vec{r}' - \vec{r}_j\right|$ may be replaced with a constant R. Looking at the time-averaged light intensity measured at the detector (I = E.E*):

$$\langle I_s \rangle = \left\langle E_s \cdot E_s^{*} \right\rangle = \frac{I_0}{R^2} \sum_{k=1}^{N} \sum_{j=1}^{N} b_j b_k \left\langle \exp(i\vec{q} \cdot (\vec{r}_j - \vec{r}_k)) \right\rangle \tag{6}$$

where the brackets indicate average over time. We can now replace the scattering length of the individual scatterers with a scattering length per volume element, thus replacing the sums in Eq. (6) with their corresponding integrals:

$$I_s = \frac{I_0}{R^2}\int_{V_s}\int_{V_s}\langle b(\vec{r}')b(\vec{r}'')\rangle \exp\left(i\vec{q}\left(\vec{r}''-\vec{r}'\right)\right)d\vec{r}'\,d\vec{r}'' \tag{7}$$

We can replace the position vectors r' and r'' with a single relative vector $\vec{r}$, and integrating over the one dummy variable we get a factor of V_s:

$$I_s = \frac{V_s I_0}{R^2}\int_{V}\langle b(0)b(\vec{r})\rangle \exp\left(i\vec{q}\vec{r}\right)d\vec{r} \tag{8}$$

The quantity b is fluctuating about its average, so that $b(\vec{r}) = b + \delta b(\vec{r})$. The autocorrelation term of fluctuations is thus

$$\begin{aligned}&\langle b(0)b(\vec{r})\rangle = \langle (b+\delta b(0))\cdot(b+\delta b(\vec{r}))\rangle = \\ &\langle b^2 + b\delta b(\vec{r}) + b\delta b(0) + \delta b(0)\delta b(\vec{r})\rangle = b^2 + \langle \delta b(0)\delta b(\vec{r})\rangle\end{aligned} \tag{9}$$

since the fluctuating terms $\delta b(\vec{r})$ and $\delta b(0)$ must average to zero. Plugging the above into Eq. (8), we get:

$$I_s = \frac{V_s I_0}{R^2}\left(\int_{V}\langle \delta b(0)\delta b(\vec{r})\rangle \exp\left(i\vec{q}\vec{r}\right)d\vec{r} + b^2\int_{V}\exp\left(i\vec{q}\vec{r}\right)d\vec{r}\right) \tag{10}$$

The second term in Eq. (12) vanishes at finite q values, as long as $|q.r_{max}| >> 1$, with r_{max} the size of the scattering volume. We need therefore consider only the first term in Eq. (10). The term $\langle \delta b(0)\delta b(\vec{r})\rangle$ falls to zero at large $\vec{r}$ since the fluctuations are not

correlated over large length scales; at vanishingly small $\vec{r}$ and $\vec{q}$ $\langle \delta b(0)\delta b(\vec{r})\rangle = \langle \delta b^2 \rangle$ and $\exp(i\vec{q}\vec{r}) \approx 1$, so that Eq. (10) becomes:

$$\mathrm{I_s} = \frac{V_s^2 I_0}{R^2}\langle \delta b^2 \rangle \quad q \to 0 \tag{11}$$

The fluctuations of b are related to temperature and density fluctuations in a pure liquid, while for a solution the concentration fluctuations of the solute should be considered. In an experiment where scattering is dominated by the solute we can rewrite Eqs. (10)-(11) as following:

$$\mathrm{I_s} = \frac{V_s I_0}{R^2}\left(\frac{\delta b}{\delta c}\right)^2 \int_V \langle \delta c(0)\delta c(\vec{r})\rangle \exp(i\vec{q}\vec{r})d\vec{r} \tag{12a}$$

$$\mathrm{I_s} = \frac{V_s^2 I_0}{R^2}\left(\frac{\delta b}{\delta c}\right)^2 \langle \delta c^2 \rangle \qquad q \to 0 \tag{12b}$$

$\langle \delta c^2 \rangle$ is inversely proportional to the osmotic compressibility $\frac{\delta \pi}{\delta c}$:

$$\langle \delta c^2 \rangle = \frac{k_b T c}{V_s}\left(\frac{\delta \pi}{\delta c}\right)^{-1} \tag{13}$$

with k_b Boltzmann's constant and T the absolute temperature.

The osmotic pressure can be expanded as a series in c:

$$\pi = N_a k_b T\left(\frac{c}{M} + A_2 c^2 + ...\right) \tag{14}$$

with A_2 the so-called second virial coefficient, M the molar mass, N_a Avogadro's number, and c the concentration in units of weight per volume. We can finally rewrite Eq. (12b) as:

$$\mathrm{I_S} = \frac{V_s\, I_0}{N_a R^2}\left(\frac{\delta b}{\delta c}\right)^2 cM\,\frac{1}{1+2A_2Mc} \quad q \to 0, c \to 0 \tag{15}$$

Let us first relate $\left(\frac{\delta b}{\delta c}\right)$ to bulk properties so that we better see how Eq. (15) is used to determine the molar mass M before returning to Eq. (14a).

For light scattering the scattering length b is related to the bulk polarizability α':

$$\mathrm{b} = k^2\alpha'\left(\overrightarrow{\mathrm{n_0}}\,\overrightarrow{\mathrm{n_s}}\right) = \frac{4\pi^2\alpha'}{\lambda^2}\left(\overrightarrow{\mathrm{n_0}}\,\overrightarrow{\mathrm{n_s}}\right) \tag{16}$$

Here n_o and n_s are unit vectors indicating the direction of polarisation of the incident and detected light, respectively. In practice most often the incident and detected light are vertically polarized if we ignore effects of depolarisation so that $\left(\overrightarrow{\mathrm{n_0}}\,\overrightarrow{\mathrm{n_s}}\right)^2 = 1$. We will assume this in the following.

We can replace the bulk polarizability α' with the molecular polarizability α, $\alpha = 4\pi\varepsilon_0\alpha'$. For a binary solution of particles with a refractive index n_m in a medium of refractive index n:

$$\alpha = \left(n_m^2 - n^2\right)\varepsilon_0\rho^{-1} \approx 2\varepsilon_0 nC\rho^{-1}\frac{\partial n}{\partial c} \tag{17}$$

with ε_0 vacuum's permittivity. Since we're considering the scattering length per unit volume, ρ cancels out and

$$\left(\frac{\delta b}{\delta c}\right) = (\vec{n}_i.\vec{n}_s)\frac{2\pi n}{\lambda^2}\left(\frac{\partial n}{\partial c}\right) \tag{18}$$

Eq. (12b) now reads

$$I_s = \frac{I_0 V_s}{R^2}\frac{4\pi^2 n^2}{\lambda^4 N_a}\left(\frac{\partial n}{\partial c}\right)^2 cM\frac{1}{1+2A_2Mc} \quad q \to 0, c \to 0 \tag{19}$$

We now turn our attention to Eq. (12a). The first term in the integral, $\langle \delta c(0)\delta c(\vec{r})\rangle$, has contributions from both inter-particle and intra-particle terms. Assuming the same scattering power over the particle, we can write the inter-particle structure factor as:

$$S(q) = \frac{\int_{V_p}\langle \delta c(0)\delta c(\vec{r})\rangle \exp(i\vec{q}\vec{r})d\vec{r}}{\int_{V_p}\langle \delta c(0)\delta c(\vec{r})\rangle} \tag{20}$$

where the integral is over a particle of volume V_p. We can expand the exponent in a Taylor series, and then integrate with the origin at the particle's centre of mass:

$$S(\mathrm{q}) = \frac{\int_{V_p} \langle \delta c(0) \delta c(\vec{r}) \rangle \exp(i\vec{q}\vec{r}) d\vec{r}}{V_p} \approx 1 - (qR_g)^2 \langle \cos^2 \phi \rangle + \ldots \quad (21)$$

ϕ is the zenith angle, the average of $\cos^2\phi$ is 1/3. The radius of gyration, R_g, is defined as:

$$R_g{}^2 = \frac{1}{2V_p} \int_{V_p} \langle \delta c(0) \delta c(\vec{r}) \rangle \vec{r}^{\,2} d\vec{r} \quad (22)$$

Eq. (12a) may be written generally as:

$$\mathrm{I_s} = \frac{I_0 V_s}{R^2} \frac{4\pi^2 n^2}{\lambda^4 N_a} \left(\frac{\partial n}{\partial c} \right)^2 cM \left(\frac{N_a k_b T}{M} \left(\frac{\partial \pi}{\partial c} \right)^{-1} \right) S(q) \quad (23)$$

The leading term of $\left(\frac{N_a k_b T}{M} \left(\frac{\partial \pi}{\partial c} \right)^{-1} \right)$ is $\frac{1}{1 + 2A_2 Mc}$,

and the leading term in S(q) is $1\text{-}q^2R_g{}^2/3$.

The term $I_0 V_s/R^2$ is difficult to measure in practice. Therefore one measures the intensity relative to a standard (e.g. toluene) with known scattering properties:

$$I_{rel} = KcM_a S(q)_z \tag{24}$$

With I_{rel} the light scattered by the solution divided by that of the standard I_s. K is a constant equal to $\frac{4\pi^2 n^2}{\lambda^4 N_a}\left(\frac{\partial n}{\partial c}\right)^2\left(\frac{n_{sta}}{n_s}\right)^2\frac{1}{R_{sta}}$; R_{sta} is the wavelength and temperature dependent Rayleigh ratio of the standard. The squared ratio of the refractive indices of the standard (n_{sta}) and sample (n_s) corrects for differences in scattering volumes. M_a is an apparent molar mass equal to $N_a k_b T\left(\frac{\partial \pi}{\partial c}\right)^{-1}$. At infinite dilution, M_a is equal to the weight average molar mass, M_w, of the solute given by:

$$M_w = \frac{\sum_i M_i^2 N_i}{\sum_i M_i N_i} = \frac{\int Mc(M)dM}{c} \tag{25}$$

With N_i the number of particles of mass M_i, and alternatively c(M) represents the total mass of particles of mass M. The structure factor is affected by polydispersity in a similar manner:

$$S(q)_z = \frac{\sum_i M_i^2 N_i S(q)_i}{\sum_i M_i^2 N_i} = \frac{\int Mc(M)S(q)_M\, dM}{\int Mc(M)dM} \tag{26}$$

It follows that the radius of gyration measured with light scattering is:

$$R_{gz} = \left[\frac{\int Mc(M) R_g^2 dM}{\int Mc(M) dM} \right]^{0.5} = \left[\frac{\sum_i M_i^2 N_i R_{g,i}^2 dM}{\sum_i M_i^2 N_i dM} \right]^{0.5} \qquad (27)$$

Since the determination of R_g from S(q) is essentially a determination of the coefficient of S(q) dependence on q^2. The term R_{gz} measured at finite concentration is proportional to the correlation length of concentration fluctuations, and is often designated R_{ga}, an apparent radius of gyration.

For fractal objects S(q) has a power-law dependence on q for $q.R_{gz} >> 1$:

$$S(q) \propto q^{-d_f} \qquad q.R_{gz} >> 1 \qquad (28)$$

Where the exponent d_f is the fractal dimension which also relates M_w to R_{gz}:

$$M_w \propto R_{gz}^{d_f} \qquad (29)$$

Dynamic light scattering

The following derivation is easier if we first return to the summation notation of Eq. (6) valid for point scatterers. We define the time

averaged autocorrelation function of the scattering intensity as a function of delay time t, $g_2(t)$:

$$g_2(q,t) = \frac{\langle I(q,0) I(q,0+t) \rangle}{\langle I(q,0) \rangle^2} = \tag{30}$$

$$\frac{\sum_{m=1}^{N} \sum_{s=1}^{N} \sum_{k=1}^{N} \sum_{j=1}^{N} b_j b_k b_s b_m \left\langle \exp(-i\vec{q} \cdot \left[\vec{r_j}(0) - \vec{r_k}(0) - \left(\vec{r_s}(\tau) - \vec{r_m}(\tau) \right) \right]) \right\rangle}{R^4}$$

There are 6 kinds of terms:

1. $N^4 - 6N^3 + 11N^2 - 6N$ terms in which all subscripts are different. These average to zero.

2. $4N^2 - 4N$ terms in which 3 subscripts refer to the same particle, the fourth being different. This corresponds to an average of one particle's phase times the average of another's; both are zero, and yield a product of zero.

3. $6N^3 - 18N^2 - 12N$ terms in which there is one and only one equality. These yield zero for the same reason as the terms above.

4. N^2 terms in which j=k, s=m. These yield unity.

5. $N^2 - N$ terms in which j=m≠k=s. These yield the term

$$\left\langle \exp(-i\vec{q} \cdot \left[\vec{r_j}(\tau) + \vec{r_j}(0) \right]) \right\rangle \left\langle \exp(i\vec{q} \cdot \left[\vec{r_k}(\tau) + \vec{r_k}(0) \right]) \right\rangle$$

These yield again zero, since an average over the sum of phases is still zero!

6. N^2-N terms in which j=s≠k=m. These yield the term

$$\left\langle \exp(i\vec{q}\cdot\left[\vec{r_j}(\tau)-\vec{r_j}(0)\right])\right\rangle\left\langle \exp(-i\vec{q}\cdot\left[\vec{r_k}(\tau)-\vec{r_k}(0)\right])\right\rangle$$

This term does not average to zero, since it depends on particle displacement, which is small for short time lags. For large values of N typically measured experimentally, we get:

$$g_2(t)=1+\left\langle \exp\left(i\vec{q}\Delta\vec{r}(t)\right)\right\rangle^2 \tag{31}$$

We now consider random fluctuations in the local concentration of solute particles that are much smaller than q^{-1}. These occur due to Brownian motion generated by random differences in pressure exerted by solvent molecules. We can start with Fick's second law of diffusion:

$$\frac{\partial\rho(\Delta r,t)}{\partial t}=D\nabla^2\rho(\Delta r,t) \tag{32}$$

with D the cooperative diffusion coefficient. At time zero no flux has taken place, so the boundary condition is:

$$\rho(\Delta r,0)=\delta(\Delta r) \tag{33}$$

The trick to solve Eq. (32) with the boundary condition Eq. (33) is to apply Fourier transform to both sides of each equation, after which we get:

$$\frac{\partial \rho(\vec{q},t)}{\partial t} = -q^2 D \rho(\vec{q},t) \tag{34}$$

$$\rho(\vec{q},0) = 1 \tag{35}$$

which yields immediately the solution

$$\rho(\vec{q},t) = \exp(-q^2 Dt) \tag{36}$$

Plugging this into Eq. (31), we finally get:

$$g_2(t) = 1 + \exp(-2q^2 Dt) \tag{37}$$

Eq. (37) is the starting point for analysis of intensity autocorrelation functions, which are measured using auto-correlators with different "channels" for different lag times. For non-interacting (dilute) particles D is equal to the self diffusion coefficient (D_0). D_0 is often interpreted in terms of the so-called hydrodynamic radius, R_h, which is equal to the radius R of a sphere of diffusion coefficient D_0:

$$D = \frac{k_b T}{6\pi\eta R_h} \tag{38}$$

Eq. 34 combines results obtained by Einstein and Stokes, and is thus appropriately called the Stokes-Einstein relation:

$$D = \frac{k_b T}{f} \tag{39}$$

$$f = 6\pi\eta R \tag{40}$$

where f in relation (39), due to Einstein, is the affine friction force on particles undergoing thermodynamic motion, and was explicitly calculated for spheres by Stokes (Eq. 40)). The value of R_h depends on the shape of the particles and the amount of draining of the solvent.

If the particles are not small compared to q^{-1} the relaxation of $g_2(t)$ will be influenced by rotational diffusion for asymmetric particles and internal dynamics for flexible particles.

If the particles interact the driving force for the cooperative diffusion coefficient, i.e. the osmotic compressibility, increases or decreases depending on whether the interaction is attractive or repulsive. In addition, the friction coefficient increases.

In the case of polydisperse solute particles we can interpret the relaxation of $g_2(t)$ in terms of a distribution of relaxation times. Interpreting autocorrelation functions in terms of relaxation time distributions is commonly done using algorithms such as REPES [58] or CONTIN [59]. The idea is to perform the Laplace inverse transform on the experimentally measured autocorrelation function:

$$g_1(t) = \int A(\tau)\exp(-t/\tau)d\tau \tag{41}$$

with g_1 the autocorrelation function of the electric field, related to g_2 through the Siegert relation [60]:

$$g_1(t) = \left(g_2(t) - 1\right)^{1/2} \tag{42}$$

The resulting distribution function of relaxation times A(τ) may be then converted to a distribution function of diffusion coefficients, D, Eqs. (37) and (42), or the corresponding hydrodynamic radii using Eq. (38), if the particles are small compared to q^{-1} and sufficiently dilute so that interaction can be neglected. It is vital to realize that this distribution function reflects the contribution of particles of relaxation time τ to the autocorrelation function g_2. The relative contribution of particles with a certain size to the average scattering intensity is proportional to its mass concentration multiplied with its molar mass. It is customary to report the harmonic average of the hydrodynamic radius:

$$R_{hz} = \frac{\left\langle \tau^{-1} \right\rangle^{-1} q^2 k_b T}{6\pi\eta} \tag{43}$$

with $\left\langle \tau^{-1} \right\rangle = \int \tau^{-1} A(\tau) d\tau$

Measurements of turbid solutions

When a significant fraction of the incident beam is scattered, the problem of multiple scattering arises. Multiple scattering interferes with both SLS and DLS measurements, since non-singly scattered photons contribute to the average light intensity at any given angle, as well as skew the autocorrelation function measured at any angle. To solve this it is possible to revert to cross-correlational light scattering. The idea is that two incident beams of equal intensity I_0, rather than a single beam, are shone at the sample, and are measured by 2 detectors. In one version, sometimes called 3D dynamic light scattering, the beams and detectors are separated in the axis perpendicular to the plane of measurement. Since the structure factor S(q) of isotropic solutions (the scattering particles may be anisotropic, as long as they don't form an anisotropic phase) is independent of the zenith angle, each detector measures twice the intensity scattered from a single beam I_s. The problem is now to identify how many photon have been singly scattered and correspond to the proper structure factor. This can be done by looking at the cross-correlation function of the light scattered, which is equal to the 2 autocorrelation functions at the 2 detectors. Since only a half of the signal comes from a single beam, one half of the signal at most can be correlated. This means that g_2 is now given with:

$$g_2(t) = 1 + B\exp(-2q^2Dt) \tag{44}$$

with B a constant not exceeding 0.25. In practice, a less than optimal experimental set-up leads to a factor B_0 lower than 0.25 even for perfectly transparent samples. Any further decrease in the intercept of g_2 (B) in the measurement of a real sample is understood in terms of non-correlated photons measured at the detector; their effect is corrected for by dividing with B_0 and taking the square-root:

$$I_{si} = I_{\text{tot}} \left(\frac{B}{B_0} \right)^{1/2} \tag{45}$$

where I_{si} is the scattered light intensity only from singly scattered photons, and I_{tot} is the total intensity of light scattered measured at the detector. Of course, one also needs to correct for the reduced transmission.

Rheology

The term rheology was coined by the polymer chemist Eugene Bingham, and is derived from the Greek word for flow. It deals with flow and deformation of materials under applications of loads, or stresses.

In rheological nomenclature, a distinction is made between 3 fundamental modes of deformation, or 3 modes of testing materials. These are the tensile deformation, shear deformation and flexion. The 3 modes of deformation are illustrated in figure 3.

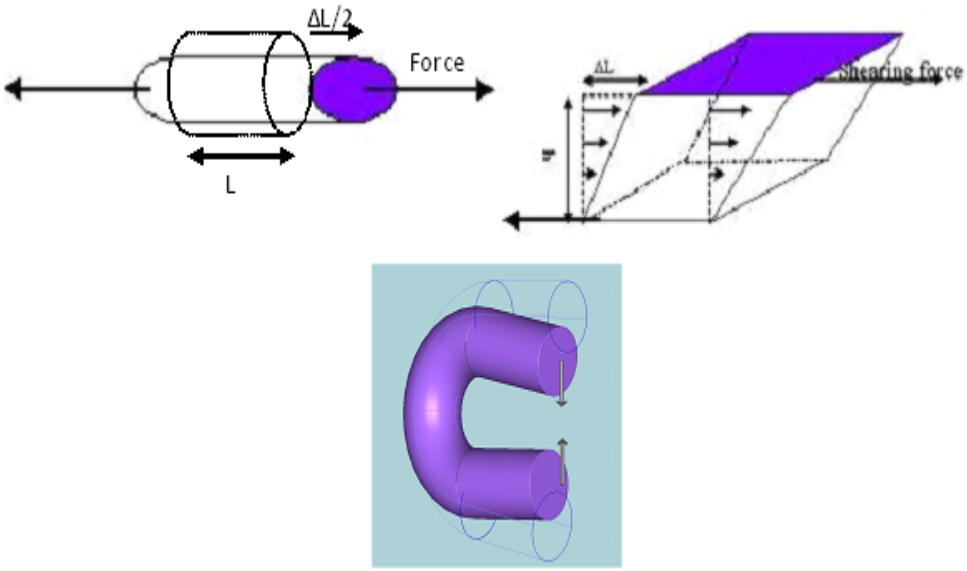

Figure 3. Upper left sketch: tensile deformation, upper right sketch : shear deformation, bottom sketch: flexion (bending). The shadowed faces represent the cross sections as defined for tensile and shear deformations in the top sketches.

Elastic materials (solids)

Perhaps the best known response of a material to a constant load is Hooke‘s law, formulated by Hooke nearly 350 years ago. Testing springs during tensile extension, Hooke found a linear relation between the spring‘s elongation ΔL, and the load m applied to the spring:

$$\boldsymbol{m} \propto \Delta \boldsymbol{L} \tag{46}$$

or, after reformulation to the known Hooke’s law:

$$\left|\boldsymbol{F}\right| = \boldsymbol{gm} = \boldsymbol{K}\Delta\boldsymbol{L} \tag{47}$$

with g the earth gravity, and K the spring constant. While Hooke found different spring constants for different springs, he never made the observation that for a given material, K was inversely proportional to the spring's length, and proportional to its cross section a. Designating ΔL/L as the strain ε, Eq. (47) would be written today as:

$$\frac{|\boldsymbol{F}|}{\boldsymbol{a}} = \sigma = \boldsymbol{E}\frac{\Delta \boldsymbol{L}}{\boldsymbol{L}} = \boldsymbol{E}\varepsilon \tag{48}$$

where we recognize E as the Young's modulus of a material under tensile extension. More importantly, perhaps, Hooke totally failed to note non-linear behaviour in his spring experiments. If he were to work with rubber at moderate strains, for instance, he'd observe a more general relation of the form [61]:

$$\sigma = \boldsymbol{G}(\alpha - \alpha^{-2}) \tag{49}$$

With α = (L+ΔL)/L = 1 + ε, and G the **elastic modulus**. Expanding α for small values of ε, we find

$$\sigma = \boldsymbol{G}(1 + \varepsilon - (1 - 2\varepsilon + 3\varepsilon^2 - ..)) \approx 3\boldsymbol{G}\varepsilon \tag{50}$$

The elastic modulus G also serves as the proportionality constant in the linear regime of shear deformation:

$$\sigma = \boldsymbol{G}\gamma \tag{51}$$

with γ, the usual symbol for strain in shear deformation, equal to ΔL/h, cf. figure 3. We see that the elastic modulus G is 1/3 of the linear regime Young's constant E, a well-known result [61].

Relating the stress to the strain as in Eq. (49) requires writing in thermodynamic terms an energy-function of the material. The undertaking of such a task requires a structural model interpreted within the frame of elasticity theory. For illustrations of the concept, see Ref. [61]. Reporting quantities such as E or G (Eqs. (48) and (51)) makes for easier comparisons between materials tested in the linear regime. Materials for which the stress increases more strongly than linearly with the strain beyond the linear regime are said to exhibit *strain-hardening*, while *strain softening* is the term applied if the increase in stress is less strong than linear with strain.

Liquids

As opposed to solids, a liquid cannot sustain stress at rest. This means that the elastic (instantaneous) response we are familiar with from springs is replaced with continuous flow in the case of liquids. An ironic sign of his rivalry with (and animosity towards) Hooke, it was none other than Sir Isaac Newton who first formulated quantitatively the relation between stress and a liquid's flow, given with:

$$\sigma = \eta \frac{\boldsymbol{d}\gamma}{\boldsymbol{dt}} = \eta \dot{\gamma} \tag{52}$$

Looking back at the shearing experiment in figure 3, we can understand the time-derivative of the strain, or the shear rate (designated $\dot{\gamma}$) as the gradient in fluid velocity, normal to the applied stress.

Liquids following Eq. (52) are said to be Newtonian. More generally, though, materials show a rate-dependent behaviour, the most general of these is the simple power-law [62]:

$$\sigma = \boldsymbol{K}\,\dot{\gamma}^{\boldsymbol{n}} \tag{53}$$

with K a constant (with unit $Pa.s^n$). Materials for which n > 1 are said to exhibit *rheological dilatancy*, or more commonly *shear thickening*. The viscosity of these materials increases with increasing shear-rate. Common examples are wet sand (mud) and dough. Materials for which n < 1 are said to exhibit *pseudoplasticity*, or more commonly *shear thinning*. Shear thinning is more common than shear thickening, and is observed for many polymer solutions. It is invariably observed for solutions of anisomeric particles, since their inclination to orient in the direction of the flow lowers the viscosity.

Time-dependence of the shear rate

The terms *thixotropy* and *anti-thixotropy* (or *rheopexy*) are applied to materials which exhibit respectively an increasing or decreasing flow-rate with time under a constant stress. The terms are ambiguous, since they are usually used to signify a decrease (thixotropy) or increase

(rheopexy) in viscosity with time, which are often interpreted in terms of fracture or formation of a net-work under shear. Viscosity is, however, a steady-state attribute; an increase in apparent viscosity (owing to a decrease in flow-rate) is seen for instance for metals during application of stresses below the yield-stress. This increase in apparent viscosity does not, in any way, reflect a formation of an elastic network under the constant stress; the metal is being deformed under the stress up to fracture (after which the shear rate increases to a constant value). The use of the terms thixotropy and rheopexy can therefore be misleading.

In this context it is worth to mention again the responses of Newtonian liquids and ideal solids to constant stresses. An ideal solid shows an elastic response, i.e. an instantaneous deformation which then totally stops. A liquid flows independently of time with a constant flow rate, which we may simply call flow. Viscoelastic materials can show an intermediate response, where the deformation is not independent of time (solids), nor is the shear rate independent of time (liquids) under constant stress. A response where the deformation depends on time less strongly than linearly is sometimes referred to as creep, and can be indicative of different changes in the material, either destructive or formative. It is therefore that it is stressed again that the terms thixotropy and rheopexy are not descriptive for the behaviour of many systems under constant stresses.

Modeling visco-elastic materials. Dashpots and springs models.

Visco-elastic behaviour can be understood quite intuitively without resorting to such specialized terms as G' and G" (see below). We have all seen materials which yield with time, but response elastically at short time-scales. Silly-putty may be the most often cited example; it bounces when dropped, but loses its shape and flows when left standing for extended periods.

Figure 4. Left: a dashpot, right: a spring.

The most common way to represent visco-elastic materials is the dashpots and springs diagram. The spring designates an elastic part of the material, while a dashpot signifies a viscous part. To solve the behaviour of the system under application of stress the next 4 rules are applied:

1. The stress on any element in a series is equal to the externally applied stress.

2. The total stress on an element in a series is equal to the sum of stresses on all its parallel-connected elements.

3. The strain on all parallel-connected elements of a single element in a series is equal.

4. The total strain is equal to the sum of strains on all elements in a series.

To illustrate how this works, we can show the solution of the creep function a under constant stress for one system, a spring connected in series to a Voigt body, which is a parallel arrangement of a spring and a dashpot.

$$\sigma = \gamma_1 \boldsymbol{G}_1 = \gamma_2 \boldsymbol{G}_2 + \dot{\gamma}_2 \eta$$
$$\gamma = \gamma_1 + \gamma_2$$
$$\dot{\gamma} = \dot{\gamma}_2 = \frac{\sigma - \gamma_2 \boldsymbol{G}_2}{\eta}$$
$$\gamma_2 = \frac{\sigma}{\boldsymbol{G}_2} + \boldsymbol{A}\boldsymbol{e}^{-\boldsymbol{G}_2 \boldsymbol{t}/\eta} = \frac{\sigma}{\boldsymbol{G}_2} + \boldsymbol{A}\boldsymbol{e}^{-\boldsymbol{t}/\tau}$$
$$\gamma = \frac{\sigma}{\boldsymbol{G}_1} + \frac{\sigma}{\boldsymbol{G}_2} + \boldsymbol{A}\boldsymbol{e}^{-\boldsymbol{t}/\tau}$$
$$\dot{\gamma}_2 \geq 0; \gamma_2 \geq 0; \gamma \leq \frac{\sigma}{\boldsymbol{G}_1} + \frac{\sigma}{\boldsymbol{G}_2}$$

In this set of equations, A is a constant to be determined from the boundary conditions which are given in the last line. The first yields A ≤ 0, as does the third. The second boundary condition yields $A \geq -\sigma/G_2$, which leaves in effect only to determine the strain at time zero. Here we use the fact that a dashpot cannot respond elastically (i.e., with a step function); this leads to using the equality sign in the second boundary condition for t = 0, which yields $A = -\sigma/G_2$.

The solution in this case is therefore a rise to a maximum:

$$\gamma = \frac{\sigma}{G_1} + \frac{\sigma}{G_2}\left(1 - e^{-t/\tau}\right)$$

This solution is illustrated in figure 5.

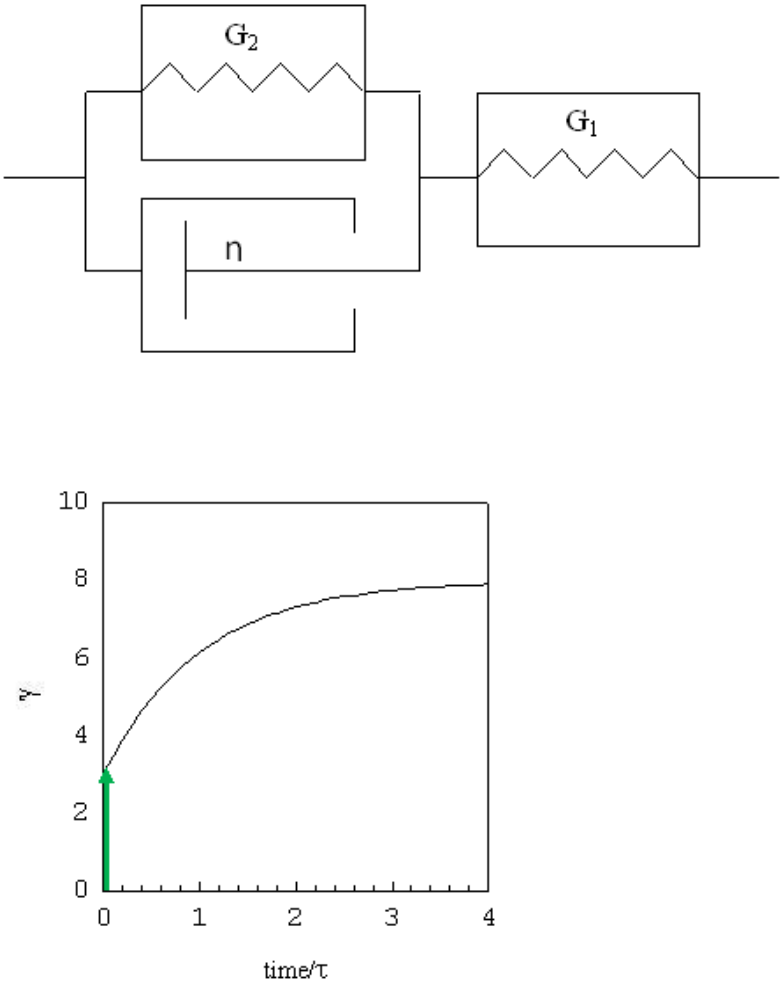

Figure 5. A schematic representation of a spring connected in series to a Voigt body (top), and the corresponding creep function under a constant stress σ (bottom); here, $\sigma/G_1 = 3$ and $\sigma/G_2 = 5$. The green arrow shows the elastic part of the response. Note $\tau = \eta/G_2$.

General visco-elastic responses

The strain and the stress are related in a general way through the modulus memory function, G(t):

$$\sigma(t) = \int_0^t G(t-\tau)\,\dot{\gamma}(\tau)\,d\tau \tag{54}$$

We can now use Eq. (54) to show how the modulus G may be interpreted in terms of 2 components, one relating to the material's tendency to deform instantly in a reversible manner (elastically), the other referring to its tendency to dissipate energy. Let's assume we now submit a material to an oscillating strain with frequency, ω so that:

$$\gamma = \gamma^0 \sin(\omega t) \tag{55}$$

where γ^0 is the maximum strain. We see that

$$\dot{\gamma} = \omega\gamma^0 \cos(\omega t) \tag{56}$$

Putting Eq. (56) into (54) we get

$$\sigma(t) = \int_0^t G(\psi)\omega\gamma^0 \cos[\omega(t-\psi)]d\psi = \omega\gamma^0 \int_0^t G(\psi)(\sin(\omega\psi)\sin(\omega t) + \cos(\omega\psi)\cos(\omega t))d\psi \tag{57}$$

where $\psi = t-\tau$. We now make a bold assumption: $\sigma(t)$ responds in a sinusoidal manner: $\sigma(t) = \sigma^0\sin(\omega t-\delta)$. This can only happen if G is independent of γ, i.e. γ^0 is still in the linear regime! Now we can obtain a solution of Eq. (57), where G is independent of t and is only a function of ω- we're left with 2 harmonics (out of phase with each other) on the right-hand side, and a single harmonic on the left-hand side. We divide the solution into 2 constants:

$$\begin{aligned}\omega\int_0^t G(\psi)\sin(\omega\psi)d\psi &= \frac{\sigma^0}{\gamma^0}\cos\delta = G^*\cos\delta = G' \\ \omega\int_0^t G(\psi)\cos(\omega\psi)d\psi &= \frac{\sigma^0}{\gamma^0}\sin\delta = G^*\sin\delta = G''\end{aligned} \tag{58}$$

and write eventually:

$$\sigma(t) = \gamma^0\left(G'\sin(\omega t) + G''\cos(\omega t)\right) \tag{59}$$

Now G' describes that part of the stress that is in phase with the strain. It is called the **storage modulus**. G" describes that part of the stress that is 90° out of phase with the strain; it is referred to as the **loss modulus**. G* is the **complex modulus**: $G^* = (G'^2+G''^2)^{1/2}$.

Results

I Purified cod myosin

Cod myosin is a highly unstable molecule [63, 64], markedly more so than myosin from fish of more temperate habitat or land-animals [64-69]. In accordance with this instability, we have found isolation of monomeric cod myosin to not be possible, at least as measured using light-scattering [6]. The 2 isolation methods used in the current study to obtain purified myosin from cod muscle are explained in detail in Ref. [6]. Both methods lead to purified myosin, present as aggregates with an aggregation number N_{agg} in the range 8-20 (given by $M_w(agg)/M_w(myosin)$), as measured using SLS. No monomeric myosin was observed from the auto-correlation functions of purified myosin; given the relatively small aggregation number of the aggregates, the fact that they completely dominate the light-scattering intensity suggests that they also dominate the size-distribution of myosin. The Laplace inversion of auto-correlation functions of myosin yielded monomodal distributions of hydrodynamic radii, see figure 6, which did not extend down to the value obtained experimentally for individual myosin molecules, 17nm [70]. The latter agrees with the calculated value of 18nm based on known structure of myosin [71].

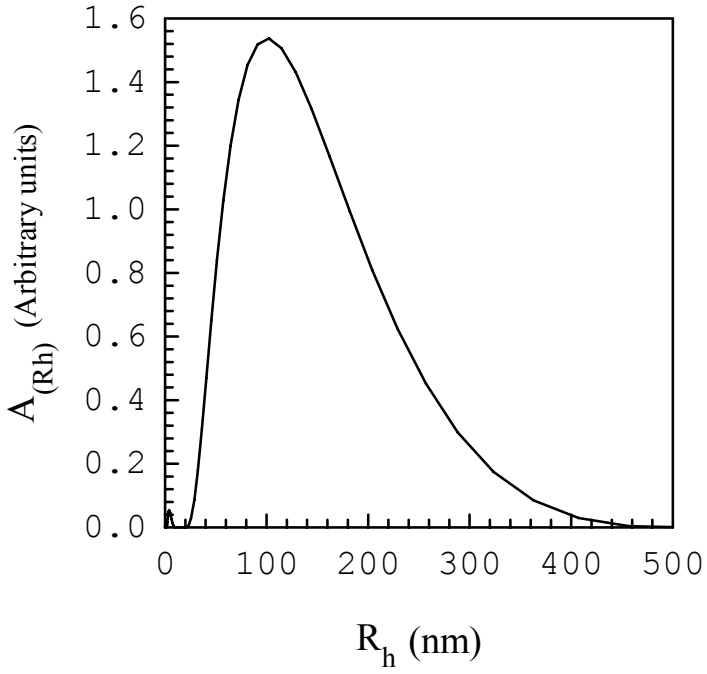

Figure 6. Size-distribution function of purified cod myosin at pH 8.

Despite the variance found in N_{agg} between different preparations, values of R_g (70-90nm) and R_h (90-120nm) were always similar. This suggests the presence of star-like myosin aggregates for which the dependence of R_g on the number of arms is very weak [72]. Since microscopy has shown that star-like aggregates consisted of globular masses up to 60nm in diameter, which are the collapsed myosin heads [29, 42], with the tails radiating out, we can compare this value of R_g to that expected from such a geometry. The upper limit for a many-armed star with a dense core of radius r and arms of length L can be calculated as follows. We first assume a total mass M, a mass M_r of

the core and M_L for the combined mass of the arms. Next, we designate f_L as the fraction of mass in the arms ($f_L = M_L/M$). Assuming L>>r, which is a good approximation for the myosin stars, $R_g \approx (f_L/3)^{1/2}.(r+L)$. Using 0.5 for f_L, 15-30nm for r (a diameter of 30-60nm) and 140-155nm for L [29, 42], R_g is in the range 64-76nm, which agrees with our findings. The assumption that one half of the mass of each myosin molecule is in the tail fraction corresponds to the known molecular weights of myosin head, tail and light chains [27], and taking into account that 60-70% of the light chains dissociate from the heads during heating [29, 43].

Star-like aggregates of the native myosin molecule were observed using electron microscopy for rabbit myosin [29, 41, 42], carp myosin [40], and finally for dog cardiac myosin [39]. Electron-microscopy showed shortening of the myosin tails after heating [29, 41, 42], which is attributed to a helix-to-coil transition. Optical rotation and CD studies have also indicated the helix-to-coil transition in the tail of myosin. For cod, the helical content of the tail was reported to decrease monotonously with increasing temperature in the range 25-65°C [46]. Similar findings have been reported for walleye pollack LMM in the range 10-60°C [43], rabbit myosin rod in the range 20-80°C [45], rabbit LMM in the range 20-80°C [44], carp rod in the range 20-70°C [7], and for myosin rod from Antarctic fish and scallop in the range 0-80°C [49].

The star-like structure and the helix-to-coil transitions serve to explain our finding that R_g and R_h decreased during heating despite a weak heat-induced aggregation process, see figure 7. Decrease of the radius-of-gyration was observed in Ref. [49], while in Ref. [52] a decrease was noted for the hydrodynamic radius of white croaker myosin during heating. The values reported in Ref. [52] imply that the measurements were made on aggregates, though this was not mentioned in the paper.

The weak aggregation noted for cod myosin in the pH range 6.5-8.0 during heating, as deducted from light scattering (figure 7a) and also turbidity measurements, see figure 8, coincides with that reported in earlier studies [67]. This increase is strong for the first 10mins, and then levels off though a very weak logarithmic increase continues. A similar increase of the turbidity which levels off very quickly was seen for rabbit myosin as well [73]. Though it is not straight-forward to conclusively determine the true extent of aggregation from in-situ light-scattering measurements during heating, for the concentrations used in figure 7, the effect of concentration is small and allows determination of M_w. From the data, it seems that only an increase in N_{agg} of the star-like primary aggregates is taking place during heating in this range of pH. Further aggregation in this pH range is only induced by cooling. It seems that at pH 6.0, however, further aggregation of the primary aggregates occurs during heating.

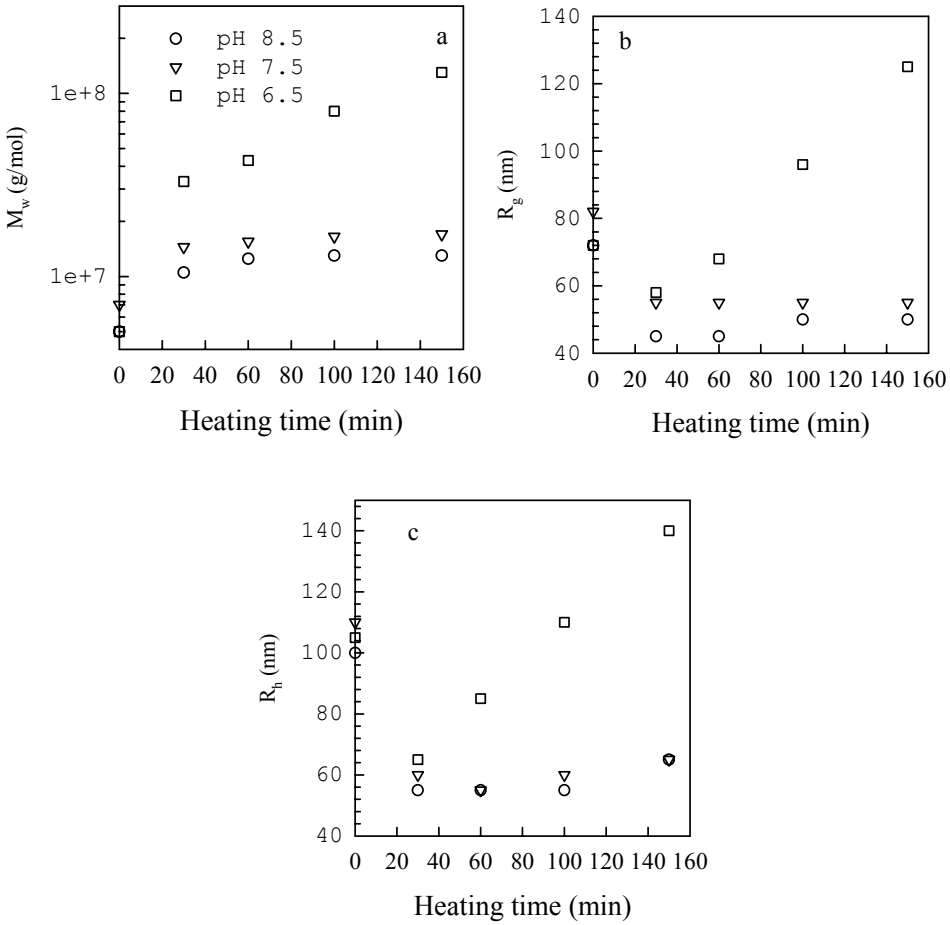

Figure 7. Molar mass M_w (a), radius of gyration R_g (b) and hydrodynamic radius R_h during heating of myosin solutions (1.5g/L) at 50°C. Different pH values are indicated in figure 7a.

The reversibility of the decrease in helical content of myosin rod segments was observed in several studies [7, 44, 45]. Coupled with the observation of extensive rod aggregation during cooling following

heating to 80°C, this led to the assumption that helices are reformed during cooling by finding other rod molecules and binding to them forming a super-helix [7]. Involvement of the tail portion of myosin in the network formation was also deduced [43] from the binding of LMM to the LMM portion of native myosin after formation of the primary aggregates. This agrees nicely with our finding that the myosin aggregate undergo a second step of thermo-reversible aggregation during cooling, at least in the pH range 6.5-8.0, which leads to a much stronger increase of both turbidity and light-scattering intensity than the first step of the aggregation. This is demonstrated in figure 9, where the turbidity increase of myosin solutions in the pH range 6.5-8.0 taking place during cooling after heating at 50°C is shown. It was reported [52] that a thermo-reversible increase of the hydrodynamic radius of myosin, as well as the storage modulus of myosin gels, takes place during cooling after heating to 65°C.

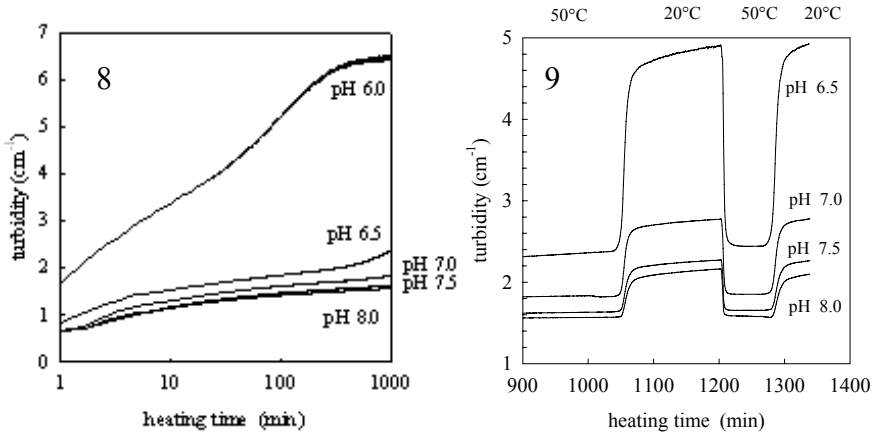

Figure 8. Dependence of the turbidity at λ=350nm on the heating time at 50°C for myosin solutions with C=5.0 g/L at different values of the pH.

Figure 9. Effect of cooling and heating cycles on the turbidity of extensively heated myosin solutions with C=5.0 g/L at different values of the pH.

The structure of myosin aggregates formed after the heating and cooling cycle was determined after dilution.

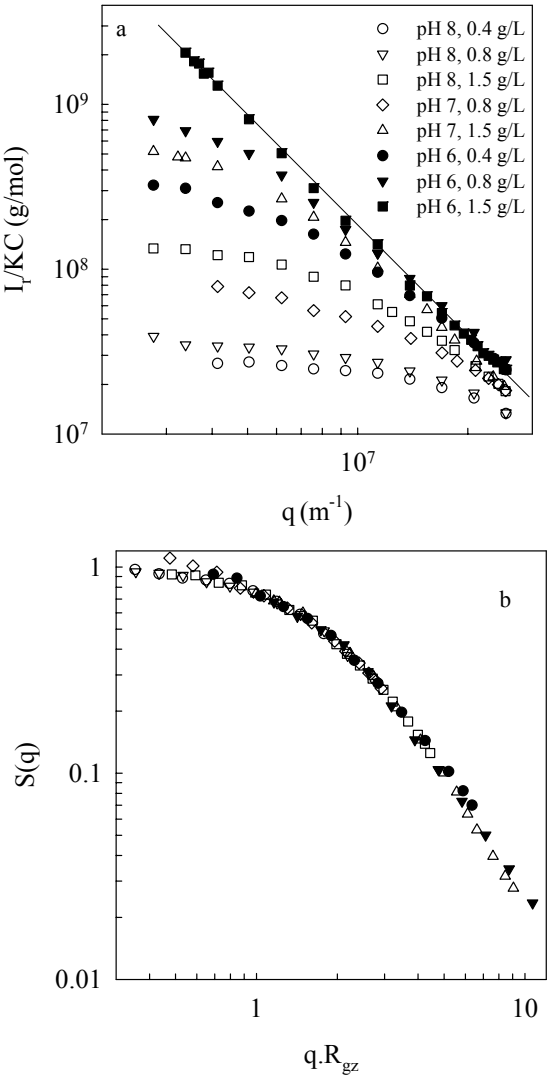

Figure 10. q-dependence (fig. 10a) of I_{rel}/Kc for highly diluted aggregate solutions obtained after heating at 70°C myosin solutions at different concentrations and pH. The solid line represents a power-law fit with exponent -2.2. The same data is shown (fig. 10b) after normalizing I_{rel}/Kc with M_w and q with R_{gz}.

Aggregates with different sizes were formed depending on the pH and the concentration, see figure 10a. The fact that the structure factor of different systems was the same when plotted as a function of $q.R_g$, see fig.10b, demonstrates their self-similar structure. For $q.Rg>>1$ we found $S(q) \propto q^{-2.2}$ implying $d_f=2.2$. This value of d_f was consistent with the dependence of M_w on R_{gz}, see figure 11. The overall structure of the myosin aggregates is close to that of aggregates formed by globular proteins (Nicolai 2007). This suggests a certain degree of universality for protein aggregation processes which take place through very different mechanisms and with a different range of binding possibilities.

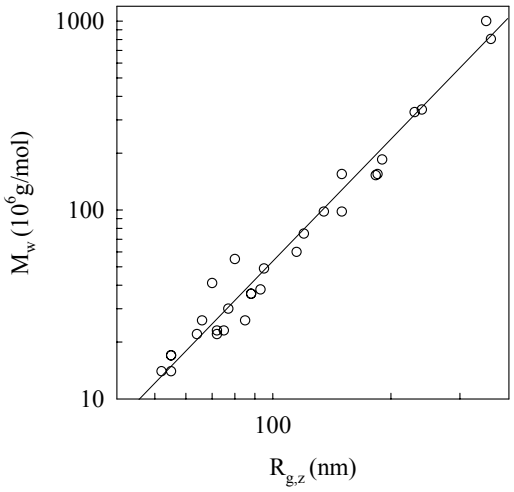

Figure 11. M_w dependence on R_{gz} for diluted aggregates obtained after heating of myosin at different concentrations and values of the pH. The solid line represents a power-law fit with an exponent 2.2.

II Fish protein isolate (FPI) from cod

As already noted in the introduction, the preparation of fish protein isolates for this study imitates that employed on an industrial scale in Iceland at 2 different processing plants. Usually, cod was purchased at a local market and delivered to the lab on ice. The white muscle tissue was homogenized in 4–5 weight equivalents of distilled water, and the pH was adjusted to a value in the range 11.0–11.2. Solutions were centrifuged for 10 min at 15,000g, followed by filtration of the supernatant over two layers of gauze. The temperature was kept under 15°C during the protein isolation. FPI solutions were stored at 4°C and used for gel preparation within 24h of extraction.

Protein composition

A typical electrophoretic pattern of the proteins extracted by this method is shown in figure 12. The electrograph shows that myosin (heavy chain 210 kDa, light chains 17–23 kDa), actin (43 kDa) and tropomyosin (38 kDa) are the most dominant proteins. Bands at higher molar mass than myosin heavy chain are tentatively assigned to titin and nebulin [26, 74]. Other weak bands may correspond to other structural proteins and proteolytic segments of the main myofibrillar proteins. The ill-separated bands between 160 and 185 kDa are thought to be proteolytic segments of myosin heavy chain [22]. The presence of these bands was reported earlier for FPI obtained through acidic and alkaline solubilization [19, 22], and for washed fish muscle post treatment with weak organic acids [75].

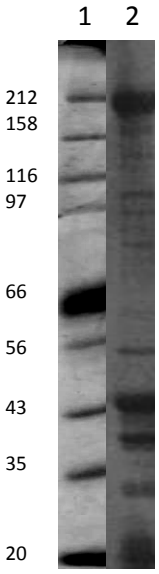

Figure 12. Protein profile of FPI (lane 2) obtained by SDS-PAGE electrophoresis compared with protein standards of different molar mass (kDa) indicated in the figure (lane 1). Protein standards shown are as followed: rabbit muscle myosin, 212kDa; MBP-β-galactosidase,158kDa; β-Galactosidase, 116kDa; Phosphorylase-b, 97kDa; Serum albumin bovine 66.4kDa; Glutamic dehydrogenase, 55.6kDa; MBP2, 42.7kDa; Thioredoxin reductase, 34.6kDa; Trypsin inhibitor, 20kDa.

Perhaps the most important aspect of the isolation method as outlined above is its yield. It was found in the current study to be 60 ± 10%. While such a yield is similar to that seen in conventional surimi processing [20], reports from the Icelandic processing plants are that the alkaline solubilization is better suited for cut-offs compared to the time-consuming refining steps required for surimi production.

Gelation

It was found that solutions with protein concentrations c=6g/L or higher a gel was obtained in the pH range 8.5-9.5 at temperatures below ~25°C. The thermo-reversible gelation observed for the FPI is perhaps its single most important feature. Figure 13 shows the storage and loss moduli of FPI at pH 9.0 during heating and subsequent cooling. At temperatures below 25°C G'>G", an indication of the more elastic (gel-like) nature of the FPI at low temperatures.

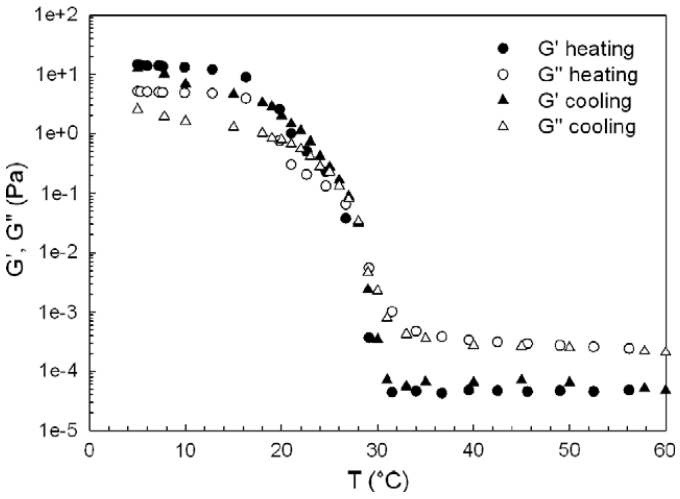

Figure 13. Temperature dependence of G' and G" at 0.01 Hz during heating and cooling of a FPI solution at pH 9.0 and C = 20 g/L.

The frequency (f) dependence of the loss and storage moduli of FPI at pH 9.0 and 5°C is shown in figure 14. It was found that preheating of the solutions before recooling led to a weaker dependence of the moduli on the shearing frequency.

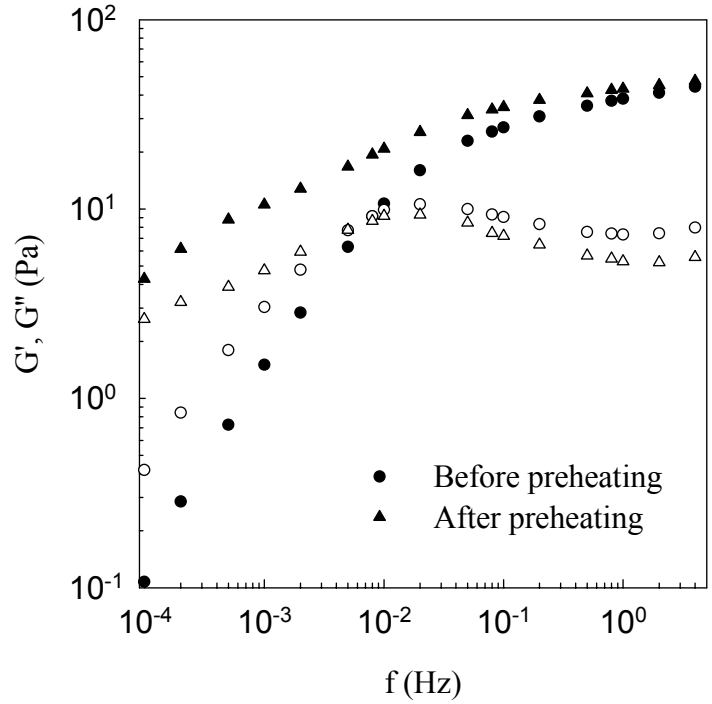

Figure 14. Frequency dependence of G' (filled symbols) and G'' (open symbols) for FPI gels at pH 9.0 (C=25g/L, 5°C) before and after preheating at 60°C for 3 minutes.

While no gel formation was found for FPI at pH > 9.5 after adjusting the pH and cooling to 5°C, gels were formed if the FPI solutions were first heated to 30°C or higher for short periods (3 mins or longer) and then cooled to 5°C. Figure 15 shows the frequency dependence of G' and G'' at for FPI (pH 11) at 5°C before and after preheating to different temperatures. Before the preheating procedure, the G'' is proportional to f, indicating the liquid like nature of the FPI. After

preheating, G'>G" and both moduli are nearly frequency independent, indicating that a gel had formed.

It is seen that while for gels produced at pH 11, the frequency dependence of G' and G" is very weak below 1Hz, for pH 9 it is more important, especially for non-preheated FPI. However, above 1Hz the frequency dependence is much weaker even for pH 9, and a near plateau is reached. We will therefore refer hereon to G' measured at 1Hz as G'_0, the high-frequency plateau value.

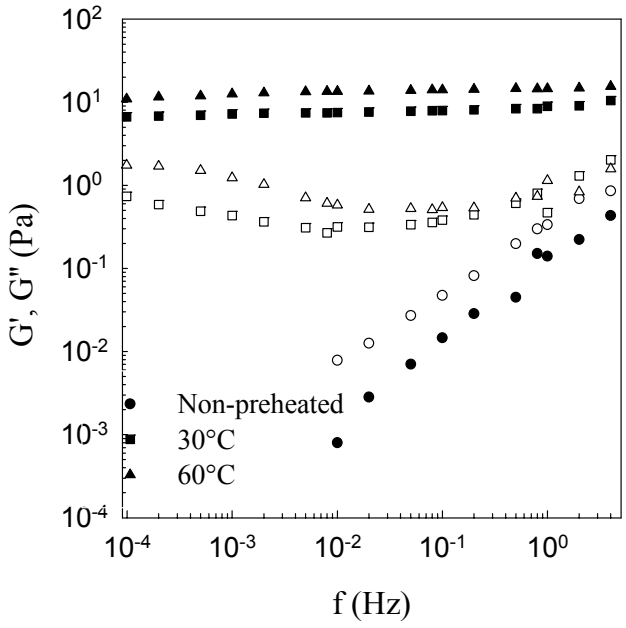

Figure 15. Frequency dependence of G' (filled symbols) and G" (open symbols) for FPI gels at pH 11.0 (C=25g/L, 5°C) before and after preheating for 3 minutes at 30°C or 60°C.

Non-linear rheology

The non-linear response to shear stress was investigated using oscillatory and continuous shear measurements at different values of the applied stress. Continuous stress sweeps of FPI showed an effect on the long-time response of the gels to weak stress When the stress was increased slowly the effective modulus G, which we define here as the ratio of stress to strain: $G \equiv \sigma/\gamma$, decreased slightly at moderate strains, see figure 16. But when the stress was increased very fast, G remained constant at the same strains. Applying weak oscillatory stress at f=0.1Hz or 1Hz did not show an effect on G', see figure 16. At low stresses, the value of G' obtained by oscillation at 1Hz is equal to the value of G obtained by continuous shear during the fastest rates ($d\sigma/dt$=2Pa/s) that was experimentally accessible ($G'_0=G_0$).

At higher stresses strain hardening was seen followed by fracture at a critical stress value above which the systems started to flow properly, see below. The critical value decreased with decreasing rate of the stress ramp.

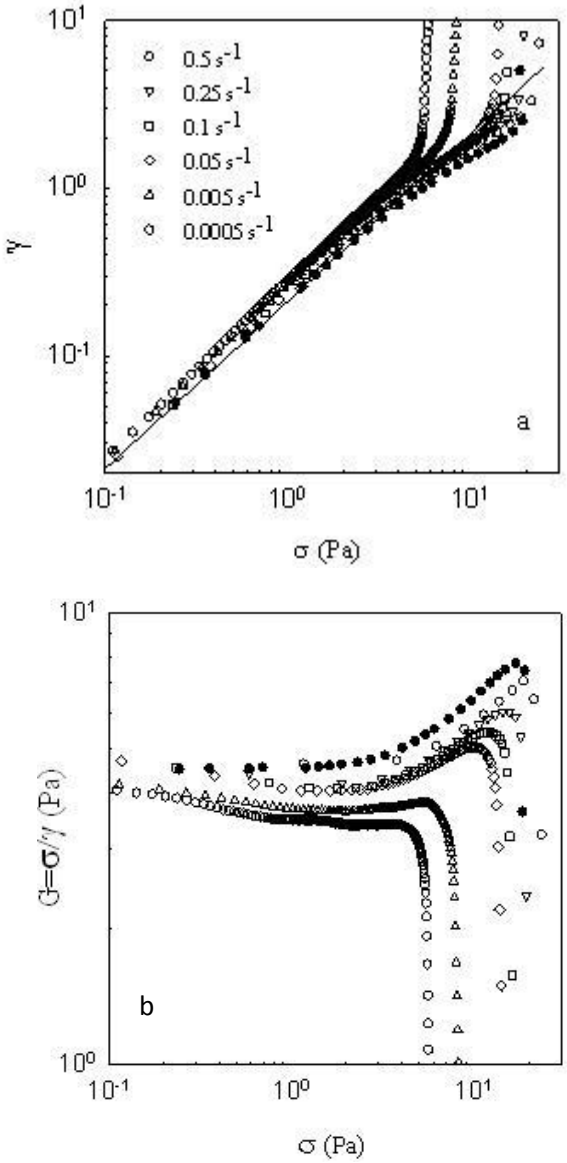

Figure 16. Strain-stress curves of FPI gels at pH 11 (C=20g/L, G'_0=4.8Pa, 5°C). The open symbols indicate continuous shear measurements at different initial flow rates ($d\gamma/dt=(d\sigma/dt)/G'_0$) indicated in the figure, while the filled symbols indicate oscillatory measurements at f=1Hz. The solid line represents $\gamma=\sigma/ G'_0$. A different representation of the same data is shown in figure 16b: $G = \sigma/\gamma$ versus σ.

The behaviour of FPI gels under constant stresses was determined and showed that creep is responsible for the rate-dependence of strain-stress curves recorded using continuous shear ramps. Figure 17 shows the time dependence of the strain under different constant stresses, indicated in the figure, for FPI at pH 11 and 9. An elastic response is built up very quickly, followed by creep that can be approximated with a power law:

$$\gamma(t) = \gamma_0\left(1 + \left(t/\tau\right)^{\alpha}\right) \tag{60}$$

As shown in figure 17c, normalizing the strain with its elastic part γ_0, which in all cases was close to σ/G_0, leads to master curves of the data at each pH. The power-law exponent α was similar for the data presented, about 1/3, but the characteristic time τ was very different for pH 9 and pH 11: about 5000s for the former and 5s for the latter. While α was always close to 1/3 for pH 11, different FPI samples at pH 9 crept with power-law exponents in the range 0.3-0.7.

Power-law creep is a known phenomenon for metals below their yield stress. Surprisingly, the strain in metals develops with the same exponent as presented here for FPI gels (1/3). For FPI, the period over which creep was observed at low stresses was very different for pH 11 and 9. For pH 11, strains were found to follow Eq. (60) for up to 10^5s. For pH 9, on the other hand, the strain stagnated after similar periods, see figure 18. At higher stresses creep was followed by fracture and ordinary flow.

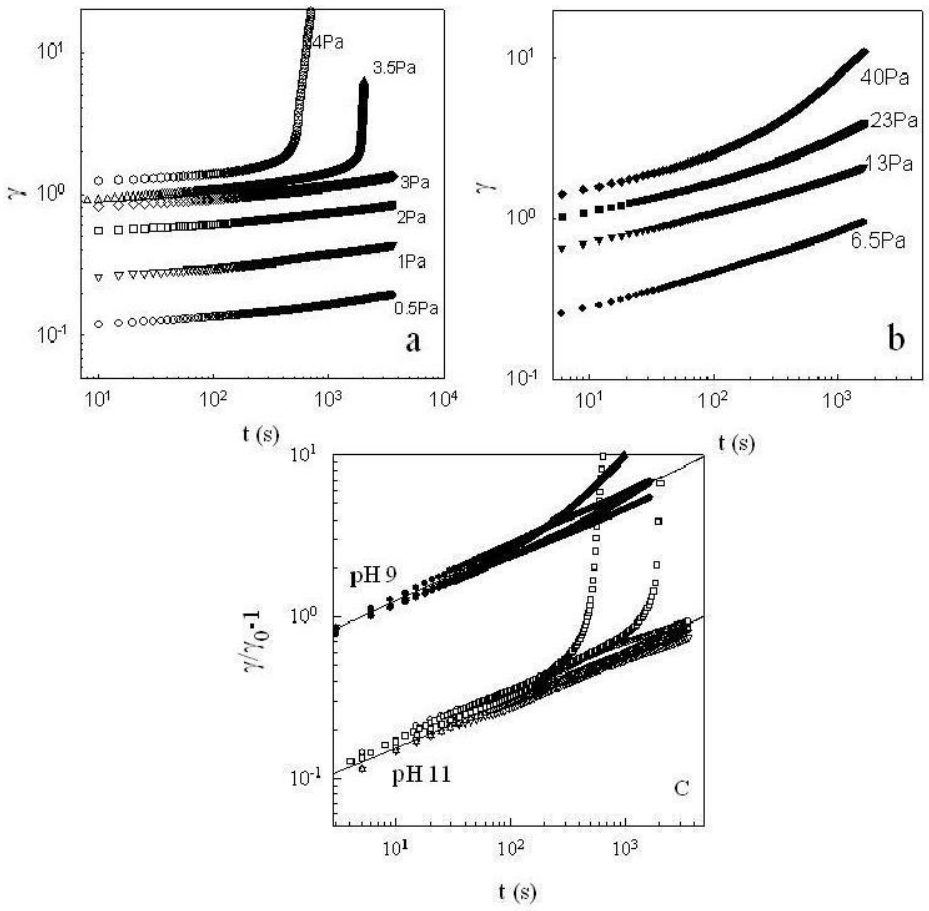

Figure 17. Strain as a function of time at different applied stresses indicated in the figures for preheated gels at pH 11 (C=20g/L, G_0 = 5Pa) (a) and at pH 9 (C=20g/L, G_0 = 40Pa) (b). Figure 17c shows the same data in a different representation. The solid lines in fig. 17c have a slope of 0.3.

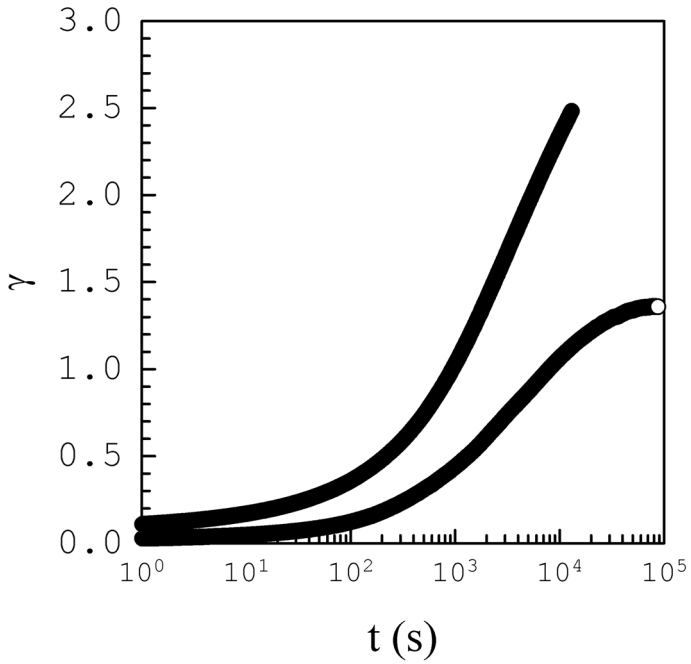

Figure 18. Strains of a FPI gel at pH 9 (G_0 = 16Pa) under stresses of 1Pa (upper curve) and 0.3Pa (lower curve).

Steady-state viscosities were measured for fractured FPI systems as a function of the shear-rate, see figure 19. It turns out that for a wide range of shear-rates, the stress is roughly constant, though it fluctuates about its mean value. We may identify this stress as the yield stress above which the systems flow properly. At lower stresses the systems may creep, but probably always stops deforming after some time as illustrated in figure 18.

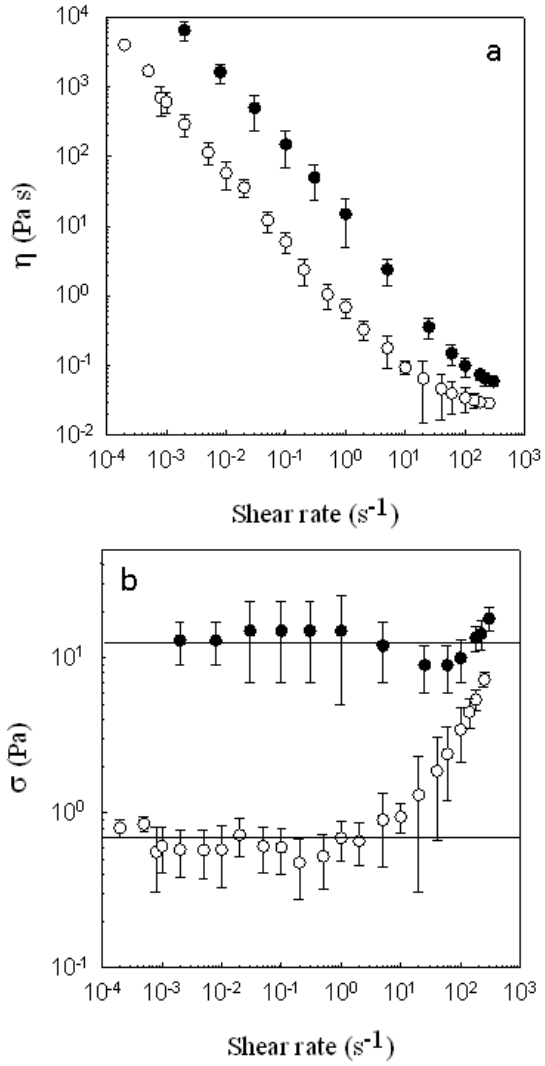

Figure 19. Viscosity (figure 19a) and shear stress (figure 19b) obtained from flow experiments. FPI gels (c=20g/L) at 5°C were broken by quickly shearing at high frequency and the stress was recorded as a function of decreasing shear rate. Filled symbols: pH 9, open symbols: pH 11.

Reproducible weak strain-hardening was seen for FPI at both pH 9 and pH 11 when measured using oscillatory measurements at 0.1Hz or

1Hz, which coincided with continuous shear measurements, see figure 16b. Figure 20 shows the dependence of G' on the strain for FPI gels at pH 9 and 11. After normalization of G' with G'_0, master curves are obtained within the experimental noise for each pH. As shown in annex A, these curves can be fitted with the model suggested in Ref. [76] for affine strain-hardening of fractal gels.

Above a critical strain the gels fractured and began to flow, but the gel reformed again at small stresses. This is consistent with the finding of a yield stress below which true flow is not possible, deduced from data such as that presented in figure 19.

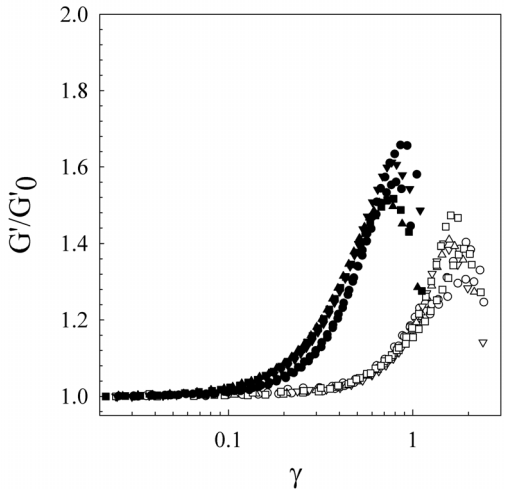

Figure 20. Strain dependence of the normalized elastic moduli of FPI gels at pH 9 (filled symbols) and pH 11 (closed symbols) after preheating at 30°C (C=25g/L, 5°C).

The strain at fracture, γ_f, was roughly independent of G_0 and protein concentration for pH 9 and decreased weakly with increasing G_0 for pH 11, see figure 21. A decrease of γ_f was reported in several investigations of protein gels in the literature, including β-lactoglobulin at neutral pH [77], gelatin [78], and mixtures of whey proteins [79-81]. It has been suggested [82] that if the force needed to break the any given link in protein blobs is concentration independent (or sufficiently weakly dependent), a decrease in fracture strain with increasing concentration would be observed, see also Appendix A.

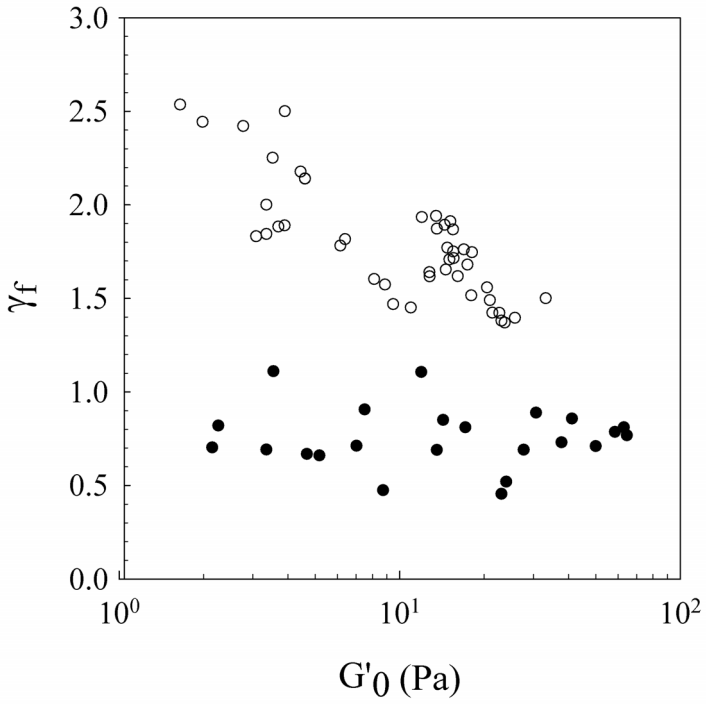

Figure 21. Strain at fracture γ_f for FPI gels at pH 9 (filled symbols) and pH 11 (open symbols) as function of G'_0.

Microscopic structure

Visually, gels at both pH 9 and 11 were seen to exhibit syneresis within about a week or longer. The use of confocal scanning laser microscopy (CSLM) allowed visualizing what could be the first step in this macro-phase separation, i.e. the formation of protein poor areas in the otherwise homogenous matrix.. Those areas were formed after a time that fluctuated strongly between samples, but was typically between 1-5 days. Several typical images obtained using CSLM are shown in figure 22. No structure of the gel could be seen at the highest resolution available (about 300nm). However, large particles of high protein concentration were visible, typically several microns in size, randomly scattered in the system. These areas are present immediately after protein isolation at pH 11 in the liquid state, and are typically 4-6 times denser than the matrix, i.e. about 150g/L which is close to that found for precipitates formed close to the iso-electric point. The presence of these large, dense protein aggregates precludes detailed and meaningful investigation of the gels using light-scattering, see also appendix A.

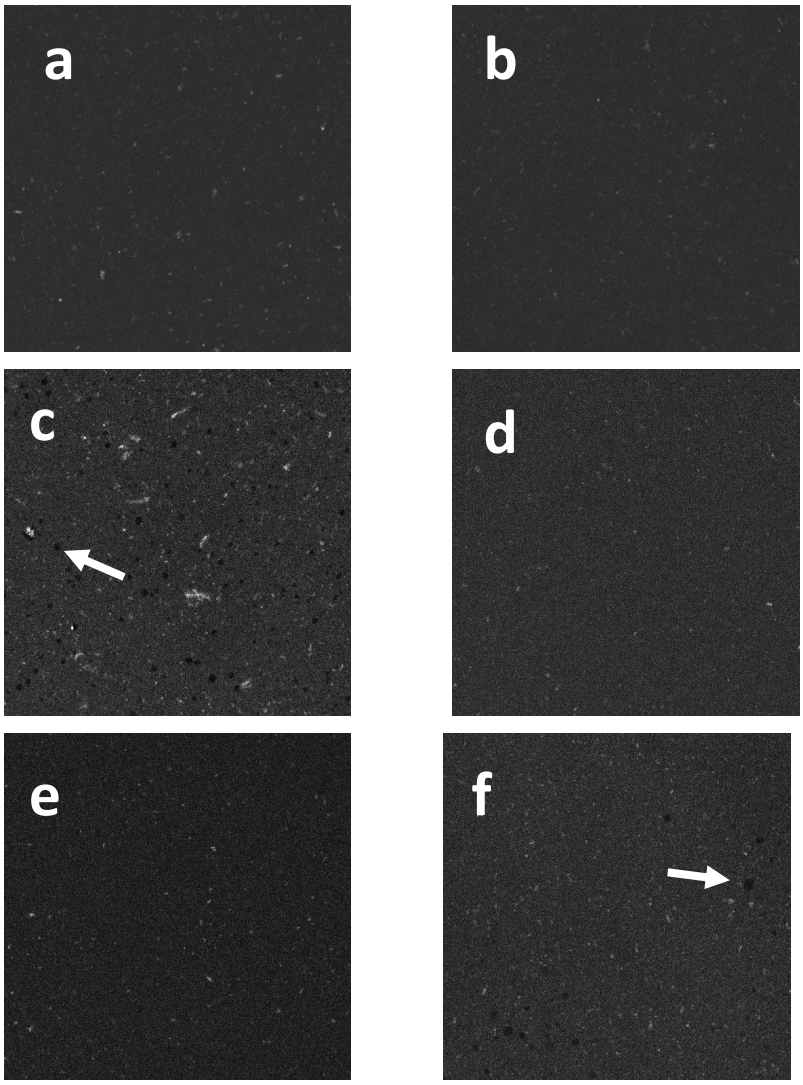

Figure 22. CSLM images of FPI. a: pH 11 at 5°C before preheating, b: pH 11 at 5°C after preheating, c: pH 11 after 4 days at 5°C, d: pH 9 at 50°C, e: pH 9 at 5°C after preheating, f: pH 9 after 1 day at 5°C. The width of the images represents in all cases 160μm. Large protein aggregates are visible as white spots, while the arrows indicate protein poor domains in figures 22c and 22f.

The effect of adding NaCl

The effect of NaCl, the most common salt in use in the food industry, on the gelation of FPI has been investigated as well. The finding was that added salt prevented gelation at the pH range 8.5-9.5, and shifted the pH range at which gelation was seen to lower values. At pH 9.0, for instance, gelation was virtually prevented by addition of 130mM NaCl, see figure 23. This effect will be noted again below in the section on current status of FPI use.

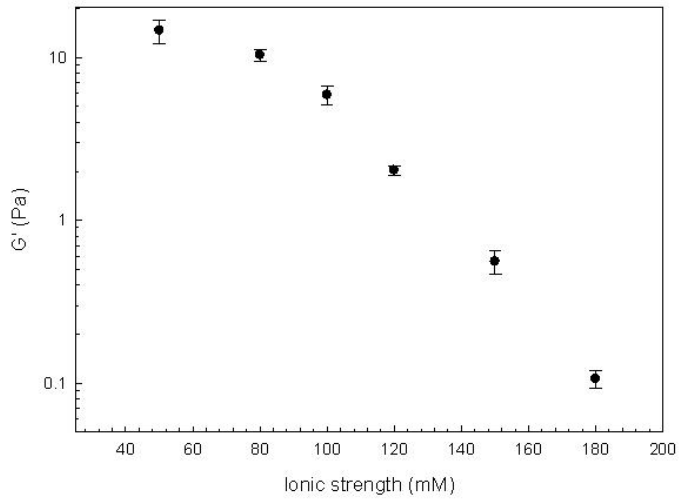

Figure 23. G' at 1Hz and 5°C for FPI at pH 9 as a function of ionic strength. NaCl was added to adjust the ionic strength which is approximated as 50mM plus the concentration of added NaCl.

Current status of FPI use

As noted in the introduction, two processing plants operate in Iceland currently which utilize similar techniques to that described herein to solubilise muscle proteins from cod cut-offs, as well as cut-offs of other fish. The estimate for the amount of cod cut-offs processed in the first processing plant is about 50 tonnes per year. Figure 24 is a drawing of the processing plant, with several of the machines designated with arrows. The cut-offs are first minced in the belt mincer, before NaOH is added and the pH adjusted in a buffer tank. Separation from insoluble material is obtained by means of centrifugation in the decanter. Next, the pH of the homogenate is lowered with a concomitant addition of NaCl, and it is then compressed at 20atm forming an opaque but macroscopically homogeneous liquid (figure 25). It has been verified that pressure treatment at 20atm does not affect the gelation properties of FPI at pH 9 without added salt, see figure 26.

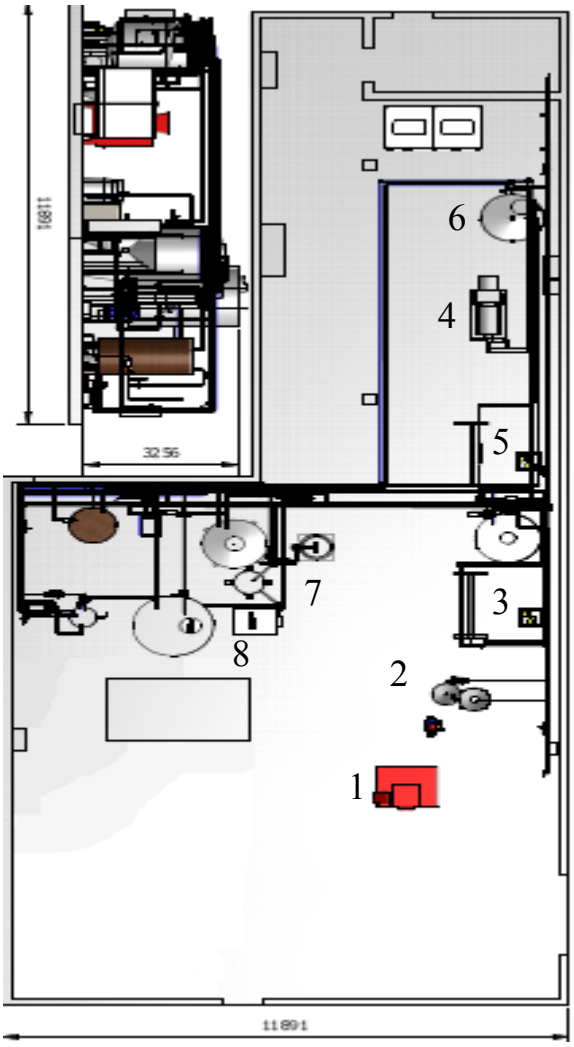

Figure 24. Drawing of the first processing plant opened in Iceland where a similar protein isolation process to that described herein is employed. Numbers in figure refer to the following equipment: 1. Belt mincer, 2. pH adjustment rack I (alkaline), 3. Buffer tank I, 4. Decanter centrifuge, 5. pH adjustment rack II - addition of acid and salt, 6. Buffer tank II, 7. Cooling tank, 8. Homogenizer

Figure 25. Protein isolate from cod as prepared in the processing plant.

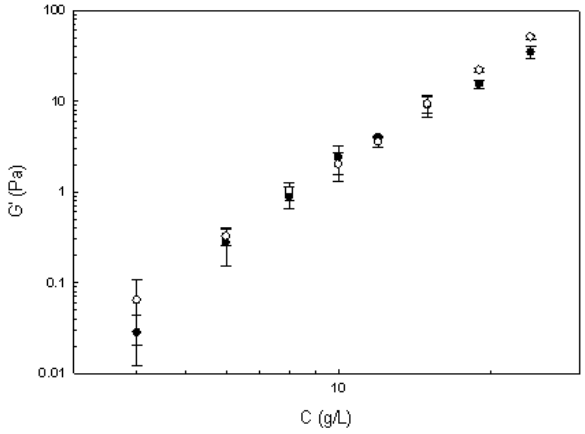

Figure 26. Concentration dependence of G' at 1Hz for FPI at pH 9 and 5°C. Open symbols represent FPI treated at 20atm before cooling to 5°C, and filled symbols represent non-treated FPI.

Though the pH of the isolate is below 9, gel formation is prevented since the ionic strength is nearly 250mM. After injection of the liquid

into cod fillets equilibration of the ionic strength takes place, with the ionic strength of muscle close to 150mM [26, 83, 84]. This leads to gelation and immobilization of the injected isolate in the muscle. So far, such fillets have been frozen within minutes of injection, and later sold frozen. The injected isolate is not visible in the injected fillet, see figure 27.

Figure 27. Injected cod fillets in the first processing plant opened in Iceland. As seen from the cross-section (fillet in the background), no visible marks are left by the injection and the FPI cannot be distinguished from the meat. Unfortunately, no better quality images were made available for the current dissertation.

Acknowledgements

This work has been funded by Matís (Icelandic Food Research) ohf. The author would like the acknowledge receipt of the following grants for the work reported herein: AVS R&D fund of the Ministry of Fisheries in Iceland, The Icelandic Technology Development Fund, Icelandic Research center (Rannís) student fund (though grant was only equal to 1/6 of grants currently awarded) and Jules Verne's Research fund.

This dissertation is dedicated to my advisors, Ragnar Jóhannsson from Matís and Taco Nicolai from Université Du Maine. Not only would the work reported herein not be completed without your help and guidance, but I also suspect the world would be a poorer place without you. As the Japanese would say, Budha is watching your work happily from the shadows of the grass blades.

I'd like to thank my family, especially my parents, for always being there for me when I needed a word of support or encouragement, and for reading critically all my manuscripts.

A big thank you to everyone at Matís for all the help, laughs, cries, beers, and generally for bearing with me for 4 years. An especially big thank you and a hug to Margrét for being her wonderful self. An executive thank you to the big guns: Sjöfn, for the fact I'm still here, Guðjón, for encouragement in a time when results were not

forthcoming, and Hörður, for *always* showing “American grade” politeness!

パトリシャ先生へ

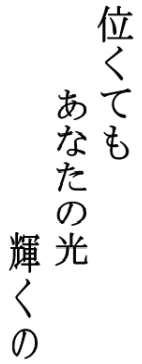

Another big thank you to Hans Kristján Árnason for making sure I stay in Iceland.

Ágúst- corro, ergo sum!

I would also like to thank Christophe Chassenieux, Dominique Durand and Lazhar Benyahia for (very!) useful discussions.

The list of fellow PhD students I’d like to acknowledge is too long, so I’ll just note the different student posses at Le Mans (summer 2006 & winter 2008-2009), Utrecht (summer school in colloid science 2007- mi avete dato il migliore regalo d’compleanno!) and Lund (advanced colloid chemistry 2008). May that we meet again, young friends.

Appendix A. Does the fractal model correctly describe the structure and rheology of FPI gels?

When a gel is assumed to be composed of monodisperse fractal spheres (blobs), geometry arguments give us a straight-forward relation of 2 fractal dimensions characterizing the gel with the concentration dependence of the elastic moduli. Following the arguments in Ref. [85], since we assume a space-filling network of monodisperse fractal spheres, it follows that:

$$c = \frac{3M}{4\pi R^3 N_A} \tag{61}$$

with M the molar mass, R the sphere's radius. It follows that $c \propto R^{df-3}$. For Eq. (61) to apply, all the percolating units (for instance, proteins) must belong to the percolating network, which is a safe assumption if the concentration is at least $2c_g$, with c_g the critical concentration for percolating or gel formation [35]. If elasticity is purely enthalpic (i.e., we may neglect the k_bT contribution of each blob), then each blob acts as an elastic spring with elastic constant $K = K_0 N_b^{-1} R^{-2}$, assuming that each blob consists of N_b links with bending constant K_0. It is further assumed that $N_b \propto R^{db}$, with d_b the fractal dimension of the stress baring backbone which is necessarily equal or smaller than d_f. Since G is inversely proportional to the number of blobs per unit length, it follows that $G \propto R^{-(3+db)}$, and from there:

$$G \propto c^{\frac{3+d_b}{3-d_f}} \tag{62}$$

It should be noted that in Ref. [85], a second limiting behaviour for the dependence of G on c is considered. If the links inside the blob are assumed to be of negligible strength compared to inter-blob links, then the blob may be approximated as a hard sphere, or a mere link in a chain. The elasticity now depends on the number of links (blobs) per chain length , i.e. $G \propto R^{-1}$ and $G \propto c^{1/(3-df)}$. From a physical point of view, however, it makes no sense to distinguish between bonds inside the blob and between blobs, since the same bonding mechanisms are at work. Only Eq. (62) therefore applies (in theory) for protein gels.

One further relation given in Ref. [85] will be discussed here. The elastic spring constant K of the blobs, as already noted, is proportional to $R^{-(2+db)}$. The force on the blob is equal to K times the absolute strain, which is proportional to R. The total force on the blob thus scales as $R^{-(1+db)}$. This force is equal to the force on the weakest links in the blob, which sustain the full force by themselves (singly connected junctions). If those weakest links rupture at a certain critical constant force, it follows that the first rupture occurs at a critical strain γ_0 which scales as R^{1+db} or $c^{-(1+db)/(3-df)}$. If no change in number of bonds is assumed, then the linear regime extends up to this γ_0, and above this strain a monotonous strain-softening should be observed, as the bonds are gradually breaking. If these arguments for the existence of a limiting strain γ_0 which defines the end of the linear regime were to

hold, then obviously no master-curve could be obtained for G'/G'_0 curves as a function of strain at different protein concentrations. It is also obvious that in such a case no strain-hardening would be observed, only strain softening following the linear regime. Though not discussed here, the starting point used as a physical argument in the derivation of the strain hardening model suggested in Ref. [76] is that the average number of bonds between blobs increases upon deformation. It seems, therefore, that the reasoning that the limit of the linear regime should depend on concentration do not hold for fractal gels. It is possible, though not at all straight-forward, that an argument could be made similar to that above, that strain-softening should follow the strain-hardening regime at a strain which would decrease with concentration, i.e. scale as $c^{-(1+db)/(3-df)}$, and therefore perhaps also the fracture strain should scale as $c^{-(1+db)/(3-df)}$. An attempt was made to replace γ_0 with the fracture strain γ_f and it seemed that it decreased less strongly with increasing concentrations of whey protein isolate, leading to the speculation that the force needed to break a sufficient number of bonds in the blob to cause a macroscopic fracture increases with increasing concentration [82].

d_f can be determined, in principle, from light scattering experiments. Figure 28 shows cross-correlation light scattering data of a FPI gel at 5°C and pH 9.Though the multiple-scattering of the sample is non-negligible (turbidity ~2 cm^{-1}), its effect on the data is not large, as can be seen from the figure. The data seem to follow a power-law with a power-law exponent -1.55, so that we may be tempted to interpret the

slope in the double-logarithmic representation in terms of the fractal dimension d_f. Herein lies a trap- according to the CSLM images shown in figure 22, the light scattered is no doubt dominated by the large (several microns) insoluble aggregates. The structure of the gel no doubt contributes to the scattering, since the large aggregates have a fractal dimension close to 2 (see also Ref. [8]), but in no way is it possible to refer to S(q) as determined in this fashion as S(q) of the gel!

The strain dependence of G'/G'_0 for gels at both pH could be fitted according to the strain-hardening model suggested in Ref. [76]. Examples are given in figure 29 for both pH 9 and 11. For pH 9, gels could be obtained for concentrations above 6g/L, and gels with $c \geq 8$g/L showed strain hardening which was similar when G' was normalized with G'_0. The data could be fitted to the strain-hardening model suggested in Ref. [76] with d_b values in the range 1.22-1.32. A smaller range of this fit parameters was found for all samples with c=25g/L, see figure 29b, where d_b was always very close to 1.30. For pH 11 (c=25g/L) the fit value was close to 2.0. It is important to note that the strain-hardening curve is not expected to follow the theoretical curve up to fracture, since microscopic fracture and a downward deviation from the curve precede the macroscopic fracture which is indicated by the very strong decrease of G' with a very small increase of γ.

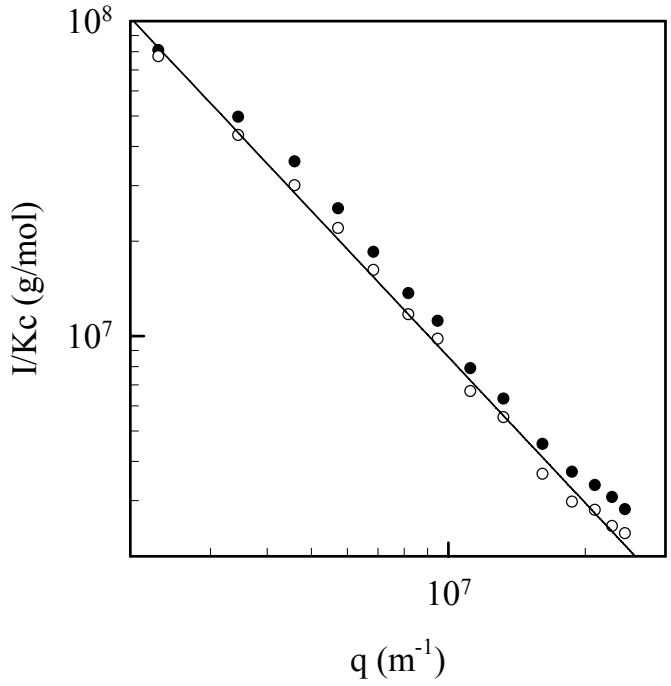

Figure 28. Light scattering data for FPI at pH 9 and 5°C before (filled symbols) and after (open symbols) correcting for the effect of multiple scattering. The solid line represents a fit to a power-law with an exponent -1.55.

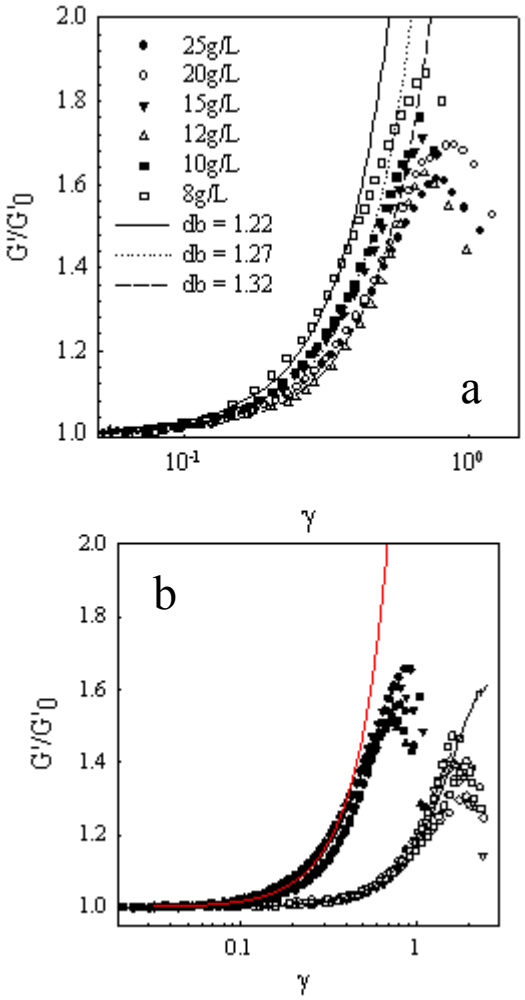

Figure 29. G'/G'_0 as a function of strain for FPI gels at 5°C. Data for different concentrations (indicated in the figure) at pH 9 are shown in figure 29a. Figure 29b shows data for a single concentration, 25g/L, at pH 11 (open symbols) and pH 9 (filled symbols). Fit parameters are indicated in figure 29a, while fits with db = 1.30 (red solid line) and 2.0 (black solid line) are shown in figure 29b.

The concentration dependence of G' could be described with a power-law for c≥10g/L, as seen from figure 30. Assuming that the critical

concentration for gelation is 5g/L, this meets the requirement of $2C_g$. The power-law exponent is 3.0, see figure 30. Lo and behold, Eq. (62) seems therefore to be fulfilled by FPI at pH 9, and the strain-hardening data (figure 29) combined with the light scattering data (figure 28) seem to predict correctly the concentration dependence of G'_0 (figure 30), since (3+1.3)/(3-1.55)=3.0. However, the warning about S(q) in figure 28 not corresponding to the gel structure still stands. The light scattering data is affected by the large insoluble aggregates, and cannot be thought of as a true measure of the gel structure. This is thus, perhaps, a wise word of caution applicable to any research: using knowledge of the systems investigated is more important than over-interpreting data with models which do not necessarily apply to the system investigated. In particular, FPI gels have not been shown to have a fractal local structure, and it is therefore unwise to treat the data of figure 30 in terms of Eq. (62).

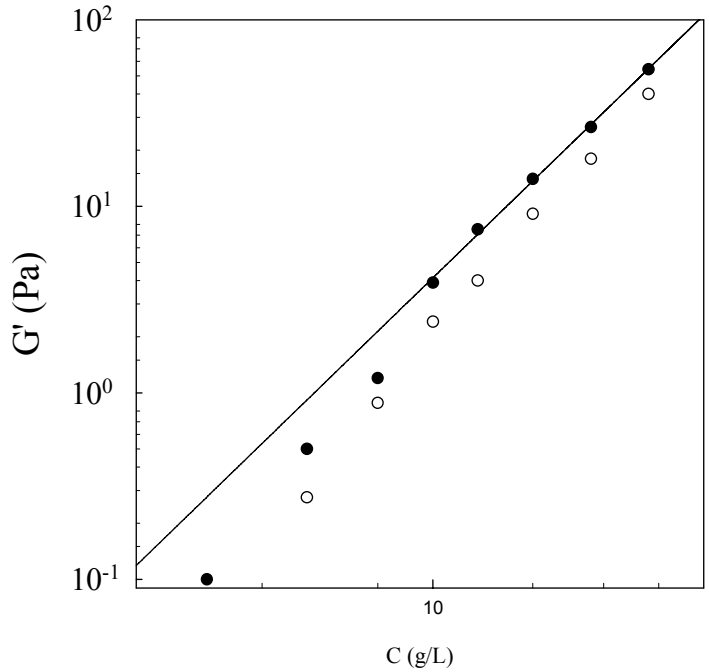

Figure 30. Concentration dependence of G'_0 for FPI gels at pH 9 and 5°C. Open symbols: non preheated FPI, filled symbols: gels obtained after 5 minutes of preheating at 30°C. The solid line represents a power-law fit with exponent 3.0.

References

1. Rustad, R., *Physical and chemical properties of protein seafood by-products* in *Maximising the value of marine by-products*, F. Shahidi, Editor. 2007, Woodhead Publishing: Cambridge. p. 3-21.
2. Kristinsson, H.G., Theodore, A.E., and Ingadottir, B., *Chemical processing methods for protein recovery from marine by-products and underutilized fish species*, in *Maximising the value of marine by-products*, F. Shahidi, Editor. 2007, Woodhead Publishing: Cambridge. p. 144-168.
3. www.statice.is. (cited; Available from: www.statice.is)
4. Clark, A.H., *Gelation of globular proteins*, in *Functional properties of food macromolecules*, S.E. Hill, D.A. Ledward, and J.R. Mitchell, Editors. 1998, Aspen Publishers: Gaithersburg. p. 77-142.
5. Nicolai, T., *Structure of self-assembled globular proteins*, in *Food colloids. Interactions, microstructure and processing*, E. Dickenson and M. Leser, Editors. 2007, The Royal Society of Chemistry: Cambridge. p. 35-56.
6. Brenner, T., Johannsson, R., and Nicolai, T., *Characterization of fish myosin aggregates using static and dynamic light scattering.* Food Hydrocolloids, 2009. **23**(2): p. 296-305.
7. Sasaki, T., Yuan, C.H., and Konno, K., *Role of cooling process in the thermal aggregate formation by carp myosin rod.* Journal of Food Science, 2006. **71**(2): p. C75-C80.
8. Brenner, T., Johannsson, R., and Nicolai, T., *Characterisation and thermo-reversible gelation of cod muscle protein isolates.* Food Chemistry, 2009. **115**(1): p. 26-31.
9. Brenner, T., Nicolai, T., and Johannsson, R., *Rheology of thermo-reversible fish protein isolate gels.* Food Research International, 2009. doi:10.1016/j.foodres.2009.04.020.
10. Knobl, G.M., Stilling.Br, Fox, W.E., and Hale, M.B., *Fish protein concentrates* Commercial Fisheries Review, 1971. **33**(7-8): p. 54-63.
11. Zein, G.N., Elbedawey, A.E.F., Elsherbiney, A.M., and Dawoud, F.M.A., *Studies on fish-protein concentate and fish-meal from river*

Nile bolti fish (Tilapia-Nilotica). Nahrung-Food, 1985. **29**(5): p. 523-532.

12. Kim, S.K. and Mendis, E., *Bioactive compounds from marine processing byproducts - A review.* Food Research International, 2006. **39**(4): p. 383-393.
13. Batista, I., *Recovery of proteins from fish waste products by alkaline extraction.* European Food Research and Technology, 1999. **210**(2): p. 84-89.
14. Hultin, H.O. and Kelleher, S.D., *Process for isolating a protein composition from a muscle source and protein composition*. 2001: US.
15. Kahn, L.N., Berk, Z., Pariser, E.R., Goldblith, S.A., and Flink, J.M., *Squid protein isolate - effect of processing conditions on recovery yields.* Journal of Food Science, 1974. **39**(3): p. 592-595.
16. Montecalvo, J., Constantinides, S.M., and Yang, C.S.T., *Optimization of processing parameters for the preparation of flounder frame protein product.* Journal of Food Science, 1984. **49**(1): p. 172-176.
17. Choi, Y.J. and Park, J.W., *Acid-aided protein recovery from enzyme-rich Pacific whiting.* Journal of Food Science, 2002. **67**(8): p. 2962-2967.
18. Kim, Y.S., Park, J.W., and Choi, Y.J., *New approaches for the effective recovery of fish proteins and their physicochemical characteristics.* Fisheries Science, 2003. **69**(6): p. 1231-1239.
19. Kristinsson, H.G. and Liang, Y., *Effect of pH-shift processing and surimi processing on Atlantic croaker (Micropogonias undulates) muscle proteins.* Journal of Food Science, 2006. **71**(5): p. C304-C312.
20. Kristinsson, H.G., Theodore, A.E., Demir, N., and Ingadottir, B., *A comparative study between acid- and alkali-aided processing and surimi processing for the recovery of proteins from channel catfish muscle.* Journal of Food Science, 2005. **70**(4): p. C298-C306.
21. Thawornchinsombut, S. and Park, J.W., *Effect of NaCl on gelation characteristics of acid- and alkali-treated Pacific whiting fish protein isolates.* Journal of Food Biochemistry, 2007. **31**(4): p. 427-455.
22. Undeland, I., Kelleher, S.D., and Hultin, H.O., *Recovery of functional proteins from herring (Clupea harengus) light muscle by an acid or*

alkaline solubilization process. Journal of Agricultural and Food Chemistry, 2002. **50**(25): p. 7371-7379.

23. Yongsawatdigul, J. and Park, J.W., *Effects of alkali and acid solubilization on gelation characteristics of rockfish muscle proteins.* Journal of Food Science, 2004. **69**(7): p. C499-C505.
24. Carlson, F.D., *The application of quasi-elastic light scattering to the study of muscular contraction*, in *The application of light scattering to the study of biological motion*, J.C. Earnshaw and M.W. Steer, Editors. 1982, ASI Proceedings: Maratea. p. 404-457.
25. Foegeding, E.A., Lanier, T.C., and Hultin, H.O., *Characteristics of edible muscle tissues*, in *Food Chemistry*, O.R. Fennema, Editor. 1996, CRC Press: New York. p. 879-942.
26. Stefansson, G. and Hultin, H.O., *On the solubility of cod muscle proteins in water.* Journal of Agricultural and Food Chemistry, 1994. **42**(12): p. 2656-2664.
27. Harrington, W.F. and Rodgers, M.E., *Myosin.* Annual Review of Biochemistry, 1984. **53**: p. 35-73.
28. Elliott, A. and Offer, G., *Shape and Flexibility of Myosin Molecule.* Journal of Molecular Biology, 1978. **123**(4): p. 505-519.
29. Sharp, A. and Offer, G., *The mechanism of formation of gels from myosin molecules.* Journal of the Science of Food and Agriculture, 1992. **58**(1): p. 63-73.
30. Takahashi, K., *Topography of myosin molecule as visualized by an improved negative staining method.* Journal of Biochemistry, 1978. **83**(3): p. 905-908.
31. Wegener, W.A., *A swivel-jointed formalism for segmentally flexible macromolecules and its application to the rotational behavior of myosin.* Biopolymers, 1982. **21**(6): p. 1049-1080.
32. Yoon, S.H., Kakinuma, M., Hirayama, Y., Yamamoto, T., and Watabe, S., *cDNA cloning of myosin heavy chain from white croaker fast skeletal muscle and characterization of its complete primary structure.* Fisheries Science, 2000. **66**(6): p. 1163-1171.
33. Rottereau, M., Gimel, J.C., Nicolai, T., and Durand, D., *Monte Carlo simulation of particle aggregation and gelation: I. Growth, structure and size distribution of the clusters.* European Physical Journal E, 2004. **15**(2): p. 133-140.

34. Strogatz, S.H., *Nonlinear dynamics and chaos*. 1994, Reading: Perseus Books.

35. Stauffer, D. and Aharony, A., *Introduction to percolation theory*. 2nd edition ed. 1992, London: Taylor & Francis.

36. Gimel, J.C., Nicolai, T., and Durand, D., *Relation between aggregation and phase separation: Three-dimensional Monte Carlo simulations.* Physical Review E, 2002. **66**(6).

37. Lanier, T.C., *Surimi: gelation chemistry*, in *Surimi and surimi seafood*, J.W. Park, Editor. 2000, Marcel Dekker: New York. p. 237-265.

38. Fazli, H. and Golestanian, R., *Aggregation kinetics of stiff polyelectrolytes in the presence of multivalent salt.* Physical Review E, 2007. **76**(4).

39. Margossian, S.S. and Slayter, H.S., *Electron-microscopy of cardiac myosin - its shape and properties as determined by the regulatory light chain.* Journal of Muscle Research and Cell Motility, 1987. **8**(5): p. 437-447.

40. Tazawa, T., Kato, S., Katoh, T., and Konno, K., *Role of neck region in the thermal aggregation of myosin.* Journal of Agricultural and Food Chemistry, 2002. **50**(1): p. 196-202.

41. Walker, M. and Trinick, J., *Electron-microscope study of the effect of temperature on the length of the tail of the myosin molecule.* Journal of Molecular Biology, 1986. **192**(3): p. 661-667.

42. Yamamoto, K., *Electron-microscopy of thermal aggregation of myosin.* Journal of Biochemistry, 1990. **108**(6): p. 896-898.

43. Higuchi, T., Ojima, T., and Nishita, K., *Heat-induced structural changes and aggregation of walleye pollack myosin in the light meromyosin region.* Fisheries Science, 2002. **68**(5): p. 1145-1150.

44. Ishioroshi, M., Samejima, K., and Yasui, T., *Further-studies on the roles of the head and tail regions of the myosin molecule in heat-induced gelation.* Journal of Food Science, 1981. **47**(1): p. 114-120.

45. Samejima, K., Ishioroshi, M., and Yasui, T., *Relative roles of the head and tail portions of the molecule in heat-induced gelation of myosin.* Journal of Food Science, 1981. **46**(5): p. 1412-1418.

46. Chan, J.K., Gill, T.A., and Paulson, A.T., *The dynamics of thermal-denaturation of fish myosins.* Food Research International, 1992. **25**(2): p. 117-123.

47. Ishioroshi, M., Samejima, K., and Yasui, T., *Heat-induced gelation of myosin - factors of pH and salt concentrations.* Journal of Food Science, 1979. **44**(5): p. 1280-1284.

48. Morita, J.I. and Yasui, T., *Involvement of hydrophobic residues in heat-induced gelation of myosin tail subfragments from rabbit skeletal-muscle.* Agricultural and Biological Chemistry, 1991. **55**(2): p. 597-599.

49. Rodgers, M.E., Karr, T., Biedermann, K., Ueno, H., and Harrington, W.F., *Thermal-stability of myosin rod from various species.* Biochemistry, 1987. **26**(26): p. 8703-8708.

50. Hermansson, A.M., Harbitz, O., and Langton, M., *Formation of 2 types of gels from bovine myosin.* Journal of the Science of Food and Agriculture, 1986. **37**(1): p. 69-84.

51. Hermansson, A.M. and Langton, M., *Filamentous structures of bovine myosin in diluted suspension and gels.* Journal of the Science of Food and Agriculture, 1988. **42**(4): p. 355-369.

52. Kouchi, S., Kondo, S., Ooi, K., Ichikawa, H., and Dobashi, T., *Viscoelastic and light scattering studies on thermally induced sol to gel phase transition in fish myosin solutions.* Biopolymers, 2003. **69**(4): p. 498-507.

53. Liu, M.N. and Foegeding, E.A., *Thermally induced gelation of chicken myosin isoforms.* Journal of Agricultural and Food Chemistry, 1996. **44**(6): p. 1441-1446.

54. Raghavan, S. and Kristinsson, H.G., *Conformational and rheological changes in catfish myosin during alkali-induced unfolding and refolding.* Food Chemistry, 2008. **107**(1): p. 385-398.

55. Imhof, A., *Scattering techniques in soft condensed matter*, in *Soft Condensed Matter & Advanced Colloid Science*. 2007: Universiteit Utrecht.

56. Kralchevsky, P.A., Danov, K.D., and Denkov, N.D., *Chemical physics of colloid systems and interfaces*, in *Handbook of Surface and Colloid Chemistry*, B. K.S., Editor. 1997, CRC Press: New York. p. 333-494.

57. Nicolai, T., *Static and Dynamic Light Scattering of Macromolecules in Solution: Theory and Practice*, University publications Universite Du Maine.

58. Stepanek, P., *chapter 4*, in *Dynamic light scattering*, W. Brown, Editor. 1993, Oxford University Press: Oxford.

59. Provencher, S.W., *Contin - a general-purpose constrained regularization program for inverting noisy linear algebraic and integral-equations.* Computer Physics Communications, 1982. **27**(3): p. 229-242.

60. Berne, B. and Pecora, R., *Dynamic light scattering*. 1976, New York: Wiley.

61. Macosko, C.W., *Rheology. Principles, measurements, and applications*. 1994, New York: VCH.

62. Hunter, R.J., *Foundations of Colloid Science*. 2001, Oxford: Oxford University Press.

63. Connell, J.J., *Studies on the properties of fish skeletal muscle .7. Denaturation and aggregation of cod myosin.* Biochemical Journal, 1960. **75**: p. 530-538.

64. Connell, J.J., *The relative stabilities of the skeletal-muscle myosins of some animals.* Biochemical Journal, 1961. **80**: p. 503-509.

65. Davies, J.R., Bardsley, R.G., Ledward, D.A., and Poulter, R.G., *Myosin thermal-stability in fish muscle.* Journal of the Science of Food and Agriculture, 1988. **45**(1): p. 61-68.

66. Davies, J.R., Ledward, D.A., Bardsley, R.G., and Poulter, R.G., *Species dependence of fish myosin stability to heat and frozen storage.* International Journal of Food Science and Technology, 1994. **29**(3): p. 287-301.

67. Gill, T.A., Chan, J.K., Phonchareon, K.F., and Paulson, A.T., *Effect of salt concentration and temperature on heat-induced aggregation and gelation of fish myosin.* Food Research International, 1992. **25**(5): p. 333-341.

68. Johnston, I.A., Walesby, N.J., Davison, W., and Goldspink, G., *Temperature adaptation in myosin of antarctic fish.* Nature, 1975. **254**(5495): p. 74-75.

69. Ogawa, M., Ehara, T., Tamiya, T., and Tsuchiya, T., *Thermal-stability of fish myosin.* Comparative Biochemistry and Physiology B-Biochemistry & Molecular Biology, 1993. **106**(3): p. 517-521.

70. Herbert, T.J. and Carlson, F.D., *Spectroscopic Study of Self-Association of Myosin.* Biopolymers, 1971. **10**(11): p. 2231-2252.

71. Garciadelatorre, J. and Bloomfield, V.A., *Conformation of myosin in dilute-solution as estimated from hydrodynamic properties* Biochemistry, 1980. **19**(22): p. 5118-5123.

72. Daoud, M. and Cotton, J.P., *Star shaped polymers - a model for the conformation and its concentration-dependence.* Journal De Physique, 1982. **43**(3): p. 531-538.

73. Liu, M.N., Foegeding, E.A., Wang, S.F., Smith, D.M., and Davidian, M., *Denaturation and aggregation of chicken myosin isoforms.* Journal of Agricultural and Food Chemistry, 1996. **44**(6): p. 1435-1440.

74. Hu, D.H., Kimura, S., and Maruyama, K., *Sodium dodecyl-sulfate gel-electrophoresis studies of connectin-like high-molecular-weight proteins of various types of vertebrate and invertebrate muscles.* Journal of Biochemistry, 1986. **99**(5): p. 1485-1492.

75. Chawla, S.P., Venugopal, V., and Nair, P.M., *Gelation of proteins from washed muscle of threadfin bream (Nemipterus japonicus) under mild acidic conditions.* Journal of Food Science, 1996. **61**(2): p. 362-366.

76. Gisler, T., Ball, R., and Weitz, D.A., *Strain hardening of fractal colloidal gels.* Physical Review Letters, 1999. **82**(5): p. 1064-1067.

77. Pouzot, M., Nicolai, T., Benyahia, L., and Durand, D., *Strain hardening and fracture of heat-set fractal globular protein gels.* Journal of Colloid and Interface Science, 2006. **293**(2): p. 376-383.

78. Bot, A., vanAmerongen, I.A., Groot, R.D., Hoekstra, N.L., and Agterof, W.G.M., *Effect of deformation rate on the stress-strain curves of gelatin gels.* Journal De Chimie Physique Et De Physico-Chimie Biologique, 1996. **93**(5): p. 837-849.

79. Foegeding, E.A., *Rheological properties of whey protein isolate gels determined by torsional fracture and stress-relaxation.* Journal of Texture Studies, 1992. **23**(3): p. 337-348.

80. Li, H., Errington, A.D., and Foegeding, E.A., *Isostrength comparison of large-strain (fracture) rheological properties of egg white and whey protein gels.* Journal of Food Science, 1999. **64**(5): p. 893-898.

81. Lowe, L.L., Foegeding, E.A., and Daubert, C.R., *Rheological properties of fine-stranded whey protein isolate gels.* Food Hydrocolloids, 2003. **17**(4): p. 515-522.

82. Ikeda, S., Foegeding, E.A., and Hagiwara, T., *Rheological study on the fractal nature of the protein gel structure.* Langmuir, 1999. **15**(25): p. 8584-8589.

83. Kilimann, M. and Heilmeyer, L.M.G., *Effect of Mg-2+ on Ca-2+-binding properties of non-activated phosphorylase kinase.* European Journal of Biochemistry, 1977. **73**(1): p. 191-197.

84. Wu, Y.J., Atallah, M.T., and Hultin, H.O., *The proteins of washed, minced fish muscle have significant solubility in water.* Journal of Food Biochemistry, 1991. **15**(3): p. 209-218.

85. Shih, W.H., Shih, W.Y., Kim, S.I., Liu, J., and Aksay, I.A., *Scaling behavior of the elastic properties of colloidal gels.* Physical Review A, 1990. **42**(8): p. 4772-4779.

PAPERS

Paper 1. Brenner Tom, Johannsson Ragnar and Nicolai Taco. *Characterization of fish myosin aggregates using static and dynamic light scattering.* Food Hydrocolloids, 2009. **23**(2): p. 296-305.

Available online at www.sciencedirect.com
ScienceDirect
Food Hydrocolloids 23 (2009) 296–305
FOOD HYDROCOLLOIDS
www.elsevier.com/locate/foodhyd

Characterization of fish myosin aggregates using static and dynamic light scattering

T. Brenner[a], R. Johannsson[a], T. Nicolai[b,*]

[a] *Matis, Biotechnology Division, Gylfaflot 5, 112 Reykjavik, Iceland*
[b] *Polymeres, Colloids, Interfaces, UMR CNRS, Université du Maine, 72085 Le Mans Cedex 9, France*

Received 17 September 2007; accepted 14 January 2008

Abstract

Myosin was extracted from Atlantic Cod (*Gadus morhua*) using different methods resulting in small aggregates of pure myosin. These aggregates consisted of between 8 and 20 myosin molecules and were relatively stable at low temperatures ($T < 20$ °C) in dilute ($C < 5$ g/L) solutions containing 0.5 M KCl in the pH range 6.0–8.0. At higher concentrations precipitation or gelation was observed. Heat-induced aggregation at low concentrations was studied using turbidimetry and light scattering. In most cases the aggregation stagnated at longer heating times, but in some cases the aggregation continued until it led to precipitation of large flocs. Cooling led to further growth of the aggregates, which was, however, reversed upon heating.

The structure of the aggregates was determined after cooling and dilution using static and dynamic light scattering. Self-similar aggregates were observed, characterized by a fractal dimension of 2.2. The size of the aggregates formed after extensive heating increased with increasing temperature (30–70 °C), decreasing pH (8.0–6.0) and increasing protein concentration (0.4–3 g/L), but the structure of large aggregates was independent of the conditions.

Keywords: Cod myosin; Aggregation; Light scattering; Mysosin; Gel

1. Introduction

The cardinal role played by myosin in muscle protein gel formation and in binding of meat is well documented by Fukazawa, Hashimoto, and Yasui (1961) and MacFarlane, Schmidt, and Turner (1977). Muscle myosin (Myosin II), the main component of the myofibrillar proteins, is comprised of two heavy chains of about 220 kDa, and 4 light chains of about 20 kDa each (Harrington & Rodgers, 1984). Myosin's heavy chain is composed of a long α-helix tail and a globular head. The two heavy chains are woven together, to form a tail and two pear-shaped heads (Elliott & Offer, 1978; Takahashi, 1978; Sharp & Offer, 1992). The tail is 155 nm long, with a diameter of 2 nm, while the heads have a long axis of about 20 nm and a short axis at the widest point of about 6 nm.

Pure myosin can be solubilized in salt water, but aggregates when heated, which may lead to gelation when the concentration is sufficiently high. Most research on myosin aggregation and subsequent gelation has been performed on mammalian myosin (Hermansson, Harbitz, & Langton, 1986; Ishioroshi, Samejima, & Yasui, 1979, 1981; Morita & Yasui, 1991; Samejima, Ishioroshi, & Yasui, 1981; Sharp & Offer, 1992; Tsai, Cassens, & Briskey, 1972). Less work has been done on aggregation of fish myosin (Fukushima et al., 2005; Gill, Chan, Phonchareon, & Paulson, 1992; Kouchi, Kondo, Ooi, Ichikawa, & Dobashi, 2003; Tazawa, Kato, Katoh, & Konno, 2002), which is less stable than mammalian myosin (Connell, 1960, 1961; Davies, Bardsley, Ledward, & Poulter, 1988; Gill et al., 1992; Johnston, Walesby, Davison, & Goldspink, 1975). Variance in myosin stability is also found between different fish species, with an apparent correlation between the thermal stability of myosin and the species habitat (Davies, Ledward, Bardsley,

*Corresponding author.
E-mail address: taco.nicolai@univ-lemans.fr (T. Nicolai).

0268-005X/$ - see front matter © 2008 Elsevier Ltd. All rights reserved.
doi:10.1016/j.foodhyd.2008.01.003

& Poulter, 1994; Johnston et al., 1975; Ogawa, Ehara, Tamiya, & Tsuchiya, 1993).

The aggregation process of myosin molecules is thought to consist of two steps (Ishioroshi et al., 1981; Morita & Yasui, 1991; Samejima et al., 1981; Sharp and Offer, 1992). In the first step, oligomers are formed by association of the heads, possibly through disulphide bridge formation. Tazawa et al. (2002) found for fish myosin that oligomerization can also occur by association of the so-called neck regions between the heads and the tails. Electron microscopy images of the oligomers showed star-like clusters with the heads assembled in the centre and the tails radiating out (Margossian & Slayter, 1987; Sharp & Offer, 1992; Tazawa et al., 2002; Walker & Trinick, 1986; Yamamoto, 1990). During the second step of the process the oligomers aggregate to form larger clusters, possibly involving association of the tails. Very little is known about the structure of these larger aggregates. Eventually, the growth of the clusters may lead to the formation of a system-spanning network. Cooling of the system was reported to have an influence both on the clusters and the gel formed by whole myosin (Kouchi et al., 2003) or the rod fraction of myosin (Sasaki, Yuan, & Konno, 2006).

The objective of the work presented here was to investigate the aggregation of myosin using static and dynamic light scattering. These techniques have so far rarely been used to study myosin aggregation, but were found to be useful for the characterization of heat-induced aggregation of other important food proteins such as ovalbumin and β-lactoglobulin (β-lg) (Nicolai, 2007). The advantage of scattering techniques compared with electron microscopy is that they require no sample treatment and that they can be used in situ during the aggregation process. The structure of large aggregates can be determined by measuring the so-called structure factor, which gives information about the organization of associated myosin on larger length scales. One of the main conclusions of the present study is that the large-scale structure is self-similar and close to that of aggregates formed by other proteins. This shows a certain degree of universality of the aggregation process on large length scales for proteins with very different structures and binding mechanisms.

The myosin used for this study was isolated from cod. Cod myosin is highly unstable and spontaneously aggregates in solution even at low temperatures. We will show that myosin solutions obtained using the isolation method recommended by Kristinsson (2001), which consisted of a slightly modified version of a method reported initially by Martone, Busconi, Folco, Trucco, and Sanchez (1986), contained oligomers of myosin and in addition larger aggregates. A simplified isolation method was also used that led to smaller oligomers and fewer large aggregates at the expense of a slightly lower purity. Further heat-induced aggregation of the oligomers was studied at different protein concentrations (0.4 3 g/L), heating temperatures (30 70 °C) and pH (6.0 8.0). The ionic strength was kept constant at 0.5 M KCl. The structure of the aggregates was determined after cooling and dilution.

2. Materials and methods

2.1. Sample preparation

White muscle (free of connective tissue) of cod fillets was treated to obtain myosin, following the method proposed by Martone et al. (1986) as modified by Kristinsson (2001) (method 1), as well as a shorter method described below (method 2). The fish was kept on ice post mortem (between 1 and 4 days) before use and was thus in the state of rigor mortis or immediate post rigor mortis.

Method 1: Chopped muscle was homogenized in solvent A (0.1 M KCl, 1 mM phenylmethylsulfponylfluoride, 0.02% NaN_3 and 0.02 M Tris HCl buffer, pH 7.5) and kept for 60 min on ice, before centrifugation at 1000*g* for 10 min. The pellet was dispersed in solvent B (0.45 M KCl, 5 mM β-mercaptoethanol (MCE), 1 mM ethylene glycol-bis (β-aminoethyl ether) *N*,*N*,*N*′,*N*′-tetraacetic acid, 0.2 M Mg^{2+} and 0.02 M Tris maleate buffer, pH 6.8), before adding either ATP or $K_2P_4O_7$ to a final concentration of 10 mM. The dispersion was kept in solvent B for 90 min during which myosin is extracted into the solution, while actin remains insoluble. After centrifugation the supernatant containing the myosin (supernatant 2) was diluted by a factor 25 in 1 mM $NaHCO_3$, which led to precipitation of the myosin. The myosin was recovered by centrifugation at 10,000*g* for 10 min and the pellet was dispersed in solution C (0.5 M KCl, 5 mM MCE and 0.02 M Tris HCl buffer, pH 7.5) using a Potter-Elvehjem tissue grinder. Myosin was precipitated again by dilution (3 ×) in 1 mM $NaHCO_3$ with 10 mM Mg^{2+} and the myosin was recovered by centrifugation after keeping the solution over night in the cold. Myosin solutions were prepared by dissolving the pellet in 0.5 M KCl.

The purity of the myosin as determined by SDS-PAGE was very high. The only impurity was a very small quantity (<3%) of actin. No difference in the myosin purity was observed when using $K_2P_4O_7$ instead of ATP, as well as when leaving MCE out of all the extraction steps. ATP has the disadvantage of absorbing light at a wavelength of 280 nm, which perturbs the determination of the protein concentration using absorbance.

Unfortunately, solutions of myosin prepared using method 1 were difficult to filter through 0.45 μm pore size filters, and obviously contained very large aggregates. Attempts to prepare solutions with higher concentrations (>5 g/L) showed the presence of large insoluble flocs. It was suspected that large aggregates were formed during the myosin precipitation step. Therefore, we modified the extraction procedure as follows in order to avoid precipitation of the myosin (method 2).

Method 2: Method 1 was followed to obtain supernatant 2. One washing step of pellet 1 with 0.05 M KCl was added

(prior to the dispersion in solvent B). MCE was not added, and $K_2P_4O_7$ was used instead of ATP. Instead of precipitating the myosin, supernatant 2 was extensively dialyzed against 0.5 M KCl buffered at the pH of choice (6.5 8) at 4 °C. NaN_3 was added (0.02%) to avoid protein degradation. Care was taken to perform all extraction steps at a temperature not exceeding 5 °C. Solutions at pH 6.0 aggregated relatively rapidly even at 4 °C. Therefore solutions at pH 6.0 were made by adjusting the pH of solutions dialysed against pH 7.

The purity of the myosin obtained by method 2 was close to that obtained by method 1 with only a small additional contamination of tropomyosin (<2%). Solutions of myosin obtained by method 2 contained fewer large aggregates, which shows that precipitation leads to irreversible aggregation of a fraction of the myosin.

The concentration of myosin in supernatant 2 was rather low (3 6 g/L). Therefore an attempt was made to concentrate myosin using reverse osmosis. Dialysis bags with myosin solutions were placed in concentrated (100 g/L) solutions of polyethylene oxide with weight average molar mass (M_w) equal to 10^4 g/mol. The approximate concentration of myosin was monitored by weighing the dialysis bag before and during dialysis. The concentration increased substantially after overnight dialysis. However, the more concentrated myosin aggregated and gelled in the dialysis bags.

For light-scattering experiments the myosin solutions were filtered through 0.45 μm pore size filters in order to remove large aggregates and spurious scatterers. The myosin concentration was determined using UV absorbance after filtration, as described below. Only relatively low concentrations (<5 g/L) of myosin prepared by method 1 could be filtered. We observed that unfiltered solutions at concentration between 7 and 10 g/L (pH 7) gelled over the course of 2 8 weeks at 4 °C exhibiting extensive syneresis especially at the lowest concentrations. Similar observations were reported by Connell (1960).

2.2. Determination of the myosin concentration using UV absorption

The extinction coefficient (ε) of cod myosin at 278 nm was determined as follows. The absorbance of myosin solutions was measured using a spectrophotometer (Varian). Most of the myosin was subsequently precipitated by dilution with distilled water. The small residual amount of myosin that did not precipitate was estimated by measuring the absorbance of the supernatant. The precipitated myosin was then dried in vacuum at 80 °C for 4 days to remove remaining water, and subsequently weighed. The value of the extinction coefficient determined in this way was 0.75 L/g/cm. This value may be compared with the values reported by Woods, Himmelfarb, and Harrington (1963) , who found the value of rabbit and lobster myosin in 0.5 M HCl to be 0.54 and 0.78 L/g/cm, respectively.

2.3. SDS-PAGE

The electrophoretic pattern of solutions was determined using pre-cast polyacrylamide 4 15% gel slabs (Bio-Rad Laboratories Inc., Herts, UK) run on an electrophoresis unit (Bio-Rad, miniprotean II Cell) with a constant current of 60 mA per gel. The gels were scanned with a GelDoc 2000 scanner (Bio-Rad Laboratories Inc., Herts, UK) and analysed using the software package GelCompar II, 2.01 (Applied Maths BVBA, Kortrijk, Belgium). Broad-range protein standards were obtained from Bio-Rad Laboratories (Bio-Rad Laboratories Inc., Herts, UK).

2.4. Turbidity

Myosin solutions were placed in quartz cells (inner diameter = 10 mm), and the lid was sealed with parafilm to avoid evaporation. The cells were placed in a holding chamber, equipped with water jackets, and the temperature was controlled to within 0.2 °C using a water bath. The turbidity at different wavelengths was measured using a spectrophotometer Varian Cary-50 Bio (Les Ullis, France).

2.5. Light scattering

Static and dynamic light-scattering measurements were made using an ALV-5000 multiple tau digital correlator (ALV-Langen, Germany) and a JDS Uniphase He Ne laser (vertically polarized beam, wavelength 632.8 nm), model 1145P-3083. This laser was provided with the ALV goniometer system (ALV/CGS-8). The range of scattering wave vectors (q) covered in the experiment was $2.8 \times 10^{-3} - 2.6 \times 10^{-2}$ nm^{-1}. The scattering vector q is given as $q = (4\pi n_s/\lambda)\sin(\theta/2)$, where n_s is the refractive index of the sample and θ is the scattering angle. The temperature of solutions in light-scattering experiments was controlled to within 0.2 °C using a thermostat water bath.

2.6. Analysis of light-scattering data

The relative excess scattering of particles is related to their weight average molar mass, M_w, and their structure factor, $S(q)$ (Brown, 1996; Higgins & Benoit, 1994)

$$I_r = KCM_wS(q), \quad (1)$$

where C is the particle mass concentration. K is an optical constant

$$K = \frac{4\pi^2 n_s^2}{\lambda^4 N_a}\left(\frac{\partial n}{\partial C}\right)^2\left(\frac{n_{tol}}{n_s}\right)^2\frac{1}{R_{tol}},$$

where N_a is Avogadro's number, $(\partial n/\partial C)$ is the refractive index increment, and R_{tol} is the Rayleigh ratio of toluene at 20 °C ($(\partial n/\partial C) = 0.19$ (Gellart & Englander, 1962; Herbert & Carlson, 1971) and $R_{tol} = 1.4 \times 10^{-5}$ cm^{-1} at $\lambda = 633$ nm (Moreels, De Ceuninck, & Finsy, 1987). $(n_{tol}/n_s)^2$ corrects for the difference in scattering volume

of the solution and the toluene standard with refractive index n_{tol}.

At infinite dilution $S(q)$ depends on the particle size and shape and can be related to the z-average radius of gyration (R_{gz})

$$S(q) = (1 + (qR_{gz})^2/3)^{-1}, \quad qR_{gz} < 1, \quad C \to 0. \tag{2}$$

If one applies Eqs. (1) and (2) to results obtained at finite concentrations one obtains an apparent molar mass (M_a) that is inversely proportional to the osmotic compressibility and an apparent radius of gyration (R_{ga}) that is proportional to the correlation length of concentration fluctuations. At low concentrations the effect of interaction between the solute particles can be described in terms of the second virial coefficient (A_2):

$$S(q) = (1 + 2A_2M_wC)^{-1}, \quad 2A_2M_wC < 1, \quad q \to 0. \tag{3}$$

M_w, R_{gz} and A_2 are obtained by extrapolation of measurements at different values of q and C. A convenient representation of the data and the extrapolations is the so-called Zimm plot in which KC/I_r is plotted as a function of data against $q^2 + bC$, with b an arbitrary constant.

With the technique of dynamic light scattering (DLS) the autocorrelation function of the scattered light intensity fluctuations is determined (Berne & Pecora, 1976; Brown, 1996). The normalized autocorrelation function ($g_2(t)$) can be analysed in terms of a distribution of exponential decays:

$$g_2(t) - 1 = \left[\int A(\tau) \exp\left(-\frac{t}{\tau}\right) d\tau\right]^2, \tag{4}$$

where $A(\tau)$ is the amplitude of the exponential with relaxation time τ. In dilute solutions and for $qR_{gz} < 1$, the relaxation of intensity fluctuations is caused by centre of mass diffusion of the particles and τ depends on the diffusion coefficient of the particles (D)

$$\tau = (q^2D)^{-1}, \quad qR_{gz} < 1, \quad C \to 0. \tag{5}$$

D is related to the hydrodynamic radius, R_h, through the Stokes Einstein relation

$$D = kT/(6\pi\eta R_h) \tag{6}$$

with T the absolute temperature, k Boltzmann's constant and η the viscosity. For polydisperse solutions a distribution of relaxation times will be observed that corresponds to the distribution of hydrodynamic radii. Eqs. (5) and (6) are only valid if $qR_g < 1$, otherwise rotation and internal dynamics may play a role in the relaxation process. For fully flexible particles $D \propto q$ if $qR_g \gg 1$. Autocorrelation functions were analysed in terms of Eq. (4) using the REPES (Stepanek, 1993) and CONTIN (Provencher, 1982) routines, which gave similar results. In all cases a monomodal relaxation time distribution was found, see Fig. 1 for an example. The average relaxation rate ($\langle\Gamma\rangle = \langle\tau^{-1}\rangle$) was used to calculate the diffusion coefficient: $\langle D\rangle = \langle\Gamma\rangle/q^2$. The z-average hydrodynamic radius (R_{hz}) was obtained from the average diffusion coefficient using Eq. (6). At finite concentration an apparent hydrodynamic radius (R_{ha}) was obtained in this way.

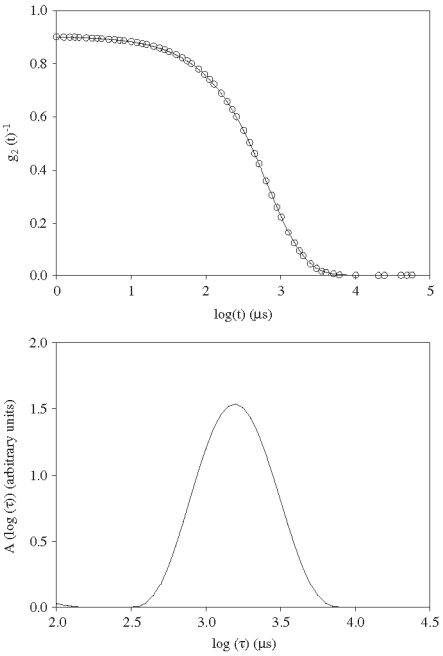

Fig. 1. Intensity autocorrelation function (top) and the corresponding relaxation time distribution (bottom) obtained for a myosin solutions at pH 8, $C = 0.8$ g/L, $q = 1.7 \times 10^7\,m^{-1}$. The solid line through the measured correlation function represents a fit to Eq. (4) resulting in the relaxation time distribution shown in the bottom figure.

3. Results and discussion

3.1. Characterization of unheated myosin solutions

Solutions of isolated myosin were characterized at 20 °C using static and dynamic light scattering. Fig. 2 shows an example of a Zimm plot for myosin obtained by method 2 at pH 8. Within the experimental error the data show a linear dependence on the concentration and on the scattering wave vector except at the largest q-values. Data extrapolated to $q \to 0$ and $C \to 0$ have been analysed using Eqs. (2) and (3). The following values for the weight average molar mass, the z-average radius of gyration and the second virial coefficient were obtained: $M_w = 6.3 \times 10^6$ g/mol, $R_{gz} = 80$ nm and $A_2 = 1.4 \times 10^{-8}$ mol L/g^2. It appears that the isolation procedure used here did not yield solutions of individual myosin. Comparison with the

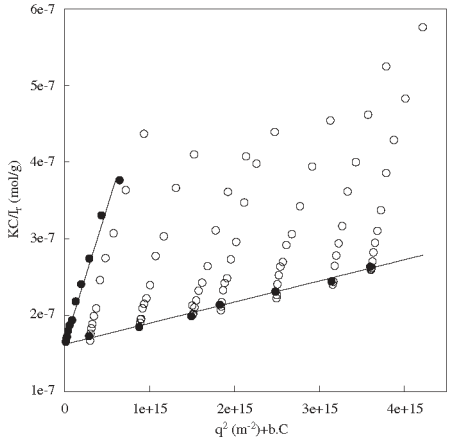

Fig. 2. Zimm plot obtained for myosin isolated using method 2 in aqueous solutions at pH 7. The filled points represent extrapolations to $q = 0$ and $C = 0$ of the data at constant C and q, respectively. The solid lines are linear least-squares fits to the extrapolated data.

values for individual myosin given by Herbert and Carlson (1971) ($M_w = 5 \times 10^5$ g/mol and $R_g = 45$ nm) shows that oligomers containing on average about 12 myosin molecules were formed during the isolation procedure in this case.

Myosin solutions obtained using different methods as described above were characterized in the same way. Oligomers with a weight average aggregation number between 8 and 20 myosin molecules were obtained in all cases. The result depended on the method used, but variations in the molar mass were found even if the same method was used. The largest oligomers were obtained with method 1. With method 2 larger oligomers were obtained if the dialysis was longer or done at higher temperatures. In the pH range between 6 and 8, generally, smaller oligomers were obtained at higher pH that grew more slowly during storage. At pH 8 the oligomers were very stable at 4 °C showing a typical increase of M_w between 20% and 30% over a period of a month. The observed effect of the pH on the stability is in agreement with the results reported by Connell (1960) who reported that cod myosin was most stable at pH 7.5 8.

In all cases a small positive second virial coefficient was observed in the range 1.4 2.5×10^{-8} mol L/g^2. The hydrodynamic radius of the oligomers was around 100 nm, while the radius of gyration was in the range 70 90 nm. These values depended weakly on the preparation method. We note that Kouchi et al. (2003) observed a hydrodynamic radius of 95 nm for myosin isolated from white croaker, which implies that their isolation method also produced oligomers. We used for the experiments described in the following, only myosin prepared by method 2.

3.2. Thermally induced aggregation of myosin

Fig. 3 shows the turbidity of myosin solutions with $C = 5$ g/L during heating at 50 °C for different values of the pH. The turbidity increased sharply during the first few minutes followed by a much weaker increase. Similar observations were reported by Gill et al. (1992) for cod and herring myosin at pH 6.5, but they plotted the data on a linear time scale so that the weak long time increase is not seen as clearly from their results. The authors studied the effect of the salt concentration (0.6 1.4 M NaCl) and the heating temperature (35 55 °C). They found that the turbidity increased faster at higher heating temperatures reaching values that increased weakly with increasing salt concentration. In the present study, we also observed a faster increase of the turbidity with increasing temperature-reaching values that increased weakly with decreasing pH from 8 to 6.5. However, at pH 6.0 the increase was much stronger and at long heating times precipitation was observed. The most likely explanation for the increase of the turbidity is, of course, that the molar mass of the myosin aggregates increased.

We have studied the variation of the apparent molar mass, radius of gyration and hydrodynamic radius of myosin during heating using light scattering. Fig. 4a shows the evolution of M_a at 50 °C for three different values of the pH with $C = 1.5$ g/L and for three concentrations at pH 8. As mentioned above, M_a is equal to I_r/KC extrapolated to $q = 0$ and is inversely proportional to the osmotic compressibility. M_a increased rapidly at first and then stagnated for pH 7 and pH 8, but it continued to

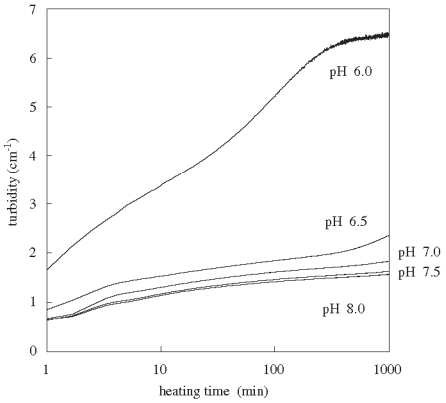

Fig. 3. Dependence of the turbidity at $\lambda = 350$ nm on the heating time at 50 °C for myosin solutions with $C = 5.0$ g/L at different values of the pH.

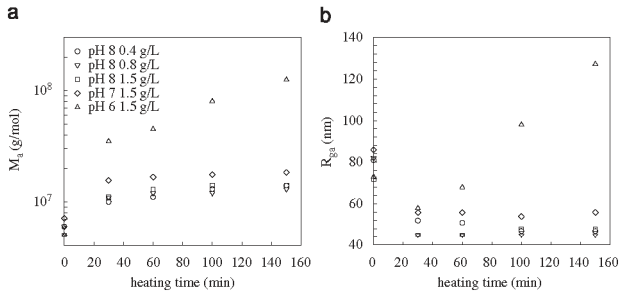

Fig. 4. Dependence of M_a (a) and R_{ga} (b) on the heating time at 50 °C for myosin solutions at different concentrations and pH.

increase at pH 6.0. The increase of M_a at pH 7 and 8 was modest, but at pH 6 it was important. In fact, the solutions at pH 6 became turbid after long heating times so that light scattering results are no longer reliable. At pH 7 and 8, similar results were obtained when the concentration was reduced indicating that the effect of interaction was small and that M_a was close to M_w. At pH 6, the strong increase of M_a was slower at lower concentrations. The results for M_a confirm those obtained from the turbidity measurements showing a modest heat-induced aggregation between pH 6.5 and 8.0 and a much more extensive aggregation at pH 6.

Surprisingly, while M_a increased, R_{ga} and R_{ha} decreased substantially. Fig. 4b shows the dependence of R_{ga} on the heating time. Similar results were found for R_h (results not shown). The effect of heating on R_{ga} and R_{ha} is thus the inverse of that on M_a. Kouchi et al. (2003) noted a similar decrease of R_{ha} for myosin of white croaker when increasing the temperature from 20 to 40 °C. At pH 7 and 8, the radii remained constant at longer heating times, but at pH 6, the values reached a minimum and increased at longer times. It is clear that the aggregation process at pH 6, at longer heating times has a different character.

Results obtained at different concentrations (0.4, 0.8, 1.5 and 3.0 g/L) and temperatures (30, 50 and 70 °C) showed in all cases initially a rapid increase of M_a and a decrease of R_{ga}, although the effect was slower and less pronounced at 30 °C. The subsequent slow increase of both M_a and R_{ga} was not observed within 15 h at pH 8. It was observed at pH 7 at 70 °C for 1.5 and 3.0 g/L. At pH 6 it was observed for 1.5 and 3.0 g/L both at 50 and 70 °C. In general, the rate of the second aggregation process at longer heating times increased with increasing protein concentration, increasing heating temperature and decreasing pH.

If the myosin oligomers are indeed formed by association of the heads as suggested on the basis of electron microscopy, then the initial increase of the M_a can be understood in terms of an increase of the association number. However, for star polymers the radius increases with increasing association number, albeit weakly (Daoud & Cotton, 1982), while for myosin oligomers a decrease of both R_g and R_h was observed. The origin of this phenomenon is probably the transition of the tail structure from a helix to a random coil (Ishioroshi et al., 1979, 1981; Morita & Yasui, 1991; Samejima et al., 1981; Sharp & Offer, 1992; Walker & Trinick, 1986). As a consequence, the tails become less rigid and therefore less extended resulting in smaller values of R_g and R_h. Chan, Gill, and Paulson (1992) reported that for cod myosin the helical content decreased gradually in the temperature range 25 65 °C.

3.3. Effect of cooling after prolonged heating

We have seen that between pH 6.5 and 8.0 heating led initially to an increase of the molar mass and a decrease of the size of the myosin aggregates, but that at longer heating times the variation was very weak. For this reason the turbidity of heated solutions increased rapidly at first and only very slowly at longer times. Fig. 5 shows the effect of cooling and reheating on the turbidity of myosin solutions ($C = 5$ g/L) after prolonged (15 h) heating at 50 °C. Cooling to 20 °C led to an increase of the turbidity, which means that the molar mass of the aggregates increased. The increase occurred at the same rate as the temperature decreases and was stronger at lower pH between 8.0 and 6.5. Interestingly, reheating to 50 °C decreased the turbidity back to the same value, implying that the increase was reversible.

The effect of cooling to 20 °C on M_a, R_{ga} and R_{ha} was determined for several myosin solutions after prolonged heating. An increase of these parameters was observed after cooling, except at pH 8 and $C = 0.4$ g/L for which no effect of cooling was observed. The effect of cooling was stronger at higher myosin concentrations, at higher heating temperature, and at lower pH. It was verified for several solutions that the effect of cooling was reversible upon reheating.

3.4. Structure of myosin aggregates

The structure of myosin aggregates formed by heating was studied at 20 °C using light scattering. Heated myosin solutions were cooled to 20 °C and highly diluted so that the influence of interactions on the measurements could be neglected. Aggregates formed at different myosin concentrations (0.4–3 g/L), different pH (6, 7 and 8) and different heating temperatures (30, 50 and 70 °C) were studied. Fig. 6a, shows the q-dependence of I_r/KC for a number of solutions containing aggregates of different size formed by heating at 70 °C at different conditions of pH and myosin concentration. M_w and R_g were derived from the initial q-dependence using Eqs (1) and (2). As mentioned above, in general, the size of the aggregates increased with increasing myosin concentration, increasing heating temperature and decreasing pH.

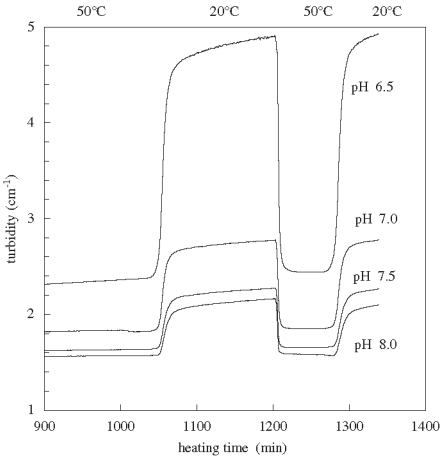

Fig. 5. Effect of cooling and heating cycles on the turbidity of extensively heated myosin solutions with $C = 5.0$ g/L at different values of the pH.

At pH 6 very large aggregates were formed that showed a power law q-dependence of KC/I_r over the whole accessible q-range

$$\frac{I_r}{KC} \sim q^{-d_f} \tag{7}$$

A power law q-dependence of the structure factor is characteristic for self-similar structures and the exponent is equal to the so-called fractal dimension (d_f). A linear least-squares fit gave $d_f = 2.2$ for myosin aggregates, see solid line in Fig. 6a. Similar results were obtained for solution heated at 50 °C. At 30 °C only relatively small aggregates were formed at the concentration and pH conditions tested in this study (data not shown).

The formation of self-similar aggregates by proteins upon heating has been reported earlier for β-lg by Gimel, Durand, and Nicolai (1994), Baussay, Le Bon, Nicolai, Durand, and Busnel (2004), for ovalbumin by Weijers, Nicolai, and Visschers (2002) and for bovum serum albumin by Hagiwara, Kumagai, and Nakamura (1996) with values for d_f close to 2. It was found that the structure factor of aggregates of different size superimposed if plotted as a function of qR_{gz}. The master curve obtained by superposition of the data plotted in Fig. 6a is shown in Fig. 6b and the values of M_w and R_{gz} are summarized in Table 1. Of course, the data for the largest aggregates cannot be superimposed without ambiguity, because they show a power law over the whole accessible q-range so that any combination of M_w and R_{gz} that respects the scaling relation results in superposition. Structure factors of myosin aggregates formed at all conditions tested

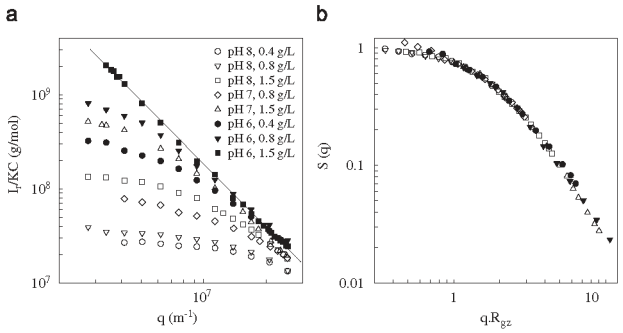

Fig. 6. (a) q-Dependence of I_r/KC for highly diluted aggregate solutions obtained by extensively heating at 70 °C myosin solutions at different concentrations and pH. The solid line has slope −2.2. (b) Same data as plotted in Fig. 6b after normalizing I_r/KC with M_w and q with R_{gz}.

superimposed on the same master curve within the experimental error, which shows that the large-scale organization of the myosin molecules in the clusters is universal.

Fig. 7 shows M_w as a function of R_{gz} for all samples. For self-similar aggregates a power law relationship is expected:

$$M_w = aR_{gz}^{d_f}, \quad (8)$$

where the prefactor a is determined by the local structure of the aggregates. The data plotted in Fig. 7 show relatively large scatter, but they are consistent with Eq. (8) using the same value for the fractal dimension ($d_f = 2.2$), see solid line. The scatter of the data is not caused by the characterization method, but probably reflects a variety of the structure on smaller length scales of aggregates obtained in different trials. Figs. 6b and 7 represent a central result of this work. They show that large cod myosin aggregates formed after heating and subsequent cooling have the same self-similar structure independent of the heating temperature, the myosin concentration and the pH. The fact that the prefactor a is independent of the heating conditions within the experimental error, shows that also the local structure of the aggregates is approximately the same.

Table 1
Weight average molar mass and the z-average radius of gyration of myosin aggregates formed after heating at 70 °C at different pH and concentrations followed by subsequent cooling to 20 °C and dilution

	M_w (g/mol)	R_{gz} (nm)
pH 8; 0.4 g/L	2.8×10^7	70
pH 8; 0.8 g/L	3.6×10^7	86
pH 8; 1.5 g/L	1.45×10^8	175
pH 7; 0.8 g/L	7.1×10^7	115
pH 7; 1.5 g/L	7.0×10^8	360
pH 6; 0.4 g/L	3.5×10^6	250
pH 6; 0.8 g/L	1.2×10^9	410
pH 6; 1.5 g/L	$>10^{10}$	>1 μm

The values were deduced from the data shown in Fig. 6a.

An independent measure of the size of the aggregates is the hydrodynamic radius. Autocorrelation functions were determined for dilute solutions of myosin aggregates obtained at different conditions. The analysis in terms of Eq. (4) yielded narrow relaxation time distributions in all cases and the average diffusion coefficient was calculated using Eq. (5). The q-dependence of D was found to be weak even for large aggregates when the q-dependence of I_r/KC was strong, which shows that the aggregates are relatively rigid. For β-lg aggregates it was found by Baussay et al. (2004) that the rigidity of the aggregates increased with increasing ionic strength which corresponded to increasing degree of branching as reported by Pouzot, Nicolai, Visschers, and Weijers (2005).

R_{hz} was calculated from the average diffusion coefficient extrapolated to $q = 0$ using Eq. (5) and the ratio R_{gz}/R_{hz} is shown as a function of M_w in Fig. 8. For non-draining particles this ratio depends on the structure and the size distribution of the particles, but for self-similar particles these parameters are independent of the molar mass. We found a weak decrease of the ratio with increasing molar mass of the aggregates tending to 0.9 ± 0.1 for large aggregates. A similar ratio was reported earlier for β-lg aggregates by Gimel et al. (1994).

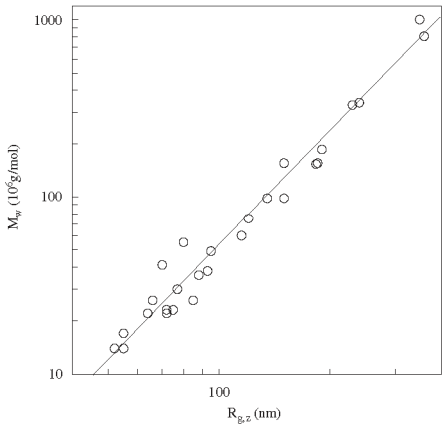

Fig. 7. Dependence of the molar mass on the radius of gyration for myosin aggregates obtained at different heating temperatures, concentrations and pH. The solid line has slope 2.2.

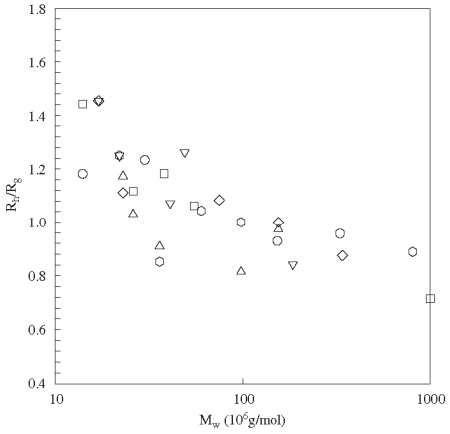

Fig. 8. Dependence of the ratio R_{hz}/R_{gz} on the molar mass for myosin aggregates obtained at different heating temperatures, concentrations and pH.

4. Discussion

It appears that it is very difficult to isolate individual cod myosin. This was already observed half a century ago by Connell (1960). He managed nevertheless to isolate individual myosin using freshly killed cod (pre rigor mortis) and a more rapid method, but probably at the cost of lower purity.

Highly purified myosin from post rigor mortis cod formed small oligomers in dilute aqueous solutions containing 0.5 M KCl at pH 6 8 even at low temperatures. The oligomers showed a relatively small variation of R_g and R_h compared with the variation of M_w. This is compatible with the proposition that star-like aggregates are formed by association of the myosin heads based on electron microscopy (Margossian & Slayter, 1987; Sharp and Offer, 1992; Tazawa et al., 2002; Walker and Trinick, 1986; Yamamoto, 1990), because for star polymers the radius varies only weakly with the association number (N_{ag}) (Daoud and Cotton, 1982).

Heating the oligomers led in first instance to weak increase of the association number of the aggregates together with a decrease of the both the radius of the gyration and the hydrodynamic radius. This apparently contradictory effect can be explained by the temperature-induced helix-coil transition that renders the myosin tails more flexible thus reducing the radius. Rodgers, Karr, Biedermann, Ueno, and Harrington (1987) studied the radius of gyration and the optical rotation of myosin rod fragments of several species. They observed a decrease of both the fraction helix and the radius of gyration with increasing temperature.

Prolonged heating led to further aggregation and finally to precipitation or gelation if the concentration was sufficiently high. Precipitation occurs either because large aggregates sediment before they can form a space filling structure or because the latter is too weak to resist gravity. One notices gel formation only when the space filling structure is strong enough, i.e. at higher myosin concentrations. It is possible that the further aggregation is caused by interaction between myosin tails of different oligomers leading to irreversible bond formation between oligomers. Cooling caused an increase of the size of the aggregates, but this increase was found to be reversible. We may speculate that the links formed during cooling involve hydrogen bonds. Another possibility is that coiled-coil structures are reformed after cooling between tails from different oligomers as suggested by Sasaki et al. (2006). We note, however, that at higher myosin concentrations large-scale aggregation and gelation was observed even at 4 °C. This means that the helix-coil transition is not a necessary step for this process.

The outcome of the second step of the aggregation process was the formation of self-similar aggregates similar to those observed by heat-induced aggregation of globular proteins. At low protein concentration, the growth of the aggregates stagnated at a value that increased with increasing protein concentration. Above a sufficiently high concentration the aggregation process led to flocculation or to gelation at still higher concentrations. Similar observations were reported for heat-induced aggregation of globular proteins (Nicolai, 2007). For the latter systems it was found that at a given protein concentration larger aggregates are formed if the electrostatic repulsion is lower (Weijers et al., 2002; Baussay et al., 2004). For myosin we also found larger aggregates when decreasing pH toward the *iso*-electric point (pI = 5.4), i.e. when reducing electrostatic repulsion.

For globular proteins it was found that the structure of the gels is highly sensitive to electrostatic interactions even though the structure of the aggregates is similar. When the electrostatic repulsion between the proteins was weak, because the pH was close to pI or salt was added, highly heterogeneous turbid gels were observed, while in the opposite case the gels were transparent and homogeneous (Clark, 1998; Nicolai, 2007). For the myosin solutions studied here the salt concentration is relatively high so that turbid heterogeneous gels are formed. Such large heterogeneity cannot be explained by simple cross-linking of space-filling fractal aggregates and suggests that strong concentration fluctuations or even micro-phase separation of the aggregates occurred in more concentrated solutions, while gelation inhibited macroscopic phase separation. Of course, these considerations are speculative and further studies are needed to resolve this issue. Unfortunately, cod myosin solutions are not stable at higher concentrations even at low temperatures so that controlled studies of the heat-induced gelation process of cod myosin are not possible.

5. Summary

Highly purified cod myosin was isolated resulting in relatively dilute solutions of oligomers containing around 10 myosin molecules. In addition, large aggregates were formed the extent of which could be reduced by avoiding myosin precipitation steps. Heating led initially to a rapid increase of the association number, but the radius of the aggregates decreased, probably due to the helix-coil transition of myosin tails. At longer times relatively slow aggregation of the oligomers occurred at a rate that increased with increasing myosin concentration (0.4 3 g/L), increasing temperature (30 70 °C) and decreasing pH (8 6). Cooling extensively heated solutions led to further aggregation, which was, however, reversible upon reheating.

The large-scale structure of the aggregates was found to be self-similar characterized by a fractal dimension of about 2.2, independent of the concentration, temperature and pH in the range studied here.

Acknowledgements

The AVS R&D fund of the Ministry of Fisheries in Iceland and The Icelandic Technology Development Fund are acknowledged for financial support of this work.

References

Baussay, K., Le Bon, C., Nicolai, T., Durand, D., & Busnel, J. (2004). Influence of the ionic strength on the heat-induced aggregation of the globular protein β-lactoglobulin at pH 7. *International Journal of Biological Macromolecules, 34*, 21–28.

Berne, B., & Pecora, R. (1976). *Dynamic light scattering*. New York: Wiley.

Brown, W. (1996). *Light scattering: Principles and development*. Oxford: Clarendon Press.

Chan, J. K., Gill, T. A., & Paulson, A. T. (1992). The dynamics of thermal-denaturation of fish myosins. *Food Research International, 25*, 117–123.

Clark, A. H. (1998). Gelation of globular proteins. In S. E. Hill, D. A. Ledward, & J. R. Mitchell (Eds.), *Functional properties of food macromolecules* (2nd ed., pp. 77–142). Gaithersburg: Aspen Publishers.

Connell, J. J. (1960). Studies on the proteins of fish skeletal muscle. 7. Denaturation and aggregation of cod myosin. *Biochemical Journal, 75*, 530–538.

Connell, J. J. (1961). The relative stabilities of the skeletal-muscle myosins of some animals. *Biochemical Journal, 80*, 503–509.

Daoud, M., & Cotton, J.-P. (1982). Star shaped polymers: A model for the conformation and its concentration dependence. *Journal de Physique, 43*, 531.

Davies, J. R., Bardsley, R. G., Ledward, D. A., & Poulter, R. G. (1988). Myosin thermal-stability in fish muscle. *Journal of the Science of Food and Agriculture, 45*, 61–68.

Davies, J. R., Ledward, D. A., Bardsley, R. G., & Poulter, R. G. (1994). Species dependence of fish myosin stability to heat and frozen storage. *International Journal of Food Science and Technology, 29*, 287–301.

Elliott, A., & Offer, G. (1978). Shape and flexibility of myosin molecule. *Journal of Molecular Biology, 123*, 505–519.

Fukazawa, T., Hashimoto, Y., & Yasui, T. (1961). The relationship between the components of myofibrillar protein and the effect of various phosphates that influence the binding quality of sausage. *Journal of Food Science, 26*, 550–555.

Fukushima, H., Satoh, Y., Yoon, S. H., Togashi, M., Nakaya, M., & Watabe, S. (2005). Rheological properties of fast skeletal myosin rod and light meromyosin from walleye pollack and white croaker: Contribution of myosin fragments to thermal gel formation. *Journal of Agricultural and Food Chemistry, 53*, 9193–9198.

Gellart, M. F., & Englander, S. W. (1962). The molecular weight of rabbit myosin A by light scattering. *Biochemistry, 2*, 39.

Gill, T. A., Chan, J. K., Phonchareon, K. F., & Paulson, A. T. (1992). Effect of salt concentration and temperature on heat-induced aggregation and gelation of fish myosin. *Food Research International, 25*, 333–341.

Gimel, J. C., Durand, D., & Nicolai, T. (1994). Structure and distribution of aggregates formed after heat-induced denaturation of globular proteins. *Macromolecules, 27*, 583–589.

Hagiwara, T., Kumagai, H., & Nakamura, K. (1996). Fractal analysis of aggregates formed by heating dilute BSA solutions using light scattering methods. *Bioscience, Biotechnology and Biochemistry, 60*, 1757–1763.

Harrington, W. F., & Rodgers, M. E. (1984). Myosin. *Annual Review of Biochemistry, 53*, 35–73.

Herbert, T. J., & Carlson, F. D. (1971). Spectroscopic study of the self association of myosin. *Biopolymers, 10*, 2231–2252.

Hermansson, A. M., Harbitz, O., & Langton, M. (1986). Formation of 2 types of gels from bovine myosin. *Journal of the Science of Food and Agriculture, 37*, 69.

Higgins, J. S., & Benoit, H. C. (1994). *Polymers and neutron scattering*. Oxford: Clarendon Press.

Ishioroshi, M., Samejima, K., & Yasui, T. (1979). Heat-induced gelation of myosin-factors of pH and salt concentrations. *Journal of Food Science, 44*, 1280–1284.

Ishioroshi, M., Samejima, K., & Yasui, T. (1981). Further studies on the roles of the head and the tail regions of the myosin molecules in heat-induced gelation. *Journal of Food Science, 47*, 114–120.

Johnston, I. A., Walesby, N. J., Davison, W., & Goldspink, G. (1975). Temperature adaptation in myosin of Antarctic fish. *Nature, 254*, 74–75.

Kouchi, S., Kondo, S., Ooi, K., Ichikawa, H., & Dobashi, T. (2003). Viscoelastic and light scattering studies on thermally induced sol to gel phase transition in fish myosin solutions. *Biopolymers, 69*, 498–507.

Kristinsson, H. G. (2001). Evaluation of different methods to isolate cod (*Gadus morhua*) muscle myosin. *Journal of Food Biochemistry, 25*, 249–256.

MacFarlane, J. J., Schmidt, G. R., & Turner, R. H. (1977). Binding of meat pieces: Comparison of myosin, actomyosin and sarcoplasmic proteins as binding agents. *Journal of Food Science, 42*, 1603–1605.

Margossian, S. S., & Slayter, H. S. (1987). Electron microscopy of cardiac myosin: Its shape and properties as determined by the regulatory chain. *Journal of Muscle Research and Cell Motility, 8*, 437–447.

Martone, C. B., Busconi, L., Folco, E. J., Trucco, R. E., & Sanchez, J. J. (1986). A simplified myosin preparation from marine fish species. *Journal of Food Science, 51*, 1554–1555.

Moreels, E., De Ceuninck, W., & Finsy, R. (1987). *Journal of Chemical Physics, 86*, 618.

Morita, J. I., & Yasui, T. (1991). Involvement of hydrophobic residues in heat-induced gelation of myosin tail subfragments from rabbit skeletal-muscle. *Agricultural and Biological Chemistry, 55*, 1597–1599.

Nicolai, T. (2007). Structure of self-assembled globular proteins. In E. Dickenson, & M. Leser (Eds.), *Food colloids. Interactions, microstructure and processing* (pp. 35–56). Cambridge: The Royal Society of Chemistry.

Ogawa, M., Ehara, T., Tamiya, T., & Tsuchiya, T. (1993). Thermal-stability of fish myosin. *Comparative Biochemistry and Physiology B-Biochemistry & Molecular Biology, 106B*, 517–521.

Pouzot, M., Nicolai, T., Visschers, R. W., & Weijers, M. (2005). X-ray and light scattering study of the structure of large protein aggregates at neutral pH. *Food Hydrocolloids, 19*, 231–238.

Provencher, S. W. (1982). CONTIN—A general purpose constrained regularization program for inverting noisy linear algebraic and integral equations. *Computer Physics Communications, 27*, 229–242.

Rodgers, M. E., Karr, T., Biedermann, K., Ueno, H., & Harrington, H. W. (1987). Thermal stability of myosin from various species. *Biochemistry, 26*, 8703–8708.

Samejima, K., Ishioroshi, M., & Yasui, T. (1981). Relative roles of the head and tail portions of the molecule in heat-induced gelation of myosin. *Journal of Food Science, 46*, 1412–1418.

Sasaki, T., Yuan, C. H., & Konno, K. (2006). Role of cooling process in the thermal aggregate formation by carp myosin rod. *Journal of Food Science, 71*, C75–C80.

Sharp, A., & Offer, G. (1992). The mechanism of formation of gels from myosin molecules. *Journal of the Science of Food and Agriculture, 58*, 63–73.

Stepanek, P. (1993). In W. Brown (Ed.), *Dynamic light scattering*. Oxford: Oxford University Press (Chapter 4).

Takahashi, K. (1978). Topography of myosin molecule as visualized by an improved negative staining method. *Journal of Biochemistry, 83*, 905–908.

Tazawa, T., Kato, S., Katoh, T., & Konno, K. (2002). Role of neck region in the thermal aggregation of myosin. *Journal of Agricultural and Food Chemistry, 50*, 196–202.

Tsai, R., Cassens, R. G., & Briskey, E. J. (1972). Emulsifying properties of purified muscle proteins. *Journal of Food Science, 37*, 286–288.

Walker, M., & Trinick, J. (1986). Electron microscope study of the effect of temperature on the length of the tail of the myosin molecule. *Journal of Molecular Biology, 192*, 661–667.

Weijers, M., Nicolai, T., & Visschers, R. W. (2002). Light scattering study of the heat-induced aggregation of ovalbumin at different ionic strength. *Macromolecules, 35*, 4753–4762.

Woods, E. F., Himmelfarb, S., & Harrington, W. F. (1963). Studies on the structure of myosin in solution. *The Journal of Biological Chemistry, 238*, 2374–2385.

Yamamoto, K. (1990). Electron microscopy of thermal aggregation of myosin. *Journal of Biochemistry, 108*, 896–898.

Paper 2. Brenner Tom, Johannsson Ragnar and Nicolai Taco. *Characterisation and thermo-reversible gelation of cod muscle protein isolates.* Food Chemistry, 2009. **115**(1): p. 26-31.

Food Chemistry 115 (2009) 26–31

Contents lists available at ScienceDirect

Food Chemistry

journal homepage: www.elsevier.com/locate/foodchem

Characterisation and thermo-reversible gelation of cod muscle protein isolates

T. Brenner [a,*], R. Johannsson [a], T. Nicolai [b]

[a] Matis, Biotechnology Division, Gylfaflot 5, 112 Reykjavik, Iceland
[b] Polymeres, Colloids, Interfaces, UMR CNRS, Université du Maine, 72085 Le Mans Cedex 9, France

ARTICLE INFO

Article history:
Received 20 April 2008
Received in revised form 10 November 2008
Accepted 13 November 2008

Keywords:
Fish protein isolate
Gel
Rheology
Light scattering
Alkaline solubilisation

ABSTRACT

Cod (Gadus Morhua) muscle proteins were solubilized using alkaline treatment of the muscle. Solutions of similar protein composition were obtained between pH 10.5 and 12.0, however, pH > 11 was required for optimal yield. Addition of salt (up to 0.25 M NaCl) did not affect protein yield or composition. Light scattering showed that a significant fraction of the proteins was present as large self similar and flexible aggregates. When the pH was decreased below 10, gelation was observed below a critical temperature of about 25 °C, which could be reversed by heating. Slow irreversible aggregation was also observed leading to coarsening and syneresis of the gels or precipitation at higher temperatures. The rate of irreversible aggregation increased with decreasing pH and was fast below pH 8. Homogeneous thermo-reversible self supporting gels that were stable for a period of days could be prepared without heating at a narrow pH range between 8.5 and 9.5.

1. Introduction

With the decline in wild fish species abundance, better utilization is called for marine by-products and underutilized fish that is currently used for animal feed. The use of extreme pH to isolate proteins from marine catch and its by-products has been reported widely (Batista, 1999; Hultin & Kelleher, 2001; Kahn, Berk, Pariser, Goldblith, & Flink, 1974; Montecalvo, Constantinides, & Yang, 1984). This method has been suggested as an alternative to the more conventional surimi production, with several authors reporting better protein yields (Choi & Park, 2002; Kristinsson & Liang, 2006; Kristinsson, Theodore, Demir, & Ingadottir, 2005; Undeland, Kelleher, & Hultin, 2002) than is obtained in processing of surimi. It has also been reported that this method is more efficient than surimi processing in removal of both neutral and charged lipids (Hultin & Kelleher, 2001; Kristinsson & Liang, 2006; Kristinsson et al., 2005; Undeland et al., 2002) which is important for prevention of rancidity (Kristinsson et al., 2005; Lanier, 2000; Undeland, Hall, Wendin, Gangby, & Rutgersson, 2005; Undeland et al., 2002). Following usage in the literature (Kristinsson & Ingadottir, 2006; Kristinsson & Liang, 2006; Kristinsson, Theodore, & Ingadottir, 2007; Kristinsson et al., 2005; Thawornchinsombut & Park, 2007; Undeland et al., 2002) we will refer to solutions obtained with muscle tissue treatment at extreme pH as fish protein isolate (FPI).

Various studies have reported the gelation of fish muscle proteins without heating or added salt. Stefansson and Hultin (1994) observed gelation in one instance of fish proteins solubilized at very low ionic strength and neutral rather than extreme pH. Chawla, Venugopal, and Nair (1996), Lian, Lee, and Chung (2002) and Venugopal, Doke, and Nair (1994) have worked with heterogeneous fish protein suspensions, not dissimilar to those obtained in conventional surimi processing, and reported gelation in the presence of weak acids without addition of salts (and, in several experiments, without heating). On the other hand, exploring the possibilities of producing consistent, edible products from FPI obtained through extreme pH solubilisation has concentrated so far on gels prepared at high temperatures, usually combined with high salt concentrations (Choi & Park, 2002; Kim, Park, & Choi, 2003; Kristinsson & Liang, 2006; Kristinsson et al., 2005; Thawornchinsombut & Park, 2007; Undeland et al., 2002; Yongsawatdigul & Park, 2004), and often in the presence of different additives (Choi & Park, 2002; Kim et al., 2003; Kristinsson & Liang, 2006; Thawornchinsombut & Park, 2007; Undeland et al., 2002). It has not been reported, as far as we know, in the literature concerning FPI solubilized through extreme pH, that the resulting solution may show cold-setting gelation without addition of salt. Other workers have investigated gel production (Choi & Park, 2002; Kim et al., 2003; Kristinsson & Liang, 2006; Kristinsson et al., 2005; Thawornchinsombut & Park, 2007; Undeland et al., 2002; Yongsawatdigul & Park, 2004) starting from a heterogeneous suspension of FPI obtained by *iso*-electric precipitation. In contrast, the work presented here deals with FPI solutions at much lower protein concentrations (<25 g/L) and low ionic strength (<100 mM), and emphasizes the possibility of producing consistent FPI gels at low temperatures without added salt.

The aim of the work presented here was to optimize alkaline solubilisation of cod muscle protein; to characterize the FPI

* Corresponding author. Tel.: +354 4225131.
E-mail address: tom@matis.is (T. Brenner).

0308-8146/$ - see front matter © 2008 Elsevier Ltd. All rights reserved.
doi:10.1016/j.foodchem.2008.11.046

solutions after isolation; and to study the behaviour of the solutions after reducing the pH.

2. Materials and methods

2.1. Sample preparation

White muscle tissue from freshly caught cod (0–2 days from catch) was used. Repeated measurements showed that the area of harvesting and time of year had no effect on the observations made and results reported here. The muscle tissue was homogenized in 4–10 weight equivalents of distilled water, and the pH was adjusted to a value in the range 10.5–12.0. To check the effect of ionic strength on the protein yield, addition of 0.15–0.25 M NaCl to extraction solvent was tested, but only solutions obtained without added salt were used for gel production and the rheological study. Solutions were centrifuged for 10 min at 15,000g (Avanti Centrifuge J-20 XPI, Beckman Coulter, Fullerton, CA, USA), followed by filtration of the supernatant over two layers of gauze. The temperature was kept under 15 °C during the protein isolation. FPI solutions were stored at 4 °C and used for gel preparation within 24 h of extraction.

2.2. Determination of the protein concentration using UV absorption

The extinction coefficient of the protein isolates was determined as follows. The absorbance as a function of wavelength (λ) was measured at pH values ranging from 7 to 12. At all pH values, a broad peak with a maximum at $\lambda = 230$ nm was observed, indicating the presence of residual amounts of conjugated substances originating in the fish muscle. At pH values above 11.5 the protein absorption peak appears at $\lambda = 289$ nm as a shoulder on the broad peak. The absorbance at $\lambda = 289$ nm was measured at pH 12 and corrected for the effect of turbidity. The total protein content was obtained through elemental analysis of nitrogen, where we used a conversion factor of 6.0 to convert N to total protein amount. The extinction coefficient for the protein mixture at pH 12 and $\lambda = 289$ nm was found to be 0.71 ± 0.01 L g^{-1} cm^{-1}.

2.3. SDS–PAGE electrophoresis

SDS–PAGE electrophoresis was performed according to Laemmli (1970). The electrophoretic pattern of FPI was determined using polyacrylamide 10% gel slabs run on an electrophoresis unit (Bio-Rad, miniprotean II Cell) with a constant current of 20 mA per gel. The gels were scanned with a GelDoc 2000 scanner (Bio-Rad Laboratories Inc., Herts, UK) and analyzed using the software package GelCompar II, 2.01 (Applied Maths BVBA, Kortrijk, Belgium). Broad range protein standards were obtained from Biolabs (Biolabs, New England, US). All other reagents were obtained from Sigma–Aldrich.

2.4. Light scattering

Static and dynamic light scattering measurements were made using an ALV-5000 multiple tau digital correlator (ALV, Langen, Germany) and a JDS Uniphase He–Ne laser (model 1145P–3083, vertically polarized beam, wavelength 632.8 nm). The range of scattering wave vectors (q) covered in the experiment was $2.8 \times 10^{-3} - 2.6 \times 10^{-2}$ nm^{-1}. The scattering vector q is given as $q = (4\pi n_s/\lambda)\sin(\theta/2)$, where n_s is the refractive index of the sample and θ is the scattering angle. The temperature of solutions in light scattering experiments was controlled to within 0.2 °C using a thermostat water bath.

The relative excess scattering of particles, I_r, is related to their weight average molar mass, M_w, and their structure factor, $S(q)$ (Brown, 1996; Higgins & Benoit, 1994)

$$I_r = \frac{I_s - I_{sol}}{I_{tol}} = KCM_w S(q) \tag{1}$$

where C is the solute mass concentration and I_{tol} is the intensity of toluene that is used as a reference. I_s and I_{sol} refer to the intensity of scattering from the sample and from the neat solvent, respectively. K is an optical constant

$$K = \frac{4\pi^2 n_s^2}{\lambda^4 N_a}\cdot\left(\frac{\partial n}{\partial C}\right)^2\cdot\left(\frac{n_{tol}}{n_s}\right)^2\cdot\frac{1}{R_{tol}} \tag{2}$$

where I_a is Avogadro's number, $(\partial n/\partial C)$ is the refractive index increment, and R_{tol} is the Rayleigh ratio of toluene at 20 °C. We used $(\partial n/\partial C) = 0.19$ for the protein mixture and $R_{tol} = 1.35 \times 10^{-5}$ cm^{-1} at $\lambda = 633$ nm. $(n_{tol}/n_s)^2$ corrects for the difference in scattering volume of the solution and the toluene standard with refractive index n_{tol}.

At infinite dilution $S(q)$ depends on the particle size and shape and can be related to the z-average radius of gyration (R_{gz}) (Brown, 1996; Higgins & Benoit, 1994)

$$S(q) = (1 + (q\cdot R_{gz})^2/3)^{-1} \qquad qR_{gz} < 1, C \to 0 \tag{3}$$

If one applies Eqs. (1) and (3) to results obtained at finite concentrations, one obtains an apparent molar mass (M_a) that is inversely proportional to the osmotic compressibility and an apparent radius of gyration (R_{ga}) that is proportional to the correlation length of concentration fluctuations. At low concentrations the effect of interaction between the solute particles can be described in terms of the second virial coefficient (A_2) (Higgins & Benoit, 1994)

$$S(q) = (1 + 2A_2 M_w C)^{-1} \qquad 2A_2 M_w C < 1,\ q \to 0 \tag{4}$$

For large self similar structures, the structure factor has a power law dependence on q for $q\cdot R_g \gg 1$ (Nicolai, 2007)

$$S(q) \propto q^{-df} \qquad q\cdot R_g \gg 1 \tag{5}$$

With the technique of dynamic light scattering (DLS), the autocorrelation function of the scattered light intensity fluctuations is determined (Berne & Pecora, 1976; Brown, 1996). The normalized autocorrelation function (g2(t)) can be analyzed in terms of a distribution of exponential decays

$$g_2(t) - 1 = \left[\int A(\tau)\exp\left(-\frac{t}{\tau}\right)\mathrm{d}\tau\right]^2 \tag{6}$$

where $A(\tau)$ is the amplitude of the exponential with relaxation time τ. In dilute solutions and for $q\cdot R_{gz} < 1$, the relaxation of intensity fluctuations is caused by centre of mass diffusion of the particles and τ depends on the diffusion coefficient of the particles (D)

$$\tau = (q^2 D)^{-1} \qquad q\cdot R_{gz} < 1, C \to 0 \tag{7}$$

D is related to the hydrodynamic radius, R_h, through the Stokes–Einstein relation (Berne & Pecora, 1976; Brown, 1996; Higgins & Benoit, 1994)

$$D = kT/(6\pi\eta R_h) \tag{8}$$

with T the absolute temperature, k Boltzmann's constant and η the viscosity. For polydisperse solutions a distribution of relaxation times will be observed that corresponds to the distribution of hydrodynamic radii. Eqs. (7) and (8) are only valid if $q\cdot R_g < 1$, otherwise rotation and internal dynamics may play a role in the relaxation process. For fully flexible particles the apparent hydrodynamic radius (R_{ha}) decreases linearly with increasing q if $q\cdot R_g \gg 1$. Autocorrelation functions were analyzed in terms of

Eq. (6) using the CONTIN (Provencher, 1982) routine. The average relaxation rate ($\langle\Gamma\rangle = \langle\tau^{-1}\rangle$) was used to calculate the diffusion coefficient: $\langle D\rangle = \langle\Gamma\rangle/q^2$. The z-average hydrodynamic radius (R_{hz}) was obtained from the average diffusion coefficient using Eq. (8).

2.5. Rheology

Oscillatory shear measurements were done using a StressTech stress-controlled rheometer (Reologica, Lund, Sweden), equipped with a thermostat water bath and water jackets. The temperature was controlled to within 0.2 °C. All measurements were done in the linear response regime. Non-linear rheology of FPI gels will be reported elsewhere. The geometry used was a couette with inner and outer diameters of 25 and 27 nm, respectively. A thin layer of paraffin oil was added to prevent evaporation.

Gels used in the rheological study were prepared in the following manner. A solution of HCl (0.1–0.2 M) was added drop-wise at 20 °C to the alkaline protein solution while stirring. During pH adjustment some precipitation of proteins was observed, but the use of a relatively low HCl concentration and vigorous stirring minimized precipitation. The solution was stirred until the precipitate was completely dispersed, and loaded into the rheometer. Only alkaline solutions obtained without added salt were used for the rheological study, and we found their ionic strength to be close to 25 mM using a Sension 7 conductivity meter (Hach Lange, Dusseldorf, Germany). Since roughly 20–25 mM of NaCl are formed by the initial NaOH addition and the subsequent HCl addition, the final ionic strength of gels at pH 9.0 was close to 50 mM. The temperature of FPI solutions used for gel production never exceeded 20 °C. Cold-gelation properties of FPI preheated to higher temperatures before recooling will be reported elsewhere.

3. Results and discussion

3.1. Protein yield

For maximum yield the pH employed during protein isolation needed to be higher than 11. Solutions of the solubilized proteins exhibited slow hydrolysis post solubilisation. Observation of hydrolysis in FPI was previously ascribed to activity of several cathepsin-like proteases originating in the fish muscle (Choi & Park, 2002; Kim et al., 2003; Lanier, 2000; Thawornchinsombut & Park, 2007). The extent of this hydrolysis was monitored by measuring the pH of the protein solution and performing SDS–PAGE electrophoresis at different times post solubilisation. The electrophoretic pattern of the proteins showed extensive degradation had taken place when solutions were kept for several weeks at room temperature. Since protein degradation affects gelation properties, measures were taken to minimize its extent as much as possible. We have found that the rate of hydrolysis was moderate when the pH was 11.0–11.2, but increased with increasing pH and became extremely rapid above pH 12. For this reason, solubilisation was performed at pH 11.0–11.2; thus, solubilizing proteins at a pH slightly above 11 ensures both a maximal protein yield and a minimal hydrolysis of the resulting protein solutions. The rate of hydrolysis was much slower when FPI were kept at 4 °C compared to room temperature. We have found that the extent of hydrolysis was negligible and did not affect rheological measurements provided solutions (at pH 11.0–11.2) were kept at 4 °C for periods not exceeding 24 h before gel preparation. This protocol was followed for all gels produced in this study.

No effect on the yield was found when the isolation was done with salt free water or with 0.15–0.25 M NaCl. Employing a muscle tissue concentration of about 15 wt% vs. 85 wt% extraction solvent was found to be a good compromise between high yield and high protein concentration. Assuming 18 wt% protein content in the cod muscle (Foegeding, Lanier, & Hultin, 1996; Stefansson & Hultin, 1994), we obtained yields of 60 ± 10%. Protein yield was calculated according to the following equation

$$Y = \frac{A \times V_p}{\varepsilon \times M_s \times 0.18} \times 100\% \quad (9)$$

where Y is the yield, A is the absorbance at pH 12, V_p is the volume of the FPI solution obtained, ε is the extinction coefficient quoted above (0.71 L g^{-1} cm^{-1}) and M_s is the initial mass of cod muscle used.

3.2. Composition of FPI

The protein composition of FPI was determined using SDS–PAGE electrophoresis and was found to be independent of the pH (10.5–12) and ionic strength (0–0.25 M NaCl) of the solvent used for the extraction. A typical electrophoretic pattern of the proteins is presented in Supplementary data.

The electrographs showed that myosin (heavy chain ~210 kDa, light chains 17–23 kDa), actin (43 kDa) and tropomyosin (38 kDa) were the most dominant proteins. Bands at higher molar mass than myosin heavy chain are tentatively assigned to titin and nebulin (Hu, Kimura, & Maruyama, 1986; Stefansson & Hultin, 1994). Other weak bands may correspond to other structural proteins and proteolytic segments of the main myofibrillar proteins. The ill-separated bands between 160 and 185 kDa are thought to be proteolytic segments of myosin heavy chain (Undeland et al., 2002). The presence of these bands was reported earlier for FPI obtained through acidic and alkaline solubilisation (Kristinsson & Liang, 2006; Undeland et al., 2002), and for washed fish muscle post treatment with weak organic acids (Chawla et al., 1996). We could not identify the band at 28 kDa which was also found by Undeland et al. (2002) after alkaline treatment of fish muscle. The intensity of the band seems too strong for the band to be a product of proteolysis.

Several authors have attributed the solubility of muscle proteins at extreme pH to electrostatic repulsion between charges on the protein molecules at pH far from the *iso*-electric point (Choi & Park, 2002; Kim et al., 2003; Kristinsson & Ingadottir, 2006; Kristinsson & Liang, 2006; Kristinsson et al., 2005; Yongsawatdigul & Park, 2004). However, electrostatic interaction can be screened by adding salt and we found no effect of adding salt on the yield. This finding is in agreement with that of Thawornchinsombut and Park (2007) and Kahn et al. (1974) who did not observe a significant effect of adding NaCl on protein solubility at extreme pH for Pacific Whiting and squid, respectively. These observations question the importance of electrostatic interaction on the solubility at extreme pH.

The ionic strength of fish muscle tissue is close to 0.15 M, with the monovalent ions chloride, potassium and sodium being dominant (Kilimann & Heilmeyer, 1977; Stefansson & Hultin, 1994; Wu, Atallah, & Hultin, 1991). This was confirmed by elemental analysis of FPI. For cod, the typical fat content in muscle is 0.3 wt% (Foegeding et al., 1996). However, extraction of the proteins from muscle tissue using extreme pH removed a considerable amount of the total lipid content through creaming and through precipitation of the membrane-bound lipids, both of which are removed in the centrifugation step (Hultin & Kelleher, 2001). The fat content of FPI was measured following the method reported by Bligh and Dyer (1959) and found to be negligible (<0.005 wt%).

3.3. Characterisation of FPI in solution

Freshly extracted FPI at pH 11, with protein concentrations (C) between 0.5 and 8 g/L, were analyzed using static and dynamic

light scattering. The light scattering intensity had a power law dependence on q over the entire accessible range, see Fig. 1a. This means that the system contained particles that were larger than 1 μm with a self-similar structure characterized by a fractal dimension of 1.8–1.9, cf. Eq. (5). The same results were obtained at different FPI concentrations. Self similar aggregates were also shown to be formed in pure cod myosin solutions after heating (Brenner, Johannsson, & Nicolai, 2009). Aggregates with very similar overall structure are also formed when globular proteins are heated in aqueous solution (Nicolai, 2007).

Sedimentation of these large aggregates under gravity could be observed visually within one day after preparation. We found that on average about 10–15% of the proteins precipitated within the week after preparation. About the same fraction of proteins was removed when the solutions were centrifuged at 50,000g for 90 min and filtered through 0.45 μm pore-size filters. The intensity scattered by filtered solutions was much reduced especially at small q-values and had a weaker q-dependence, see Fig. 1b.

The apparent molar mass and radius of gyration could be calculated as a function of the concentration. The radius of gyration varied little with the protein concentration in the range used in the experiment and was found to be about 150 nm which is much larger than that of the individual protein components. Filtration through 0.2 μm pore-size filters was not possible, which shows that a significant fraction of the proteins was aggregated and blocked the pores of the filters. It is likely that the size distribution of the aggregates is very broad and that centrifugation and filtration simply removed the fraction of largest aggregates. We have not been able to establish if and how much protein is present as individual molecules. KC/I_r was found to increase linearly with the concentration, see Fig. 2, which shows that interaction between the protein aggregates is repulsive. The weight average molar mass and second virial coefficient could be determined from a linear least squares fit, cf. Eq. (4): $M_w = 7.8{*}10^6$ g/mol, and $A_2 = 5.0{*}10^{-9}$ mol L g^{-2}.

Intensity autocorrelation functions could be described by a single relaxation time distribution. The apparent hydrodynamic radius decreased linearly with increasing q over the whole q-range, see Fig. 3, implying that the very large aggregates were flexible. After centrifugation and filtration the q-dependence was weaker which allowed us to estimate R_h as about 180 nm.

We measured the light scattering intensity of FPI solutions at pH 11 both before and after filtration as a function of the temperature between 5 °C and 80 °C and found it to be insensitive to temperature in this pH and concentration range (0.5–8 g/L). The bonds between the aggregates were strong in the sense that they resisted

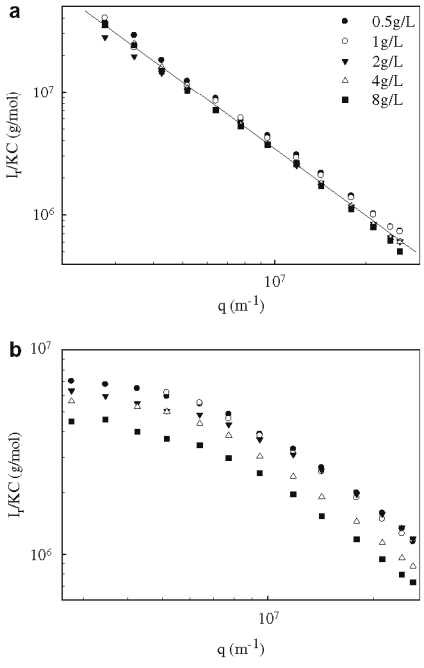

Fig. 1. Dependence of I_r/KC on the scattering wave vector of freshly prepared FPI solutions at pH 11 for different concentrations indicated in the figure. Fig. 2a shows the results before centrifugation and filtration, while Fig. 2b shows the results after centrifugation and filtration. The solid line in Fig. 2a has a slope of −1.8.

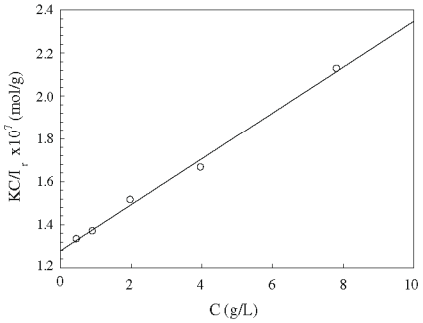

Fig. 2. Concentration dependence of KC/I_r (extrapolated to $q = 0$) for filtered FPI solutions at pH 11. The solid line represents a linear least-squares fit.

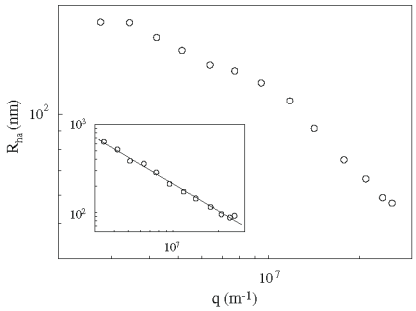

Fig. 3. Dependence of the apparent hydrodynamic radius on q of a filtered FPI solution at pH 11.0 and C = 1 g/L. The inset shows the results obtained without filtration. The solid line has slope −1.

heating and dilution. However, SDS–PAGE electrophoresis showed that there were no covalent bonds.

3.4. Reversible gelation

The systems stopped flowing when tilted if the pH was decreased below 9.5 at room temperature after a waiting time on the order of minutes in the range of pH 8.5–9.5. Down to pH 8.5, gels were formed that remained visually homogeneous for a period of at least one week. Below pH 8.5, large scale heterogeneity and syneresis appeared after a time that decreased with decreasing pH. Below pH 8 this occurred very quickly after setting the pH and no homogeneous gels were formed down to about pH 4.2. Between pH 4.2 and 3.8 gels were formed, but again heterogeneity appeared after some time. Finally, below pH 3.5 homogeneous solutions were obtained that resembled those at pH 11 showing some precipitation with time.

Fig. 4 shows the storage (G') and loss (G'') moduli of a FPI solution (pH 9.0, C = 20 g/L) at a shearing frequency f = 0.01 Hz during heating from 5 °C to 60 °C and subsequent cooling back to 5 °C. At high temperatures the system is a liquid with $G'' > G'$. During cooling, both G' and G'' increase steeply below about 30 °C and G' crosses G'' at about 25 °C. The same cross-over temperature was found for repeated measurements at pH 8.5 and 9.0 at this concentration, but the gelling point shifted to lower temperatures at lower protein concentrations.

Apart from the reversible cross-over from $G'' > G'$ at high temperatures (liquid) to $G' > G''$ at low temperatures (gel) and the strong increase of both moduli below 30 °C, another strong indicator of the reversible gelation is the dependence of G' and G'' on the shearing frequency f at high and low temperatures. At high temperatures we found that $G'' \propto f$ and $G \propto f^2$, as expected for viscous liquids, see Fig. 2 in Supplementary data. At 5 °C both G' and G'' were almost independent of the frequency, see Fig. 5, showing that the system had gelled. Gelation induced by cooling could be reversed by heating that showed melting of the gel at approximately the same temperature, see Fig. 4. Gel formation and melting was observed in repeated cooling and heating cycles. We speculate that hydrogen bonds are formed when the system is cooled, but more work is needed to elucidate the reversible gelation mechanism.

Besides thermo-reversible bonds, slow irreversible aggregation leading to precipitation from solution (or gel disintegration) was observed at all pH values. The rate of irreversible cross-linking increased with decreasing pH down to pH 5.5. Rheological measurements of self supporting gels were thus limited to pH 8.5–9.5, since only in this range gels were stable at a time scale of days.

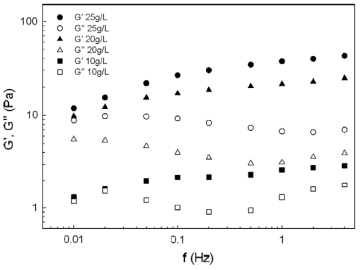

Fig. 5. Frequency dependence of G' and G'' of FPI gels (pH 9.0, 5 °C) at different concentrations indicated in the figure.

Fig. 5 shows the frequency dependence of G' and G'' of gels formed by direct cooling from 20 °C to 5 °C and pH 9.0 for different protein concentrations. Similar results were obtained at pH 8.5. G' was constant at high frequencies, but decreased slightly at lower frequencies. G'' was lower than G' over the whole frequency domain and showed a weak upturn at low frequencies indicating a dissipation process at low frequencies.

Both storage and loss moduli of FPI cooled directly from 20 °C to 5 °C and 1 Hz increased strongly with decreasing pH in the pH range 10.0–9.0. G' was typically two orders of magnitude higher at pH 9.0 than at pH 10.0 for protein concentrations between 15 and 25 g/L, but exhibited only a weak dependence on the pH between pH 9.0 and 8.5. We typically observed very low storage moduli for gels at pH 10.0; such weak gels were observed to break and flow when tilted. Above pH 10.0 the system is clearly a liquid with $G'' \propto f$. The same conclusion can be drawn from the fact that G' is larger than G'' at 1 Hz only at pH < 10.0, see Fig. 3 in Supplementary data.

The storage and loss moduli at 1 Hz are plotted as a function of the protein concentration in Fig. 6 for pH 9.0 at 5 °C. With decreasing concentration the gels become weaker and flow when tilted for

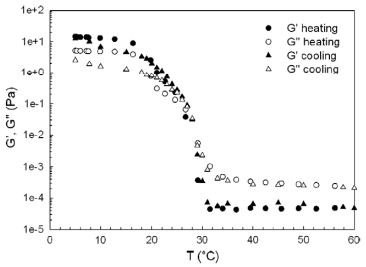

Fig. 4. Temperature dependence of G' and G'' at 0.01 Hz during heating and cooling of a FPI solution at pH 9.0 and C = 20 g/L. Filled symbols: G', open symbols: G''.

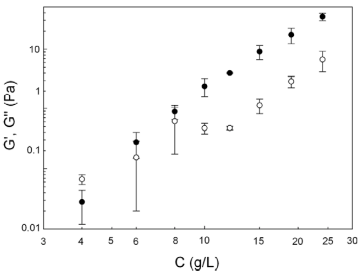

Fig. 6. Concentration dependence of G' (filled symbols) and G'' (open symbols) at 1 Hz of FPI gels (pH 9.0, 5 °C). The data represent averages of 4 trials and the error bars represent the standard deviation.

concentrations below 10 g/L. For pH 9.0, at $C = 5$ g/L and lower, G' at 1 Hz was less than G'' indicating that at such low concentration the system can no longer be considered a gel. At higher concentrations, G' increases strongly with increasing concentration and reaches about 35 Pa at 25 g/L. At pH 8.5 we found the same concentration dependence as at pH 9.0, but G' was roughly 50% higher than at pH 9.0 over the entire concentration range, see Fig. 4 in Supplementary data.

We only mention here that heating the systems above 30 °C influences the cold-setting gelation. The influence was small below pH 9.5 at the concentrations and frequencies studied here. However, it was important at higher pH at which self supporting gels did not form without preheating. When concentrated FPI solutions ($C = 25$ g/L) were heated above 30 °C and cooled down again, gelation was observed below a critical temperature of about 25 °C at pH values up to the pH at which FPI was isolated (11.0–11.2). These gels also exhibited reversible cold-setting, and melted when reheated again above 25 °C. A detailed study of the effect of preheating on cold-setting gelation of FPI will be reported elsewhere.

4. Summary

Cod muscle proteins could be solubilized to a large extent (about 60%) in alkaline solutions at pH > 11. Solutions of similar protein composition were obtained between pH 10.5–12.0, however, pH > 11 was required for optimal yield. Addition of salt (up to 0.25 M NaCl) did not affect protein yield or composition. A significant fraction of proteins was present in the solutions as large aggregates that slowly precipitated. These aggregates had a self similar structure with a fractal dimension close to two. When the pH was decreased below about 10, additional bonds were formed upon cooling leading to gelation below about 25 °C. The gels melted again at approximately the same temperature when the system was reheated. Irreversible aggregation also occurred at a rate that was very slow down to pH 8.5, but became increasingly faster with decreasing pH and was very fast below pH 8 and almost instantaneous below pH 7. Irreversible aggregation led to coarsening of the gel and syneresis at low temperatures or precipitation at high temperatures.

Acknowledgements

The AVS R&D fund of the Ministry of Fisheries in Iceland, The Icelandic Technology Development Fund, the Icelandic Research Center Student Fund and Jules Verne's Research fund are acknowledged for financial support of this work.

Appendix A. Supplementary data

Supplementary data associated with this article can be found, in the online version, at doi:10.1016/j.foodchem.2008.11.046.

References

Batista, I. (1999). Recovery of proteins from fish waste products by alkaline extraction. *European Food Research and Technology, 210*(2), 84–89.

Berne, B., & Pecora, R. (1976). *Dynamic light scattering*. New York: Wiley.

Bligh, E. G., & Dyer, W. J. (1959). A rapid method of total lipid extraction and purification. *Canadian Journal of Biochemistry, 37*, 911–917.

Brenner, T., Johannsson, R., & Nicolai, T. (2009). Characterisation of fish myosin aggregates using static and dynamic light scattering. *Food Hydrocolloids, 23*(2), 296–305.

Brown, W. (1996). *Light scattering: Principles and development*. Oxford: Clarendon Press.

Chawla, S. P., Venugopal, V., & Nair, P. M. (1996). Gelation of proteins from washed muscle of threadfin bream (*Nemipterus japonicus*) under mild acidic conditions. *Journal of Food Science, 61*(2), 362–366.

Choi, Y. J., & Park, J. W. (2002). Acid-aided protein recovery from enzyme-rich Pacific whiting. *Journal of Food Science, 67*(8), 2962–2967.

Foegeding, E. A., Lanier, T. C., & Hultin, H. O. (1996). Characteristics of edible muscle tissues. In O. R. Fennema (Ed.), *Food chemistry* (pp. 879–942). New York: CRC Press.

Higgins, J. S., & Benoit, H. C. (1994). *Polymers and neutron scattering*. Oxford: Clarendon Press.

Hu, D. H., Kimura, S., & Maruyama, K. (1986). Sodium dodecyl-sulfate gel-electrophoresis studies of connectin-like high-molecular-weight proteins of various types of vertebrate and invertebrate muscles. *Journal of Biochemistry, 99*(5), 1485–1492.

Hultin, H. O., & Kelleher, S. D. (2001). *Process for isolating a protein composition from a muscle source and protein composition*. US.

Kahn, L. N., Berk, Z., Pariser, E. R., Goldblith, S. A., & Flink, J. M. (1974). Squid protein isolate – Effect of processing conditions on recovery yields. *Journal of Food Science, 39*(3), 592–595.

Kilimann, M., & Heilmeyer, L. M. G. (1977). Effect of Mg^{2+} on Ca^{2+}-binding properties of non-activated phosphorylase kinase. *European Journal of Biochemistry, 73*(1), 191–197.

Kim, Y. S., Park, J. W., & Choi, Y. J. (2003). New approaches for the effective recovery of fish proteins and their physicochemical characteristics. *Fisheries Science, 69*(6), 1231–1239.

Kristinsson, H. G., & Ingadottir, B. (2006). Recovery and properties of muscle proteins extracted from tilapia (*Oreochromis niloticus*) light muscle by pH-shift processing. *Journal of Food Science, 71*(3), E132–E141.

Kristinsson, H. G., & Liang, Y. (2006). Effect of pH-shift processing and surimi processing on Atlantic croaker (*Micropogonias undulates*) muscle proteins. *Journal of Food Science, 71*(5), C304–C312.

Kristinsson, H. G., Theodore, A. E., Demir, N., & Ingadottir, B. (2005). A comparative study between acid- and alkali-aided processing and surimi processing for the recovery of proteins from channel catfish muscle. *Journal of Food Science, 70*(4), C298–C306.

Kristinsson, H. G., Theodore, A. E., & Ingadottir, B. (2007). Chemical processing methods for protein recovery from marine by-products and underutilized fish species. In F. Shahidi (Ed.), *Maximising the value of marine by-products* (pp. 144–168). Woodhead Publishing: Cambridge.

Laemmli, U. K. (1970). Cleavage of structural proteins during the assembly of the head of bacteriophage T4. *Nature, 227*(5259), 680–685.

Lanier, T. C. (2000). Surimi: Gelation chemistry. In J. W. Park (Ed.), *Surimi and surimi seafood* (pp. 237–265). New York: Marcel Dekker.

Lian, P. Z., Lee, C. M., & Chung, K. H. (2002). Textural and physical properties of acid-induced and potassium-substituted low-sodium surimi gels. *Journal of Food Science, 67*(1), 109–112.

Montecalvo, J., Constantinides, S. M., & Yang, C. S. T. (1984). Optimization of processing parameters for the preparation of flounder frame protein product. *Journal of Food Science, 49*(1), 172–176.

Nicolai, T. (2007). Structure of self-assembled globular proteins. In E. Dickenson & M. Leser (Eds.), *Food colloids. Interactions, microstructure and processing* (pp. 35–56). The Royal Society of Chemistry: Cambridge.

Provencher, S. W. (1982). Contin – A general-purpose constrained regularization program for inverting noisy linear algebraic and integral-equations. *Computer Physics Communications, 27*(3), 229–242.

Stefansson, G., & Hultin, H. O. (1994). On the solubility of cod muscle proteins in water. *Journal of Agricultural and Food Chemistry, 42*(12), 2656–2664.

Thawornchinsombut, S., & Park, J. W. (2007). Effect of NaCl on gelation characteristics of acid- and alkali-treated Pacific whiting fish protein isolates. *Journal of Food Biochemistry, 31*(4), 427–455.

Undeland, I., Hall, G., Wendin, K., Gangby, I., & Rutgersson, A. (2005). Preventing lipid oxidation during recovery of functional proteins from herring (*Clupea harengus*) fillets by an acid solubilisation process. *Journal of Agricultural and Food Chemistry, 53*(14), 5625–5634.

Undeland, I., Kelleher, S. D., & Hultin, H. O. (2002). Recovery of functional proteins from herring (*Clupea harengus*) light muscle by an acid or alkaline solubilisation process. *Journal of Agricultural and Food Chemistry, 50*(25), 7371–7379.

Venugopal, V., Doke, S. N., & Nair, P. M. (1994). Gelation of shark myofibrillar proteins by weak organic acids. *Food Chemistry, 50*(2), 185–190.

Wu, Y. J., Atallah, M. T., & Hultin, H. O. (1991). The proteins of washed, minced fish muscle have significant solubility in water. *Journal of Food Biochemistry, 15*(3), 209–218.

Yongsawatdigul, J., & Park, J. W. (2004). Effects of alkali and acid solubilisation on gelation characteristics of rockfish muscle proteins. *Journal of Food Science, 69*(7), C499–C505.

Paper 3. Brenner Tom, Nicolai Taco and Johannsson Ragnar. *Rheology of thermo-reversible fish protein isolate gels*. Food Research International, doi:10.1016/j.foodres.2009.04.020.

Rheology of thermo-reversible fish protein isolate gels

Tom Brenner[a,*], Taco Nicolai[b], Ragnar Johannsson[a]

[a]Matis, Biotechnology Division, Gylfaflot 5, 112 Reykjavik, Iceland

[b]Polymeres, Colloids, Interfaces, UMR CNRS, Université du Maine, 72085 Le Mans Cedex 9, France

Abstract.

Fish protein isolates (FPI) from cod muscle were studied at pH 9.0 and 11.0. Thermo-reversible gels, stable at and below room temperature could be produced at both pH values. Application of low shear stress to the gels led to an initial elastic response followed by a power-law deformation (creep) at both pH. Above a critical shear stress gels fractured and flowed regularly with a viscosity of about 0.05 Pa.s.

Strain-stress curves were recorded using both flow and oscillatory measurements. For all systems strain hardening was observed followed by fracture. Fracture occurred at approximately the same deformation, but the amplitude of strain hardening and the yield stress decreased with decreasing rate of the stress ramp. Results obtained from oscillatory shear at 1 or 0.1 Hz were close to those obtained with continuous shear during the fastest stress ramps.

The structure of the gels was investigated using confocal laser scanning microscopy and turbidity measurements.

Keywords: fish protein isolate; thermo-reversible gels; rheology; strain hardening; power-law creep

Introduction

Fish muscle proteins can be isolated by solubilising at extreme pH. The protein can be precipitated at the iso-electric point, which yields a heterogeneous suspension with a protein content close to 200g/L. Such suspensions of fish protein isolate (FPI) have been shown to undergo heat-induced irreversible gelation after addition of salt (Choi & Park, 2002; Kim, Park & Choi, 2003; Kristinsson & Liang, 2006; Kristinsson, Theodore, Demir & Ingadottir, 2005; Thawornchinsombut & Park, 2007; Undeland, Kelleher & Hultin, 2002; Yongsawatdigul & Park, 2004).

Recently, we have shown (Brenner, Johannsson & Nicolai, 2008) that non-precipitated FPI solutions extracted from cod muscle at pH 11 form homogeneous gels at room temperature if their pH is lowered to between about 9.5 and 8.5 and if the protein concentration is above about 6g/L. These gels melt when heated above about 25°C, but are reformed when cooled at the same temperature. Thermo-reversible gels can also be formed at pH 11 for C>15g/L, but only if they are preheated above 30°C. An advantage of these thermo-reversible gels is that they may be processed at higher temperatures as liquids after which gelation may be induced when desired by cooling.

The dynamic mechanical properties in the linear regime have been reported in a previous work (Brenner et al., 2008) for FPI gels formed at pH 9 and 8.5 without preheating. At high frequencies (f), the storage (G') and loss (G") shear moduli are almost frequency independent with G'>>G", but they decrease weakly at lower frequencies. For a given frequency, both G' and G'' increase with decreasing temperature and increasing concentration.

Here we report on the effect of preheating on the linear dynamic mechanical properties of FPI gels at pH 9 and pH 11. In addition, we have studied the non-linear rheology using both

continuous shear and large amplitude oscillatory shear. Non-linear rheology of food systems is important for sensory attributes (Montejano, Hamann & Lanier, 1985; vanVliet & Walstra, 1995), as well as the design of manufacturing processes. We determined complete stress-strain curves and creep measurements, which have rarely been reported for food systems.

Materials and Methods

Sample Preparation

Cod white muscle tissue was homogenized at pH 11, followed by centrifugation at 15000g for 10min. The supernatant was separated over gauze. During this procedure the temperature was kept below 10°C. Fresh cod was either used directly or frozen at -18°C and thawed prior to sample preparation. No effect of freezing on the rheology was observed. Cod caught near Iceland's shores, as well as near France, was used in the study. No difference in results presented here was found, but preparing protein solutions with concentrations above 20g/L was easier using cod caught near Iceland, independent of time of year. FPI at pH 11 was found to be stable during storage at 4°C for about 1 day, after which precipitation was usually observed.

The composition of the FPI obtained in this manner has been previously reported (Brenner et al., 2008). Protein concentration was determined by measuring the absorption at pH 12 and at a wavelength λ=289nm. The previously reported (Brenner et al., 2008) extinction coefficient (0.71 $L.g^{-1}.cm^{-1}$) was used after correcting for the effect of turbidity.

Freshly prepared FPI solutions were loaded into the rheometer at a given heating temperature. After a given heating time the solution was cooled to 5°C at a rate of 15°C/min

leading to gelation. Gels at pH 9 were also obtained by lowering the pH of the solution from 11 to 9 at 20°C while vigorously stirring before loading into the rheometer.

Rheology

Flow measurements were done on an AR-G2 stress-controlled rheometer (TA Instruments, New Castle, Delaware, USA) using cone-plate geometry (diameter 60mm, angle 1°). Oscillatory shear measurements were done with the aforementioned rheometer and set-up, as well as using a StressTech stress-controlled rheometer (Reologica, Lund, Sweden) with a couette geometry with inner and outer diameters of 25 and 27mm, respectively. A thin layer of paraffin oil was added to prevent evaporation. Measurements were done at 5°C unless otherwise indicated.

Confocal microscopy and turbidity

Confocal scanning light microscopy (CSLM) images were obtained using a Leica TCS-SP2 microscope (Leica Microsystems Heidelberg, Germany). The water-immersion objective lens used was HCx PL APO 63x NA=1.2, and its specified theoretical resolution in the x-y plane was 0.3µm. The turbidity of FPI solution was measured using a spectrophotometer Varian Cary-50 Bio (Les Ullis, France).

Results

Low amplitude oscillatory shear measurements

The FPI gels were studied at 5°C, which is the typical temperature for chilled food products and gives higher shear moduli than at room temperature. Figure 1 shows the frequency dependence of G' and G'' of FPI gels (C=25g/L) at pH 9.0 both before and after preheating at 60°C for 3 minutes. The effect of heating time on the frequency-dependence of G' and G'' was found to be insignificant beyond 3 minutes at 30°C or higher. The frequency dependence was weak in the high frequency regime and the values before and after preheating were close. Before preheating the shear moduli decreased at lower frequencies and G" was larger than G' for f<0.01Hz, and the curves tended towards the limiting behaviour for liquids ($G' \propto f^2$, $G'' \propto f$) at the very lowest frequencies close to $f=10^{-4}$Hz. After preheating, G' and G" showed much weaker frequency dependence of both moduli in the low-frequency regime and G'>G" down to at least 10^{-4} Hz.

Figure 2 shows the frequency dependence of G' for FPI heated for 3 minutes at different temperatures. Preheating at 30°C already led to much weaker frequency dependence. Increasing the heating temperature from 30°C to 40°C led to even weaker frequency dependence, but further increase in the range 40°C-80°C had only a weak effect on the frequency dependence.

G' of the sample preheated at 80°C was significantly lower than at lower temperatures, see figure 2. We already noted in earlier work (Brenner et al., 2008) that the high frequency shear modulus G'_0 defined as G' at f=1Hz was only weakly affected by preheating, with the caveat that preheating did not lead to extensive hydrolysis. Isolation of fish proteins at extreme pH does not deactivate proteases endogenous to the muscle that cause protein degradation (Brenner et al., 2008; Choi et al., 2002; Kim et al., 2003; Thawornchinsombut et al., 2007), especially above 50°C (Lanier, 2000). In general, we found degradation to be noticeable if the heating time exceeded several hours at 30°C, about 30 minutes at 50°C and a few minutes at 80°C.

At pH 9.5-11 FPI did not readily form gels unless first heated for several minutes above 30°C and subsequently cooled down again below 25°C. Preheating of FPI at pH 11 led to gels for

C>15g/L with G'_0 at 5°C in the range 8-30 Pa for C=25g/L and 2-10 Pa for C=20g/L. The variance of G'_0 between different sample preparations was stronger than any effect of the heating temperature or heating time, see below. The frequency dependence of elastic moduli of gels at pH 11 formed after preheating is even weaker than for gels formed after preheating at pH 9, see figure 3. As at pH 9, the effect of heating-time beyond 3 minutes and heating temperature beyond 30°C on G' and G'' is very weak unless it leads to significant hydrolysis. As mentioned earlier, at pH 11 FPI solutions kept at 20°C did not gel when cooled, but they did gel after several hours of preheating at 25°C.

Continuous shear flow

Creep measurements. The strain of FPI gels was recorded as a function of time (t) at constant applied stress (σ) at T=5°C. Figure 4a shows the time-dependence of γ for gels at pH 9.0 and 11.0 preheated for 5 minutes at 30°C. After applying stress the systems deform initially very rapidly to γ_0 followed by slow creep. γ_0 increased linearly with σ: $\sigma=G_0.\gamma_0$, with G_0 close to the high frequency shear modulus (G'_0) obtained from low amplitude oscillatory shear. The initial rapid deformation was followed by an increase of the deformation that was weaker than linear with time. After cessation of the stress the initial deformation was recovered immediately and part of the subsequent slow deformation was also recovered slowly.

At both pH, the time-dependent increase of the strain at different stresses could be described by a power-law, see fig. 4:

$$\gamma(t) = \gamma_0\left(1 + \left(t/\tau\right)^{\alpha}\right) \qquad (1)$$

Above a critical strain of about 1.5 the systems started to flow, probably caused by large scale fracture of the gel. Fracture was more difficult to discern at pH 9 than at pH 11, compare figures 4a and 4b, as the deviation from the power law creep was weaker. The power-law creep is observed more readily in figure 4c where $(\gamma(t)/\gamma_0-1)$ is plotted as a function of time. Using this representation, we obtained within the experimental error master-curves for individual samples measured at different stresses. For the data shown in figure 4, the power law exponent α was close at both pH, 0.3, but the characteristic times τ differed significantly (5000s and 5s at pH 11 and 9, respectively). Creep measurements of different preparations could not be represented by a single master-curve at each pH. The power-law exponent α was in the range 0.3-0.4 for pH 11, and a variance was found also in the characteristic time τ (1000-5000s). Greater variance of both parameters was found for pH 9, with α in the range 0.3-0.7 and τ in the range 1-25s. Of course, for high values of α, any deviation towards a steady-state flow may strongly influence the apparent power-law observed before fracture. While we observed upward deviations from the power-law and fracture for both pH, we observed downward deviations and a plateau only for pH 9. Samples at pH 11 which did not fracture followed power-law creep up to 10^5s.

For σ>5Pa at pH 11 and for σ>40Pa at pH 9 the systems shown in figure 4 immediately fractured and flowed with a constant flow rate. We may define a yield stress as the lowest stress at which the systems flow immediately. Similar behaviour was found for all gels with yield stresses that increased with increasing G'_0, see below.

Stress ramps. The deformation was recorded as a function of applied stress that was increased linearly with time at different rates ($d\sigma/dt$). Strain-stress curves of a system at pH 11.0 (C=20g/L, G'_0 = 4.8Pa) are shown in figure 5a. In order to show more clearly the non-linear behaviour the same data are shown in figure 5b in terms of the inverse of the compliance, or an

effective shear modulus, $G \equiv \sigma/\gamma$ as function of σ. At small deformations and in the absence of significant creep, i.e. for fast rates, G should be a constant G_0 close to G'_0. Results obtained for gels with different G'_0 were found to be close if they were compared at the same initial flow rates: $d\gamma/dt=(d\sigma/dt)/G_0$.

At all rates the systems fractured at approximately the same deformation ($\gamma_f \approx 1.5$), but the stress at fracture (σ_f) increased with increasing rate. Before fracture the strain increased less than the stress, which is usually called strain hardening. Strain hardening caused the maximum (G_{max}) of G as a function of σ seen in figure 5b. The amplitude of strain hardening (G_{max}/G_0) decreased with decreasing flow rates, because the effect of creep became more important leading to weak shear softening before shear hardening became significant. Notice that for $d\gamma/dt<0.005\ s^{-1}$ the amplitude was less than unity, because the initial strain softening due to creep became more important than the subsequent strain hardening. The increase of σ_f (defined as the stress at G_{max}) with increasing shear rate can be explained by the combination of increasing shear hardening and decreasing effect of creep. Strain-stress curves of gels at pH 9.0 were similar to those at pH 11.0, see figure 6.

At both pH strongly sheared samples slowly gelled again after cessation of the stress. The linear rheological properties of these gels were similar, but their yield stress was lower. This indicates that broken cross-links reformed, but that the network had more defects. Strongly sheared gels could be fully regenerated by heating for a short time above 30°C. Repeated measurements after reheating gave the same yield stress within the experimental error.

When the applied stress was larger than the yield stress, the systems at both pH flowed rapidly ($\dot{\gamma} > 100 s^{-1}$) with a viscosity of about 0.05Pa.s. The flow rate was subsequently reduced in steps and the stress was measured at each flow rate as a function of time. With decreasing flow

rate the stress decreased towards an average value close to σ_f and then remained constant, see figure 7. However the stress fluctuated significantly around the average value as indicated by the error bars in figure 7. These results can be explained by a dynamic equilibrium between breaking and formation of bonds. If the stress increases above σ_f bond breaking dominates causing an increase of the shear rate while if it is lower bond formation dominates causing a decrease of the shear rate. The fluctuation with time occurs, because the dynamics of bond breaking and formation are relatively slow. On time scales longer than a few hours the system evolved irreversibly at a given flow.

Large Amplitude Oscillatory Shear

The strain response of the system to imposed sinusoidal stress became increasingly non-sinusoidal with increasing stress or strain beyond the linear regime. However, maximum stress - maximum strain curves obtained using oscillation with frequencies of 1Hz or 0.1 Hz coincided with stress-strain curves obtained using continuous shear measurements at the highest rates accessible experimentally, see e.g. figures 5 and 6. The calculated values of G' were close to G derived from continuous shear measurements up to fracture, which is expected since G'>>G". The advantage of using oscillatory shear over continuous shear is that creep can be neglected at the frequencies used here.

Gels produced at both pH values showed linear dependence of the stress on the strain at moderate strains (up to ~0.1 for pH 9 and ~0.3 for pH 11), followed by strain hardening up to fracture. Figure 8 shows normalized values of the storage modulus G'/G'_0 of gels prepared after preheating at different temperatures of FPI at pH 11. The strain (γ_f) and stress (σ_f) at fracture were defined as the values where $G'=G'_{max}$. These measurements were done at 1 Hz, but results obtained

214 at 0.1 Hz were the same within the experimental error. No significant effect was observed of the
215 preheating temperature or of the preheating time. The stress at fracture obtained in this way is
216 equal to the yield stress above which the systems flow immediately during constant application of
217 stress.

218 Figure 9 shows G'/G'_0 as a function of strain for FPI gel produced at pH 9 (C=25g/L)
219 without preheating and after preheating for 10 min at different temperatures. Non-preheated gels
220 fractured at strains in the range 0.3-0.4 and showed only weak strain hardening. Gels preheated at
221 30°C showed reproducible results of G'/G'_0 versus γ with strain-hardening behaviour similar to
222 that observed at pH 11. G'_{max}/G'_0 values were in the range 1.5-1.7 and γ_f was in the range 0.75-
223 0.85, independent of the heating time. Gels preheated at 40°C or higher often showed fracture at
224 small strains with no strain-hardening, as illustrated in figure 9. However, sometimes they
225 exhibited strain-hardening resembling that of gels preheated at 30°C. We emphasize that the
226 difference in behaviour was caused by the heating temperature and not by the heating time.

227 We have previously reported that for gels formed at pH 9 without preheating G'_0 increased
228 strongly with increasing protein concentration in the concentration range 6-25g/L (Brenner et al.,
229 2008). As noted above, G'_0 was only slightly affected by preheating so that the concentration range
230 at which we could measure gels using rheology was not changed after preheating. Gels at C=6g/L
231 showed no strain-hardening and broke at very low stresses, while for C=8g/L we observed
232 sometimes strain hardening and sometimes immediate fracture. Gels in the concentration range
233 10-25g/L exhibited always strain-hardening behaviour after preheating at 30°C.

234 Figure 10a shows the strain dependence of G' for gels in the concentration range 8-25g/L at
235 pH 9, and figure 10b shows the same data after normalisation with G'_0. The preheating
236 temperature for this experiment was chosen as 30°C because, as noted above, at this temperature
237 gels showed the most reproducible and strongest strain hardening. The strain dependence of G'/G'_0

238 was similar for all concentrations, but the variance of G'_{max}/G'_0 and γ_f was larger at lower
239 concentrations. For all concentrations, γ_f was in the range 0.5-1.1 and G'_{max}/G'_0 in the range 1.3-
240 2.0.

241 The dependence of the normalized moduli on the strain was different for gels at pH 11 and
242 pH 9 even at the same concentration and heat treatment. This is illustrated in figure 11, where the
243 strain dependence of the normalized moduli is plotted for different gels with C=25g/L after
244 preheating at 30°C. At each pH there was some variance of γ_f and G'_{max}/G'_0, but this was only
245 weakly correlated to the much larger variance of G'_0, see below. Clearly, the onset of strain
246 hardening and fracture starts at larger strains at pH 11 than at pH 9.

247 The strain and stress at fracture, and the maximum strain hardening are plotted in figure 12
248 as a function of G'_0 for all systems that were investigated both at pH 9 and 11. All three parameters
249 show significant scattering, but certain tendencies can be distinguished. Figure 12a shows that the
250 strain at fracture of gels at pH 9 did not depend on G'_0 and was smaller than at pH 11 where it
251 decreased weakly with increasing G'_0. The relative amplitude of the shear hardening decreased
252 very weakly with increasing G'_0 at both pH and was slightly larger at pH 9, see figure 11b. Finally,
253 σ_f increased almost linearly with G'_0, see figure 11c, which is, of course, a direct consequence of
254 the weak dependence of γ_f and G'_{max}/G'_0.

255

256 **Structure**

257

258 The structure of the gels on length scales larger than about 0.3μm can be investigated using
259 CSLM. Typical CSLM images of FPI at 5°C are shown in figure 13. At pH 11, the images were
260 homogeneous both before preheating when the system was liquid, and after preheating when the

261 system has gelled. Also at pH 9, no features could be observed either in the liquid state at 50°C or
262 in the gelled state at 5°C. This means that the gel was homogeneous at least down to 0.3μm.
263 However, in all systems protein rich domains with a diameter of a few microns could be
264 seen that were randomly distributed in the homogeneous matrix. These domains were found to
265 have a protein density 4 to 6 times higher than the average, i.e. about 100-150g/L, which is close
266 to typical protein concentrations of precipitates formed at pI. We previously reported (Brenner et
267 al., 2008) the presence of very large protein aggregates, characterized with a fractal dimension
268 close to 2, which were present in FPI already after solubilization at pH 11. The presence of these
269 large aggregates precludes structural studies of the gel with light-scattering, since they dominate
270 the intensity of light scattered from the samples. The aggregates could be removed by filtration at
271 lower protein concentrations, which led to a decrease of about 15% of the protein concentration
272 (Brenner et al., 2008). We were not able to remove the aggregates by centrifugation or filtration at
273 high protein concentrations due to the high viscosity of the solutions.
274 Interestingly, protein poor domains appeared at both pH after a waiting time that fluctuated
275 strongly between different samples, but was typically 1-4 days at 5°C. The protein poor domains
276 were spherical with a radius of a few microns and also randomly distributed in the homogeneous
277 matrix. The protein concentration in these domains was typically 25%-50% of the average protein
278 concentration, i.e. 5-10g/L. We speculate that the protein poor domains are caused by the slow
279 phase separation of the system.
280 Although CSLM showed no difference between the liquid and the gelled state on length
281 scales larger than 0.3μm, turbidity measurements showed that the gel structure did change.
282 Unheated FPI solutions (C=25g/L) at pH 9 and pH 11 were inserted in the spectrophotometer. The
283 solutions were subsequently heated at 50°C; cooled to 5°C; and finally heated again to 50°C. The
284 turbidity during this heat treatment is plotted in Figure 14. At both pH gelation leads to an increase

of the turbidity which is reversed by melting at higher temperatures. At all temperatures the turbidity is higher at pH 9 than at pH 11. These results imply that the system is more homogeneous at pH 11, probably because electrostatic repulsion is more important. They also imply that cross-linking leads to an increased heterogeneity, as might be expected. Unfortunately, as mentioned above, the presence of the large protein aggregates rendered a more detailed investigation of the structure using light scattering impossible.

Discussion

FPI solutions gel when the pH is decreased to below 9.5, i.e. when the charge density of the proteins is lowered. This suggests that cross-linking is made possible by reduced electrostatic repulsion. Homogeneous gels are formed only in a narrow pH range between 9.5 and 8.5. At even lower pH the system becomes rapidly heterogeneous and visible protein flocs are formed. Even at pH 9 gels become increasingly heterogeneous over a period of days, showing that the system is basically unstable at all values of the pH where cross-linking occurs.

We speculate that homogeneous gels are formed only when electrostatic repulsion is low enough to allow cross-linking, but still important enough to inhibit rapid densification, and the contribution of attractive opposite-charge interactions facilitates gel formation at an intermediate pH range, i.e. 8.5-9.5. The evolution of the gels with time shows that the bonds are to some extent reversible, which may also explain the decrease of G' and G" with decreasing frequency at low frequencies. Preliminary measurements showed that adding salt to FPI solutions caused a lowering of the pH where the gels were formed. However, it also reduced the pH range in which homogeneous gels could be formed. The effect of adding salt indicates that opposite charges might

be involved in the cross-links. On the other hand, the gel strength increased with decreasing temperature indicating possible involvement of hydrogen bonds.

Heating FPI solutions above about 30°C modifies at least some of the proteins in the mixture. As a consequence, gels are formed at all pH up to at least 11, when FPI solutions are cooled below about 25°C. Bonding in this case is probably caused by a temperature reversible conformational transition of some proteins, because the gels melt again when heated above 25°C. One could imagine that gelation induced by lowering the pH was caused by the same conformational transition. However, the frequency dependence of G' and G" was not the same at low frequencies before and after preheating, demonstrating the effect of heating even at lower pH. After fracture the bonds reformed slowly, demonstrating their reversibility even at 5°C, but gels formed from highly sheared systems had a lower yield stress. Gels with the original higher yield stress were formed only after reheating the sheared systems above 30°C. We note here that currently 2 processing plants in Iceland take advantage of an isolation process from fish cut-offs, similar to that reported herein. The thermo-reversible gelation described, as well as the ability of gels to reform at rest after fracture, allow for use of the FPI in solutions injected back into fish fillets. The injected FPI is allowed to gel in-situ in the fillet, and increases the weight of the fillet. No problems of FPI "dripping" after injection have been observed.

At low applied stresses the systems crept with a strain that increased more weakly than linearly with the time, but did not reach a plateau. At pH 11, and some of the samples at pH 9, the strain could be fitted to a power-law with an exponent close to 1/3, which is, interestingly, also observed for metals (Nabarro, 2004). We could not identify a stress below which no creep occurred, though for pH 9 it was observed in one instance that creep totally stagnated after 1 day. Macroscopically the gels showed no flow when the vials were left tilted overnight even though they showed large deformation.

When the applied stress exceeded a certain value, the gels fractured and started to flow. In a small range of applied stresses the flow started only after a period of creep that increased rapidly with decreasing stress. Apparently, in this range the tension in the system accumulated with time until it led to fracture. Remarkably, fracture occurred at approximately the same deformation independent of the time it took to reach this deformation.

Creep measurements on food related systems and aqueous gels in general are rare, but recently, Caton and Baravian (2008) studied creep of several food products. They observed similar behaviour to that reported here, i.e. a fast elastic response, followed by a power law creep and finally fracture leading to regular flow. They also found that the duration after which the systems fractured increased with decreasing applied stress, but that the deformation at fracture was approximately constant. They made the interesting observation that the time of fracture increased exponentially with decreasing stress. They also noted that for the lowest stress in their presented data, no fracture was observed within a time one order of magnitude longer than that calculated with the (empirical) exponential relation of stress and time-to-fracture. Their interpretation was that "...there exists a minimal stress necessary to fluidize the material. This minimal stress defines a critical stress below which flow seems forbidden… there seems to exist a critical stress below which the material will never experience apparent or true flow". Our observations of a plateau reached during application of low stresses to FPI gels at pH 9 lead to the same conclusion. We could not find such a plateau during creep measurements at pH 11. It was observed for both pH, however, that fractured systems reformed under application of low stresses. In these cases reformation under shear was indicated by a very sharp decrease in deformation rate, after which the deformation rate kept decreasing, indicating that true flow cannot be reached at these stresses.

Creep accounts for the dependence of strain-stress curves on the rate of the stress ramp. Slow stress ramps allow for more creep and thus fracture will occur at lower stress. A dependence

356 on the rate of the stress ramp has been observed before for protein gels, e.g. whey protein gels
357 (Lowe, Foegeding & Daubert, 2003), emulsion filled whey protein gels (Sala, van Vliet, Cohen
358 Stuart, van Aken & van de Velde, 2008) and gelatin gels (Bot, vanAmerongen, Groot, Hoekstra &
359 Agterof, 1996), but was not shown experimentally to be related to creep.

360 Shear hardening has also been observed for other protein gels. For gelatin gels, strain
361 hardening was reported at strains exceeding 0.5 in shearing experiments and 0.1 in compression
362 experiments (Bot et al., 1996; Groot, Bot & Agterof, 1996). For whey protein isolates, strain-
363 softening followed by strain hardening above strains of about 1 (Lowe et al., 2003) as well as
364 monotonous strain hardening above strains of 0.1 (Li, Errington & Foegeding, 1999) have been
365 reported. Gels of bovine serum-albumin (Hagiwara, Kumagai & Matsunaga, 1997) and β-
366 lactoglobulin (Pouzot, Nicolai, Benyahia & Durand, 2006) strain-harden to various extents
367 depending on total protein concentration (and therefore elastic modulus) before fracture.
368 Observations of the dependence of strain at fracture (γ_f) on gel strength have been reported for
369 several food systems and protein gels in particular. γ_f was found to be roughly a constant up to
370 G_0=100Pa and decreased less strongly than linearly with increasing G_0 above 100Pa for gels of β-
371 lactoglobulin at neutral pH (Pouzot et al., 2006). Conversely, a monotonous decrease of γ_f with
372 increasing protein concentrations (and therefore G_0) was found for gelatin gels (Bot et al., 1996)
373 and gels of whey protein mixtures (Foegeding, 1992; Li et al., 1999; Lowe et al., 2003), at least up
374 to protein concentrations of 15%.

375 For globular protein gels it was shown by scattering techniques that they are self-similar
376 below the gel's correlation length and are characterized by a single fractal dimension at certain
377 conditions of pH and ionic strength (Nicolai, 2007). Therefore strain hardening of β-lactoglobulin
378 gels could be described with the model proposed by Gisler, Ball and Weitz (1999) for strain-
379 hardening of fractal gels. This was done by Pouzot et al. (2006) who also showed structural results

380 from strain-hardening analysis and light scattering predicted correctly concentration dependence
381 of the linear regime elastic modulus of β-lactoglobulin gels. The same strain-hardening model of
382 fractal gels could also be used to describe the shear hardening of FPI gels observed in this study,
383 but we were not able to establish whether FPI gels had a self-similar structure.

384 As was noted above, the reversible increase of turbidity during cooling at both pH
385 indicates a reversible gelation mechanism is at work, which we had previously deduced from a
386 reversible increase of the elastic modulus during cooling. Reversible aggregation of purified cod
387 myosin at pH 6-8 and a high salt concentration was previously deduced from a reversible increase
388 of both turbidity and scattered light intensity during cooling of preheated cod myosin solutions
389 (Brenner, Johannsson & Nicolai, 2009). Such thermo-reversible aggregation of myosin may be
390 related to, or explain in part, the gelation we observe for FPI. At pH 11, the turbidity at 5°C is
391 higher after preheating than before preheating, which we expect since gel formation was observed
392 using rheology only after preheating. At pH 9, the turbidity is very similar at 5°C before and after
393 heating, which suggests a similar structure is formed in both cases. The different rheology of gels
394 at pH 9 before and after preheating suggests that preheating promotes stronger bond formation
395 without modifying structure significantly. As mentioned above, the lower turbidity at pH 11
396 compared to at pH 9 is probably caused by the stronger electrostatic repulsion at pH 11. This
397 might also explain why the gel strength decreases much more rapidly with decreasing protein
398 concentration at pH 11.

399

400 **Summary**

401

402 Gelation of FPI solutions obtained by dissolving fish muscle proteins at pH 11 can be
403 induced either by decreasing the pH to below pH 9.5 or by preheating above 30°C. Although

preheating is not required for gelation below pH 9.5, it leads to gels with a weaker low frequency dependence of the shear moduli. Duration and temperature of heating have very little influence on the rheological properties of the gels beyond 3 min and 40°C, respectively. FPI gels melted above about 25°C and reformed rapidly after cooling to below about the same temperature.

At low constant shear stresses, the gels showed slow power law creep, while above a certain stress the gel fractured leading to flow. Strongly sheared systems were macroscopically homogeneous liquids with relatively low viscosity, but slowly gelled again after cessation of the stress, as well as under low stresses below the minimal stress needed to fluidize the system. The stress at fracture decreased when the stress ramp was slower, while the strain at fracture was independent of the rate of stress increase. Oscillatory stress at 1Hz yielded results that were close to those obtained with the fastest stress ramps available experimentally.

Gels showed similar strain hardening patterns independent of preheating temperature at pH 11. The strain-hardening of gels produced at pH 9 depended on the temperature. It was always found for gels preheated at 30°C, but preheating at higher temperatures most often led to gels that fractured at low stresses and with very weak or no strain hardening.

The strain at fracture varied weakly with the elastic shear modulus of the gels, but it was systematically larger at pH 11 than at pH 9 even when the latter was preheated to 30°C. The amplitude of shear hardening also depended only weakly on the elastic modulus of the gels, implying that the stress at fracture increased almost linearly with G'_0.

FPI solutions were homogeneous at length scales above 0.3μm both in the liquid and in the gel state, but contained micron sized protein aggregates. Turbidity measurements showed that the gel structure on smaller length scales was more homogeneous at pH 11 than at pH 9 and that gelation increased the heterogeneity.

Acknowledgements

We thank Lazhar Benyahia for critical reading of the manuscript and stimulating discussions on creep behaviour. The AVS R&D fund of the Ministry of Fisheries in Iceland, The Icelandic Technology Development Fund, the Icelandic Research Center Student Fund and Jules Verne's Research fund are acknowledged for financial support of this work.

References

Bot, A., vanAmerongen, I. A., Groot, R. D., Hoekstra, N. L., & Agterof, W. G. M. (1996). Effect of deformation rate on the stress-strain curves of gelatin gels. *Journal De Chimie Physique Et De Physico-Chimie Biologique*, *93*(5), 837-849.

Brenner, T., Johannsson, R., & Nicolai, T. (2008). Characterisation and thermo-reversible gelation of cod muscle protein isolates. *Food Chemistry*, *doi:10.1016/j.foodchem.2008.11.046*.

Brenner, T., Johannsson, R., & Nicolai, T. (2009). Characterization of fish myosin aggregates using static and dynamic light scattering. *Food Hydrocolloids*, *23*(2), 296-305.

Caton, F., & Baravian, C. (2008). Plastic behavior of some yield stress fluids: from creep to long-time yield. *Rheologica Acta*, *47*(5-6), 601-607.

Choi, Y. J., & Park, J. W. (2002). Acid-aided protein recovery from enzyme-rich Pacific whiting. *Journal of Food Science*, *67*(8), 2962-2967.

Foegeding, E. A. (1992). Rheological properties of whey protein isolate gels determined by torsional fracture and stress-relaxation. *Journal of Texture Studies*, *23*(3), 337-348.

Gisler, T., Ball, R., & Weitz, D. A. (1999). Strain hardening of fractal colloidal gels. *Physical Review Letters*, *82*(5), 1064-1067.

Groot, R. D., Bot, A., & Agterof, W. G. M. (1996). Molecular theory of strain hardening of a polymer gel: Application to gelatin. *Journal of Chemical Physics*, *104*(22), 9202-9219.

Hagiwara, T., Kumagai, H., & Matsunaga, T. (1997). Fractal analysis of the elasticity of BSA and beta-lactoglobulin gels. *Journal of Agricultural and Food Chemistry*, *45*(10), 3807-3812.

Kim, Y. S., Park, J. W., & Choi, Y. J. (2003). New approaches for the effective recovery of fish proteins and their physicochemical characteristics. *Fisheries Science*, *69*(6), 1231-1239.

Kristinsson, H. G., & Liang, Y. (2006). Effect of pH-shift processing and surimi processing on Atlantic croaker (Micropogonias undulates) muscle proteins. *Journal of Food Science*, *71*(5), C304-C312.

Kristinsson, H. G., Theodore, A. E., Demir, N., & Ingadottir, B. (2005). A comparative study between acid- and alkali-aided processing and surimi processing for the recovery of proteins from channel catfish muscle. *Journal of Food Science*, *70*(4), C298-C306.

Lanier, T. C. (2000). Surimi: gelation chemistry. In: J. W. Park, *Surimi and surimi seafood* (pp. 237-265). New York: Marcel Dekker.

Li, H., Errington, A. D., & Foegeding, E. A. (1999). Isostrength comparison of large-strain (fracture) rheological properties of egg white and whey protein gels. *Journal of Food Science*, *64*(5), 893-898.

Lowe, L. L., Foegeding, E. A., & Daubert, C. R. (2003). Rheological properties of fine-stranded whey protein isolate gels. *Food Hydrocolloids*, *17*(4), 515-522.

Montejano, J. G., Hamann, D. D., & Lanier, T. C. (1985). Comparison of torsional failure and texture profile characteristics of selected heat-induced protein gels. *Journal of Texture Studies*, *16*(4), 403-424.

Nabarro, F. R. N. (2004). Do we have an acceptable model of power-law creep? *Materials Science and Engineering a-Structural Materials Properties Microstructure and Processing*, *387*, 659-664.

Nicolai, T. (2007). Structure of self-assembled globular proteins. In: E. Dickenson, & M. Leser, *Food colloids. Interactions, microstructure and processing* (pp. 35-56). Cambridge: The Royal Society of Chemistry.

Pouzot, M., Nicolai, T., Benyahia, L., & Durand, D. (2006). Strain hardening and fracture of heat-set fractal globular protein gels. *Journal of Colloid and Interface Science*, *293*(2), 376-383.

Sala, G., van Vliet, T., Cohen Stuart, M. A., van Aken, G. A., & van de Velde, F. (2008). Deformation and fracture of emulsion-filled gels. Effect of oil content and deformation speed. *Food Hydrocolloids*, *doi: 10.1016/j.foodhyd.2008.11.016*.

Thawornchinsombut, S., & Park, J. W. (2007). Effect of NaCl on gelation characteristics of acid- and alkali-treated Pacific whiting fish protein isolates. *Journal of Food Biochemistry*, *31*(4), 427-455.

Undeland, I., Kelleher, S. D., & Hultin, H. O. (2002). Recovery of functional proteins from herring (Clupea harengus) light muscle by an acid or alkaline solubilization process. *Journal of Agricultural and Food Chemistry*, *50*(25), 7371-7379.

vanVliet, T., & Walstra, P. (1995). Large deformation and fracture behaviour of gels. *Faraday Discussions*, *101*, 359-370.

Yongsawatdigul, J., & Park, J. W. (2004). Effects of alkali and acid solubilization on gelation characteristics of rockfish muscle proteins. *Journal of Food Science*, *69*(7), C499-C505.

Figure captions

Figure 1. Frequency dependence of G' (filled symbols) and G'' (open symbols) for FPI gels at pH 9.0 (C=25g/L, 5°C) before and after preheating at 60°C for 3 minutes.

Figure 2. Frequency dependence of G' for FPI gels at pH 9.0 (C=25g/L, 5°C) preheated for 3 minutes at different temperatures indicated in the figure.

Figure 3. Frequency dependence of G' (filled symbols) and G'' (open symbols) for FPI gels at pH 11.0 (C=25g/L, 5°C) before and after preheating for 3 minutes at 30°C or 60°C.

Figure 4. Strain as a function of time at different applied stresses indicated in the figures for preheated gels at pH 11 (C=20g/L, G_0 = 5Pa) (a) and at pH 9 (C=20g/L, G_0 = 40Pa) (b). Figure 4c shows the same data in a different representation. The solid lines in fig. 4c have a slope of 0.3.

Figure 5. Strain-stress curves of FPI gels at pH 11 (C=20g/L, G_0=4.8Pa, 5°C) are shown figure 5a. The open symbols indicate flow measurements at different initial flow rates ($d\gamma/dt=(d\sigma/dt)/G_0$) indicated in the figure, while the filled symbols indicate oscillatory measurements at f=1Hz. The solid line represents $\gamma=\sigma/ G'_0$. A different representation of the same data is shown in figure 5b: $G = \sigma/\gamma$ versus σ.

Figure 6. Strain-stress curves for FPI gels at pH 9 (C=17g/L, G_0=11Pa). The open symbols indicate flow measurements at different initial flow rates ($d\gamma/dt=(d\sigma/dt)/G_0$) indicated in the figure,

519 while the filled symbols indicate oscillatory measurements at f=1Hz. The solid line represents
520 $\gamma=\sigma/ G'_0$.
521
522 Figure 7a. Steady-state viscosities as a function of the shear-rate for FPI gels at pH 11 (open
523 symbols) and pH 9 (filled symbols) (C=20g/L, 5°C). Error bars are indicated in the figure.
524 Figure 7a. The same data as in figure 7a, given as the measured shear stress as a function of the
525 shear rate. Error bars are indicated in the figure. The horizontal lines represent estimates of the
526 yield stress of each sheared system; for pH 9, σ_f = 13Pa and for pH 11 σ_f = 0.7Pa.
527
528 Figure 8. Normalized elastic modulus as a function of the strain for FPI gels at pH 11 after
529 preheating for 10 min at different temperatures indicated in the figure (C=25g/L, 5°C).
530
531 Figure 9. Normalized elastic modulus as a function of the strain for FPI gels at pH 9 after
532 preheating for 10 min at temperatures indicated in the figure (C=25g/L, 5°C).
533
534 Figure 10. Strain dependence of the elastic moduli before (9a) and after normalization (9b) at pH
535 9. Protein concentrations are indicated in figure 10b.
536
537 Figure 11. Strain dependence of the normalized elastic moduli of FPI gels at pH 9 (filled symbols)
538 and pH 11 (closed symbols) after preheating at 30°C (C=25g/L, 5°C).
539
540 Figure 12. Fracture strain γ_f (a), normalized elastic modulus G'_m/G'_0 (b) and stress σ_f (c) as a
541 function of G'_0. Filled symbols: pH 9, open symbols: pH 11.
542

543 Figure 13. CSLM images of FPI. a: pH 11 at 5°C before preheating, b: pH 11 at 5°C after
544 preheating, c: pH 11 after 4 days at 5°C, d: pH 9 at 50°C, e: pH 9 at 5°C after preheating, f: pH 9
545 after 1 day at 5°C. The width of the images represents in all cases 160µm. Large protein
546 aggregates are visible as white spots, while the arrows indicate protein poor domains in figures
547 14c and 14f.
548
549 Figure 14. Turbidity at a wavelength of 633nm for FPI solutions (C=25 g/L) at pH 9 and 11.
550 Unheated samples were first measured at 5°C, then heated to 50°C, cooled to 5°C and finally
551 heated again to 50°C.
552
553

554 Figure 1

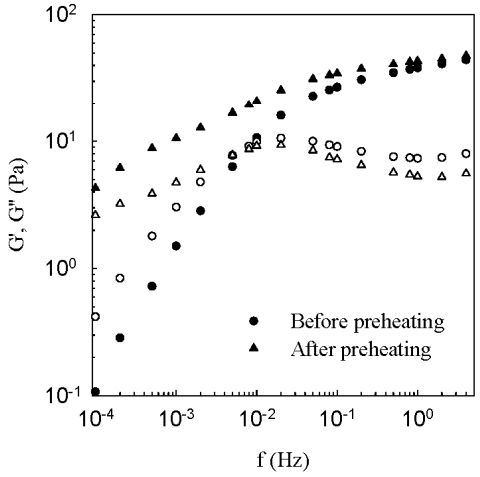

555

556

557 Figure 2

558

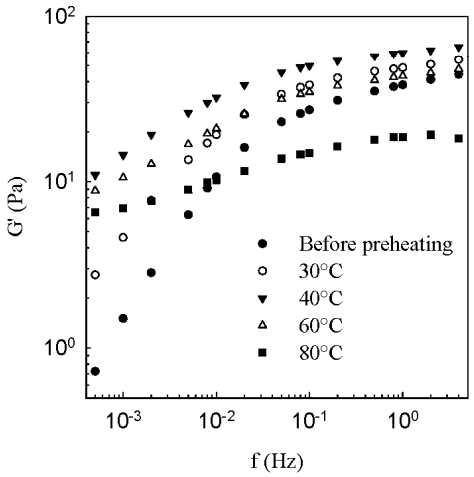

559

560

561 Figure 3

562

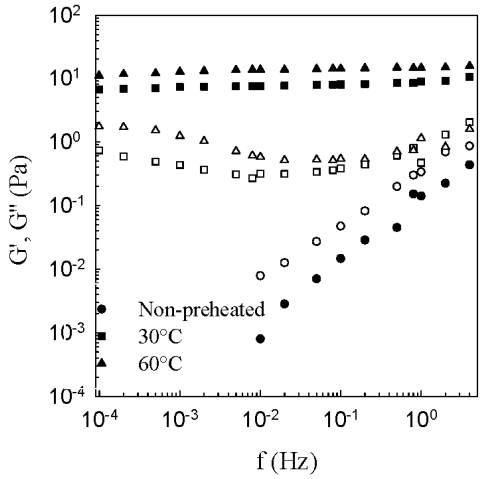

563

564

565 Figure 4

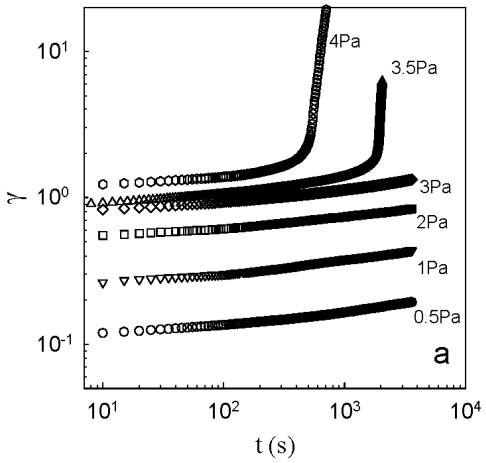

566

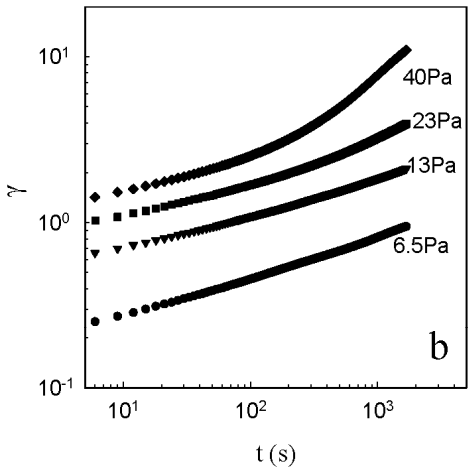

567

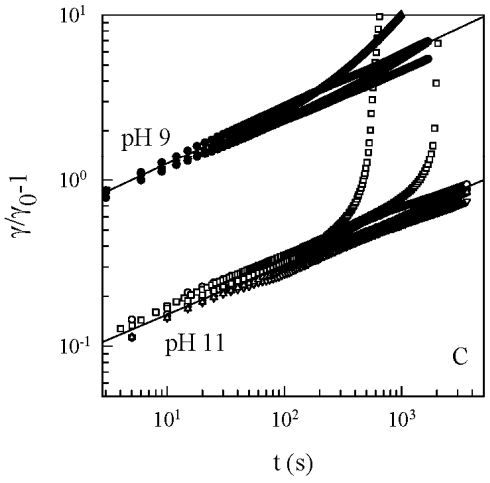

568

569

570 Figure 5

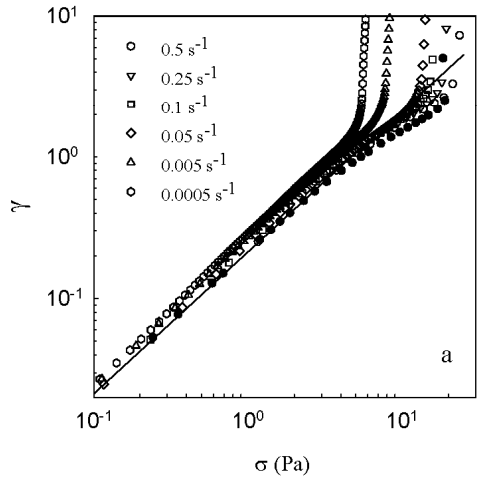

571

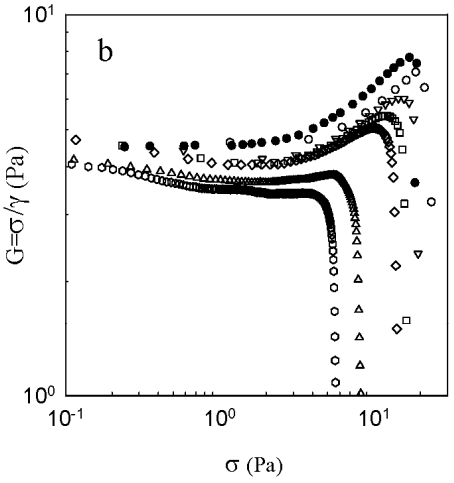

572

573

574 Figure 6

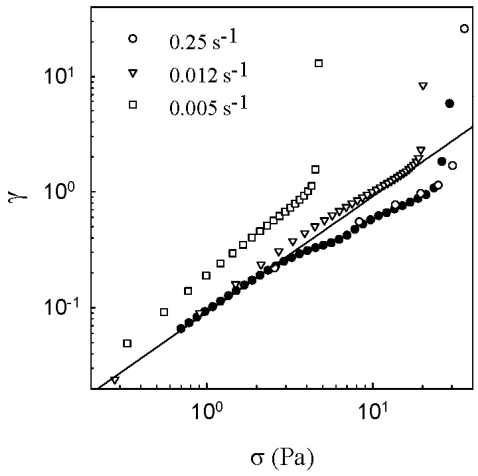

575

576

577

578

579 Figure 7

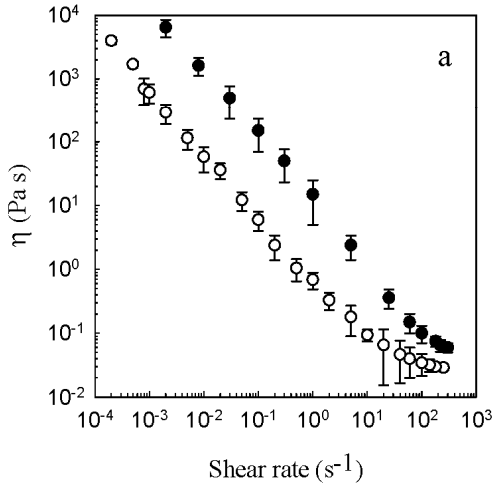

580

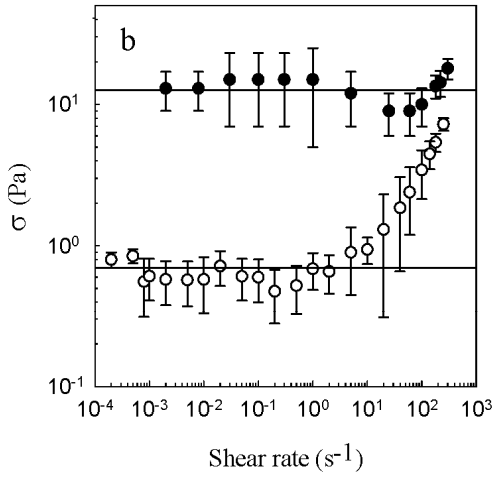

581

582 Figure 8

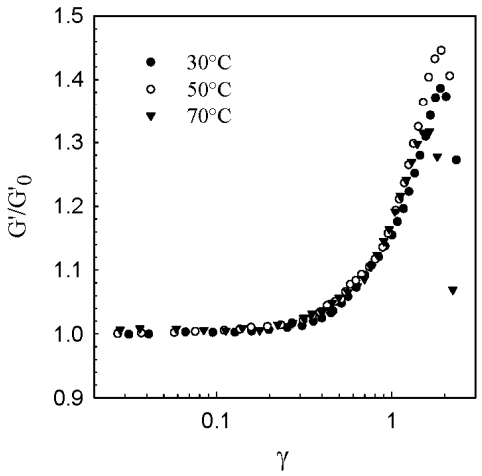

583

584

585 Figure 9

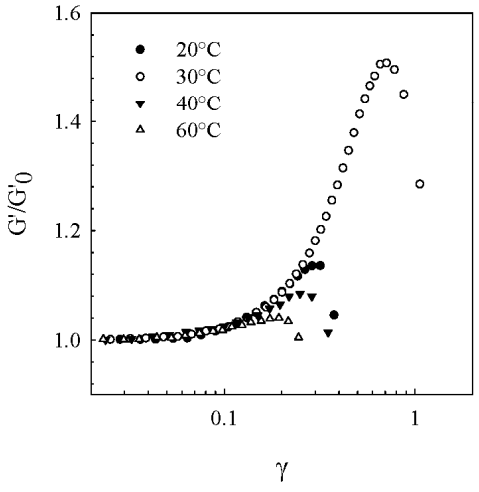

586

587

588 Figure 10

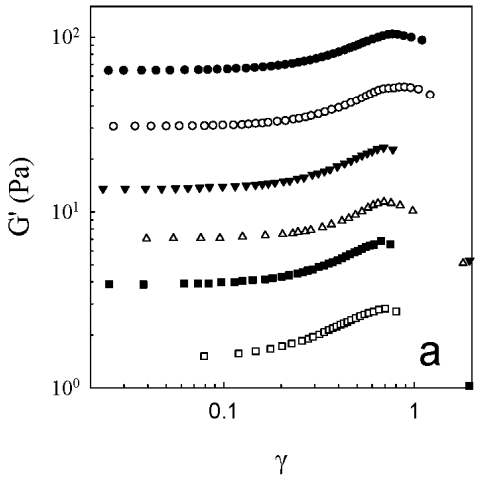

589

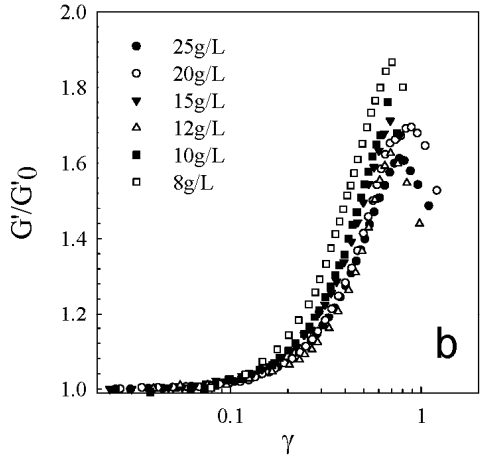

590

591 Figure 11

592

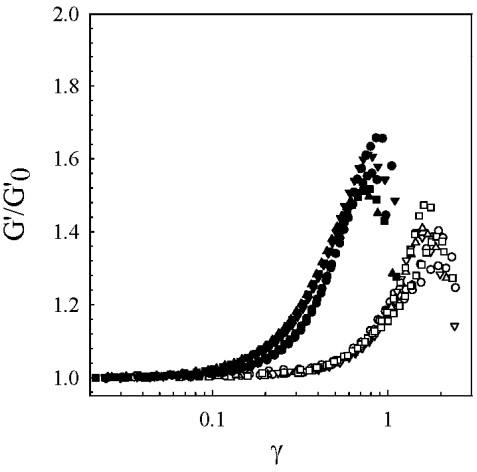

593

594

595 Figure 12

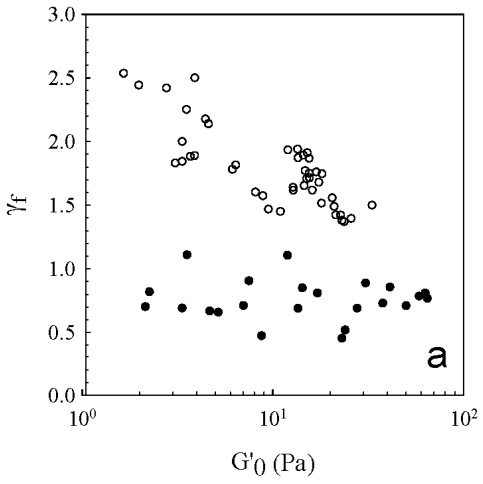

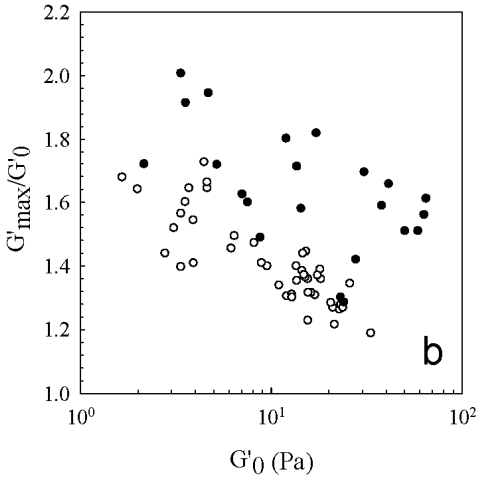
2.2
2.0
1.8
1.6
1.4
1.2
1.0
G'max/G'0
b
10^0
10^1
10^2
G'0 (Pa)

596

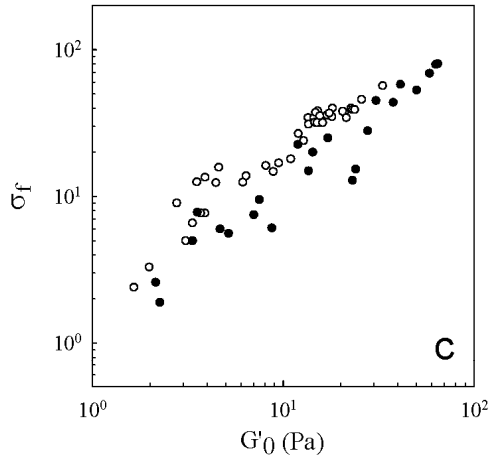
10^2
10^1
10^0
σf
c
10^0
10^1
10^2
G'0 (Pa)

597

598

599 Figure 13

600

601

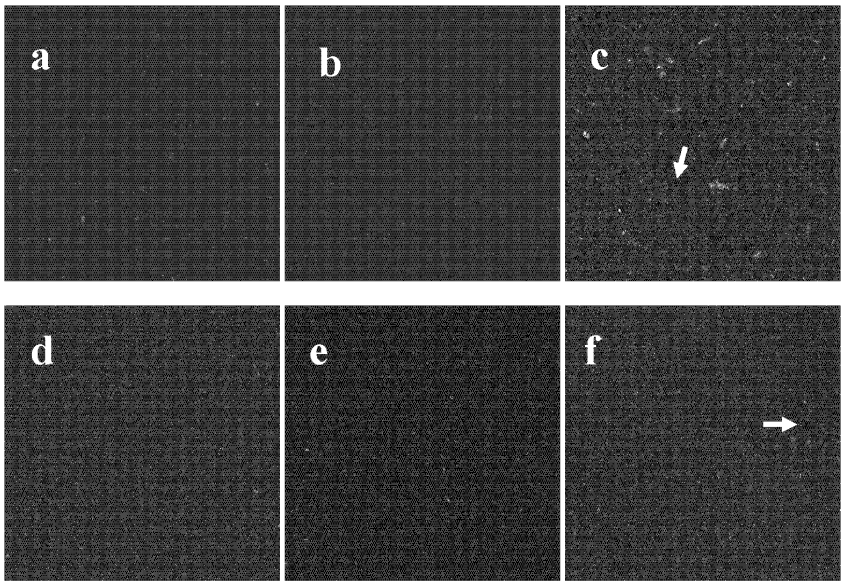

602

603

604

605

606 Figure 14

607

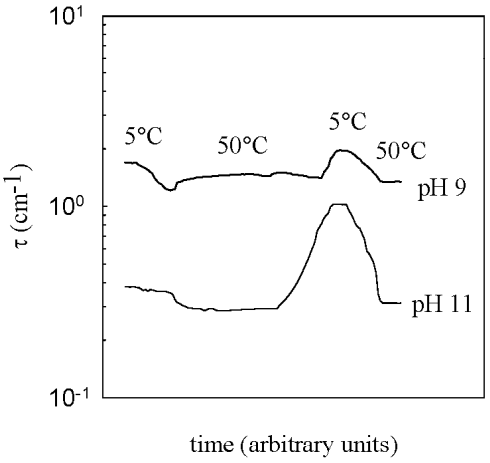

608